2008

Surface Engineering Of Gold Nanoparticles And Their Applications

Qiu Dai
University of Central Florida

SURFACE ENGINEERING OF GOLD NANOPARTICLES AND THEIR APPLICATIONS

by

QIU DAI
B.S. Northwestern Polytechnical University, 2000
M.S. University of Science and Technology of China, 2003

A dissertation submitted in partial fulfillment of the requirements
for the degree of Doctor of Philosophy
in the Department of Chemistry
in the College of Sciences
at the University of Central Florida
Orlando, Florida

Fall Term
2008

Major Professor: Qun Huo

ABSTRACT

Gold nanoparticles (AuNPs) with their unique sizes, shapes, and properties have generated much enthusiasm over the last two decades, and have been explored for many potential applications. The successful application of AuNPs depends critically on the ability to modify and functionalize their surface to provide stability, compatibility, and special chemical functionality. This dissertation is aimed at exploring the chemical synthesis and surface modification of AuNPs with the effort to (1) control the number of functional groups on the particle surface, and to (2) increase the colloidal stability at the physiological conditions.

To control the functionality on the particle surface, a solid phase place exchange reaction strategy was developed to synthesize the 2 nm AuNPs with a single carboxylic acid group attached on the particle surface. Such monofunctional AuNPs can be treated and used as molecular nanobuilding blocks to form more complex nanomaterials with controllable structures. A "necklace"-like AuNP/polymer assembly was obtained by conjugating covalently the monofunctional AuNPs with polylysine template, and exhibited an enhanced optical limiting property due to strong electromagnetic interaction between the nanoparticles in close proximity.

To improve the colloidal stability in the psychological condition, biocompatible polymers, polyacrylic acid (PAA), and polyethylene glycol (PEG) were used to surface modify the 30 nm citrate-stabilized AuNPs. These polymer-modified AuNPs are able to disperse individually in the high ionic strength solution, and offer as the promising optical probes for bioassay applications. The Prostate specific antigen (PSA) and target DNA can be detected in the low pM range by taking advantages of the large scattering cross section of AuNPs and the high sensitivity of dynamic light scattering (DLS) measurement.

In addition to the large scattering cross section, AuNPs can absorb strongly the photon energy at the surface plasmon resonance wavelength and then transform efficiently to the heat energy. The efficient photon-thermal energy conversion property of AuNPs has been used to thermal ablate the Aβ peptide aggregates under laser irradiation toward Alzheimer's disease therapy.

ACKNOWLEDGMENTS

I would like to thank my advisor, Professor Qun Huo for providing me the opportunity and facilities to conduct my Ph.D research in her lab. I want to thank her for not only those always helpful and in-time instructions, but also for encouraging me to accomplish without fear, for teaching me to walk with my own legs in the field of science, and finally build my own confidence. I believe all I have learned from her as a scientist will be invaluable for my further career.

I am also very thankful to my other thesis committee members: Professor Lei Zhai; Professor Andre J. Gesquiere; Professor Jiyu Fang; Professor Stephen M. Kuebler for their precious advice and time.

I am very grateful to all of the members from Professor Qun Huo's research group. Dr. James G. Worden is the person who taught me everything as a beginner on the nanoparticle chemistry when I started my experiments. I also appreciate fruitful discussions, helps and suggestions from Dr. Jinhai Wang, and Dr. Jianhua Zou. My appreciation is also for other members, Andrew W. Shaffer, Yuhua Li, Harish Muthuraman, Dr. Hui Chen, Xiong Liu, Lauren Austin, Janelle Coutts, for being not only wonderful colleagues, but also for being such good friends to be with.

I would like to thank Professor Theodore Goodson III from University of Michigan, and Professor Wenfang Sun from North Dakota State University, for conducting nonlinear optical measurement, and for their invaluable suggestions during the preparation of our manuscript based on those studies. I would like to express my sincere gratitude to Professor Stephen M. Kuebler for providing the optical instruments for our experiments. I also appreciate him for his

patience and confidence in me and so many valuable discussions on our experiments. I am indebted to Professor Roger M. Leblanc and Dr. Robert C. Triulzi from University of Miami for studying the photothermal ablation of Amyloid (Aβ) peptides, and for their fruitful discussions, helps, and suggestions.

I would like to thank my father, Changhong Dai and mother, Qiaodi Yin for their support, encouragement, and love during my life. Finally, I would like to thank my dear wife, Yixin Yu who always loves and supports me at any time. I can not do anything without her sacrificial love.

TABLE OF CONTENTS

LIST OF FIGURES

LIST OF TABLES

LIST OF ABBREVIATIONS

AuNPs	Gold Nanoparticles
AFM	Atomic Force Microscopy
Boc	*tert*-Butoxy carbonyl carbomate
CD	Circular Dichroism
CTAB	Cetyltrimethylammonium Bromide
cAb	Capture Antibody
DLS	Dynamic Light Scattering
DMAP	4-(Dimethylamino) pyridine
DNA	Deoxyribonucleic Acid
DIPCDI	1,2-Diisopropylcarbodiimide
dAb	Dector Antibody
EG_3-SH	Thiol-functional Triethylene Glycol
EDC	Ethyl Dimethylaminopropyl Carbodimide
FT-IR	Fourier Transform Infrared Spectroscopy
GNRs	Gold Nanorods
^{1}H-NMR	Proton Nuclear Magnetic Resonance
HOBT	4-Hydroxybenzotriazole
MSA	Mercaptosuccinic Acid
MUA	11-Mercaptoundecanoic Acid
NIR	Near Infrared
PAMAM	Polyamidoamine
PAA	Polyacrylic Acid
PEG	Polyethylene Glycol
PSA	Prostate Specific Antigen
PVP	Polyvinylpyrrolidone
SEM	Scanning Electron Microscopy
SPR	Surface Plasmon Resonance

SERS	Surface Enhanced Raman Scattering
Sulfo-NHS	N-hydroxysulfosuccinimide
TEM	Transmission Electron Microscopy
TLC	Thin Layer Chromatography
TFA	Trifluoroacetic Acid
TEOS	Tetraethylorthosilicate
UV-Vis	Ultraviolet Visible
XPS	X-ray Photoelectron Spectroscopy

CHAPTER 1 : INTRODUCTION

1.1 : History of Gold Nanoparticles

The first examples of nanotechnology, some historians might be inclined to argue, could be accredited to some glassblowers from the days of imperial Rome. The ancient craftsmen were able to embed colloidal gold nanoparticles (AuNPs) in the glass art works to enhance the lustrous qualities of the glass. Although the nanoscale nature of the gold colloids was not revealed during that time, this did not prevent the craftman from appreciating the enigmatic hues produced upon a change of incident light. One of the most striking examples of such Roman glasses is the famed Lycurgus cup (Figure 1-1), which dates back to the 4th century A.D. The chalice has a dark greenish tint under reflected light (left), but appears in red color (right) when illuminated from inside the goblet. This phenomenon was later attributed to the optical response of colloidal AuNPs dispersed throughout the glass.

Figure 1-1: The photograph of the Lycurgus cup (4th century A.D.).

Although the technology for producing colloidal AuNP-stained glass has been practiced for centuries, the originality of their brilliant colors remain in mystery until the mid-nineteen century, when Faraday published his experiments revealing the colloidal nature of "red" gold.[1] He found that the brilliant colloidal gold dispersion could be prepared by reducing an aqueous solution of gold salts with a phosphorous solution in carbon disulfide. He then investigated the optical properties of thin films prepared from colloidal solutions and observed reversible color changes (from bluish-purple to green) of the films upon mechanical compression. Although Faraday did not reveal the exact particle size, he speculated that the gold colloids were much smaller than the visible light wavelength.

Following Faraday's work, Mie originally calculated the surface plasmon resonance (SPR) in 1908 by solving Maxwell's equations for small spherical particles interacting with an electromagnetic field, which provided the foundations for theoretical understanding of the physical behavior and optical responses of AuNPs.[2] Mie found that the interesting optical attributes of AuNPs, as reflected in their bright intense colors, were due to their unique interaction with light. In the presence of an oscillating electromagnetic field of the light, the free electrons of AuNPs undergo a collective oscillation with respect to the positive metallic lattice. This process is in resonant at a particular frequency of the light, which for gold, appears around 520 nm. Gan and others extended Mie's theory to apply to cylindrical and oblate nanoparticles using a dipole approximation theory.[3] It was observed that the SPR of cylindrical gold particles is splited into two bands, and the maximum peak depends closely on the aspect ratio, which is defined as the length/width ratio of the particles.

When AuNPs were placed in close proximity to one another, the interparticle dipole coupling effect became important and Mie's theory developed for isolated particles failed to account for the optical spectrum. Effective medium theories developed by Maxwell-Garnett, had been successfully used to address the optical behavior of the assemblies of AuNPs.[4] It was found that when the interparticle distance become smaller than the spherical particle dimensions, or even when particle aggregation occurred, the SPR band began to red shift, and sometime a second band at longer wavelength can be observed.

Other than Faraday and Garnett's theoretical studies of individual and aggregated AuNPs, little limited work was done on the chemical synthesis and characterization of AuNPs. Turkevitch developed a simple but effective method for chemical synthesis of colloidal AuNPs in aqueous solution in 1951 which has been extensively utilized ever since.[5] In Turkevietch method, a sodium citrate solution was used to reduce gold salts at the boiling point to form colloidal AuNPs with a diameter of 15-20 nm. This procedure was then later optimized systemically by Frens in 1973.[6] It was proposed that the number of growing nanoparticle nuclei would be dependent on the relative concentration of gold salt to that of sodium citrate. Uniform colloidal AuNPs with sizes ranging from 16 nm to 150 nm could be prepared conveniently by varying the ratio of sodium citrate to gold salt.

In the early 1970's, Schmid pioneered in the preparation of a uniform triphenylphosphene ligand-stabilized AuNPs with a diameter of 1.4 nm consisting of 55 gold atoms.[7] It was found that the electric properties of these AuNPs changed tremendously from that of bulk materials when the size decreased to a few nanometers. Such particles could not simply be treated or

referred to as “divided metals”. Another important property of such particles is their high catalytic activity with decreased particle size.

A significant milestone was made by Brust and others to chemically synthesize alkanethiol monolayer-stabilized AuNPs with a diameter of 1-8 nm in 1994.[8] These particles exhibited remarkable stability in both dry state and solution when compared with the previously mentioned citrate-stabilized and triphenylphosphine-stabilized AuNPs. Over the last 15 years this technique has been the most extensively used synthetic methodology for obtaining monodisperse AuNPs. Following Brust’s work, Murray and others developed a simple place exchange reaction to effectively functionalize thiol monolayer-stabilized AuNPs.[9, 10] The initial ligands on the particle surface may be replaced by adding functional thiol ligands under mild experimental conditions. Additional functionality could be further incorporated onto AuNPs through chemical reactions.

The past two decades have witnessed rapid advances in the ability to chemically synthesize AuNPs with sufficient degree of control over the size, shape, composition, and functionality. Existing spectroscopy and microscopy tools have further facilitated the characterization and understanding of AuNPs. Currently, there is a great motivation to exploit the unique properties of AuNPs for applications in electric and optical devices, biochemical detection, catalysis, cancer diagnostic and therapy etc.

1.2 : Important Properties of Gold Nanoparticles

It is well known that when the size and the dimensionality of a material are reduced to the nanometer length scale, its properties change drastically as the density of states and the spatial length scale of the electron motion are reduced with decreasing size.[11] For AuNPs, the coherent

collective oscillation of free electrons in the conduction band induces large surface electric fields which greatly enhance the irradiative properties when they interact with resonant electromagnetic radiation.[12] This makes the absorption cross section of these AuNPs orders of magnitude stronger than the strongest absorbing molecules and the scattering light becomes orders of magnitude more intense than fluorescent dyes.[13] These unique optical properties provide great potential for AuNPs to be used in many applications, such as biochemical sensors, biological imaging and medical therapeutics as well as catalysis due to their high surface-to-volume ratios.[11, 14]

1.2.1 : Surface Plasmon Resonance Absorption of Gold Nanoparticles

Spherical AuNPs (1 ~100 nm) exhibit a surface plasmon resonance (SPR) absorption band in the visible light region. The SPR absorption results from the dipole oscillations of the free electrons with respect to the ionic core of a spherical metal nanoparticle. In a classical description as shown in Figure 1-2, the electric field of an incoming light wave induces a polarization of the electrons with respect to the much heavier ionic core of a spherical nanoparticle.[13] A net charge difference is only felt at the nanoparticle surface, which in turn acts as a restoring force to create a dipolar oscillation of all the electrons with the same phase. When the frequency of the electromagnetic field becomes resonant with the coherent electron motion, a strong absorption band around 520 nm can be observed as shown in Figure 1-3, which is the origin of the observed reddish color of AuNPs in solution.

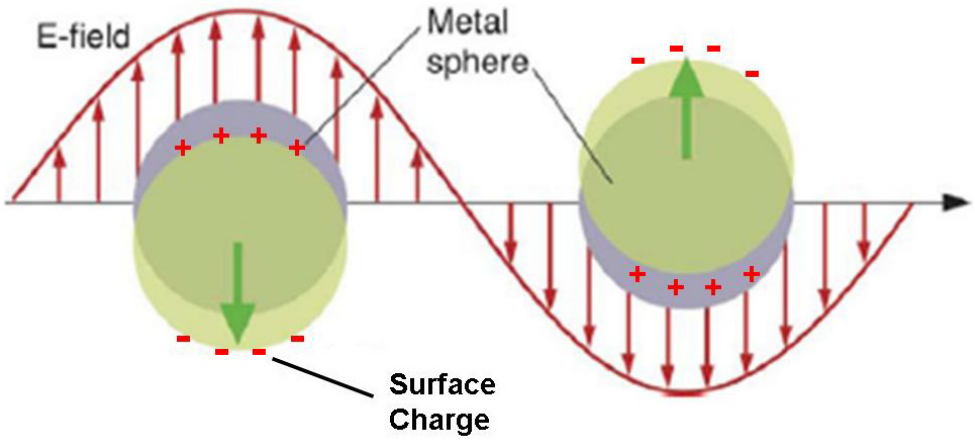

Figure 1-2: A schematic illustration of the dipole SPR oscillation in spherical **AuNPs.**

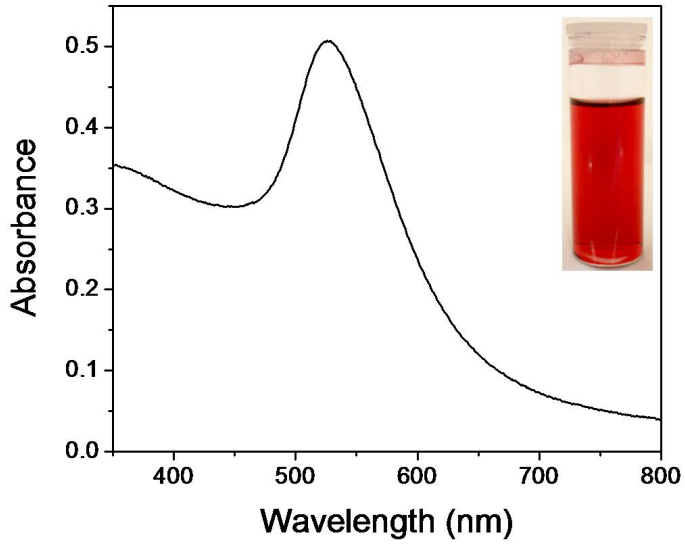

Figure 1-3: A typical SPR spectrum of spherical AuNPs.

Mie is the first to explain theoretically the SPR property of spherical AuNPs. He solved Maxwell's equation for an electromagnetic light wave interaction with a small sphere. For particles much smaller than the light wavelength (<20 nm), only the dipole oscillation

contributed significantly to the extinction cross section and thus Mie's theory was simplified to the following equation:

$$\sigma_{ext} = \frac{9 \bullet V \bullet \varepsilon_m^{3/2}}{C} \bullet \frac{\omega \bullet \varepsilon_2(\omega)}{[\varepsilon_1(\omega) + 2\varepsilon_m]^2 + \varepsilon_2(\omega)^2} \quad (1\text{-}1)$$

Where V is the particle volume, ω is the angular frequency of the exciting light, and C is the speed of light, ε_m and $\varepsilon(\omega) = \varepsilon_1(\omega) + i\varepsilon_2(\omega)$ are the dielectric functions of the surrounding medium and the material itself respectively. The resonance condition is fulfilled when $\varepsilon_1(\omega) = -2 \cdot \varepsilon_m$ if ε_2 is small or weakly dependent on ω.

From Equation 1-1, it was calculated that the optical extinction coefficient (σ) of spherical AuNPs of 40 nm in diameter is around 7.7×10^9 M^{-1} cm^{-1} at a wavelength maximum around 530 nm, which is four orders of magnitude higher than the absorption coefficient of Rhodamine 6G ($\varepsilon = 1.5 \times 10^5$ M^{-1} cm^{-1} at 530 nm).[15] Also, it can be seen that the peak intensity and position of the SPR absorption band is dependent on the sizes, the shapes of the particles, the dielectric constant of the metals, and the medium surrounding the particle. For example, Figure 1-4 shows that the SPR absorption band is red shifted and the peak bandwidth becomes broad with increased particle size.[16]

It is also indicated from Equation 1-1 that the SPR absorption band is dependent on the particle shapes. For example, gold nanorods (GNRs) exhibit two distinct SPR absorption bands in comparison with the single SPR absorption peak of the spherical nanoparticles as shown in Figure 1-5. The transverse SPR band around 520 nm is due to the excitation across the short dimension of the rods, and the longitudinal SPR band is associated with the excitation along the long axis of the rods.

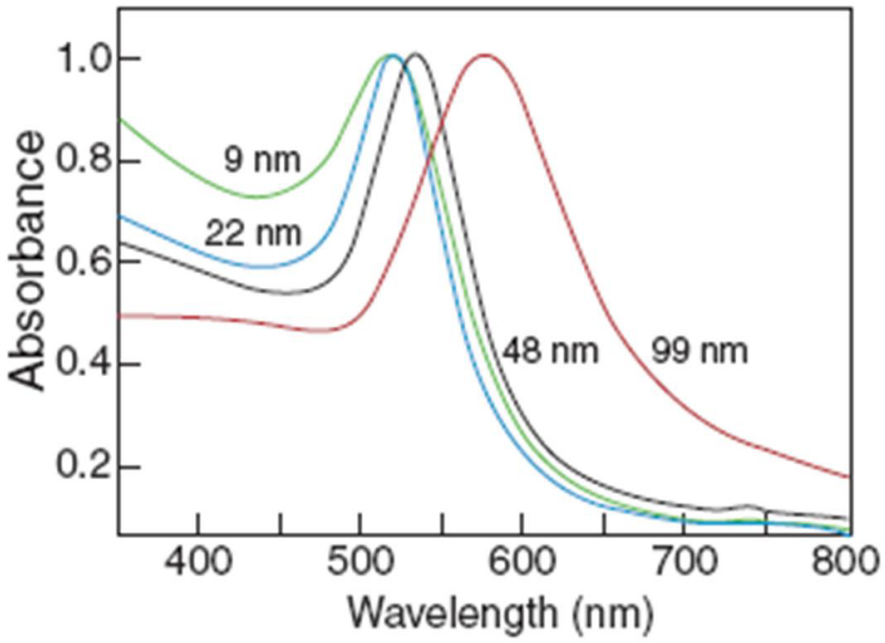

Figure 1-4: UV-vis absorption spectra of spherical AuNP with different diameters (9-99 nm).

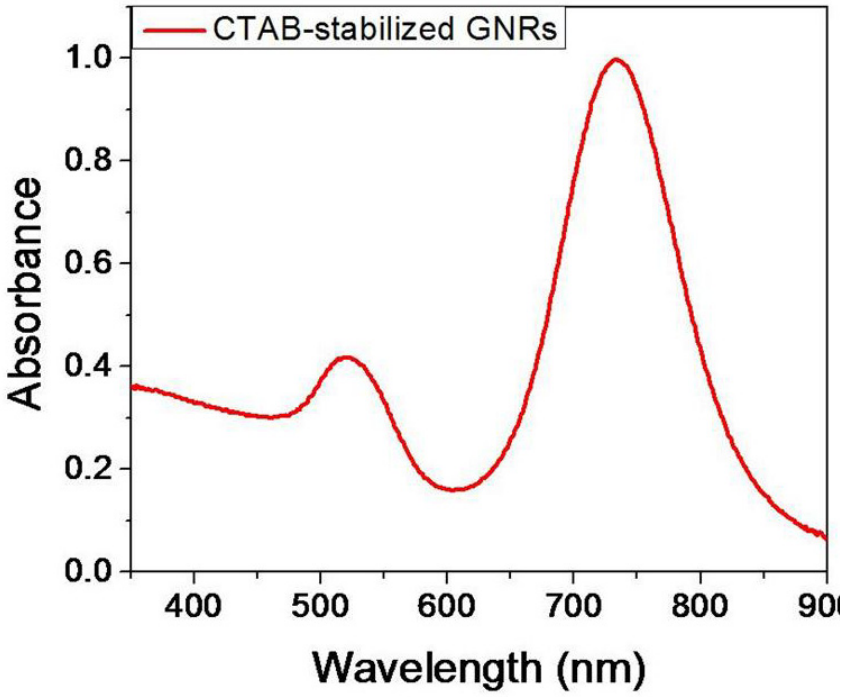

Figure 1-5: UV-vis absorption spectrum of GNRs with aspect ratio of 4 (10 × 40 nm).

The optical absorption spectrum of GNRs with aspect ratio *R* can be simulated using an extension of the Mie theory. Within the dipole approximation according to the Gans treatment, the extinction cross-section for elongated ellipsoids is given by the following equation.[3]

$$\sigma_{ext} = \frac{\omega}{3C} \bullet \varepsilon_m^{3/2} \bullet V \bullet \sum_j \frac{\left(1/P_j^2\right)\varepsilon_2}{\left\{\varepsilon_1 + \left[\left(1-P_j\right)/P_j\right]\varepsilon_m\right\}^2 + \varepsilon_2^2} \tag{1-2}$$

Where P_j are the depolarization factors along the three axes A, B, and C of the nanorods

With A > B = C, defined as:

$$P_A = \frac{1-e^2}{e^2}\left[\frac{1}{2e}\ln\left(\frac{1+e}{1-e}\right) - 1\right]$$

$$P_B = P_C = \frac{1-P_A}{2} \tag{1-3}$$

And the aspect ratio *R* is included in *e* as follows:

$$e = \left[1 - \left(\frac{B}{A}\right)^2\right]^{1/2} = \left(1 - \frac{1}{R^2}\right)^{1/2} \tag{1-4}$$

It has been found that the transverse SPR absorption band is relatively insensitive to the rod aspect ratio and coincides spectrally with the SPR absorption of spherical nanoparticles.[17] Different from the transverse SPR absorption band, the longitudinal SPR absorption band is very sensitive to the aspect ratio.[18] Figure 1-6 shows experimentally how the SPR bands of the GNRs shift with increasing aspect ratios.[19] When the aspect ratio increase, the absorption maximum of the longitudinal SPR band is greatly red shifted. This absorption difference of the longitudinal SPR band causes the color difference of the nanorods in solution. For short nanorods with the maximum of longitudinal SPR lower than 700 nm, the GNR solution appear in blue color. When the longitudinal SPR maximum is between 700 nm and 800 nm, the solution appears in deep red

color, and when the nanorods have a longitudinal SPR maximum longer than 800 nm, the solution appears in pink color.

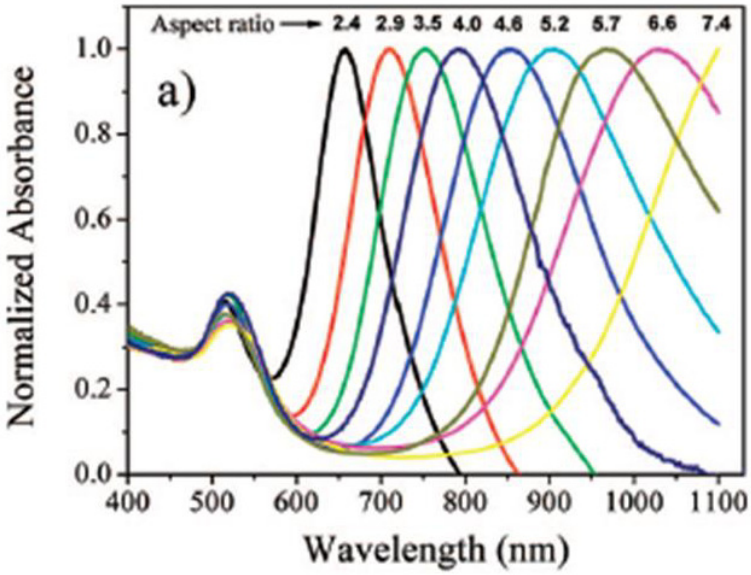

Figure 1-6: The SPR absorption spectra of GNR solution with different aspect ratios varying from 2.4 to 7.4.

It is found that the SPR absorption is dependent on the interparticle distance as well. Mie's theory is based on the assumption that individual particles are noninteracting and separated far enough that the electric field created around one particle by the excitation of a SPR is not felt by other neighboring particles. However, when spherical gold particles come into close proximity to one another, interparticle dipole coupling becomes effective for particle-particle distances smaller than five times of the particle radius ($d < 5R$, where, d is the center to center distance and R is the radius of the particles). This interaction may lead to complicated absorption spectra depending on the size and shape of the formed particle aggregate.[20] The effective-medium theories, developed by Maxwell-Garnett have been successfully applied to this problem to account for the optical absorbance behavior of AuNPs present in a closely packed assembly.[4]

The resulting spectra are a combination of the conventional SPR due to single spherical particles and the new broad peak associated with the particle-particle coupling interactions at longer wavelength region. Figure 1-7 shows the calculated absorption spectra for linear assemblies of AuNPs with 40 nm diameter. A systematic red shift in λ_{max} is expected with increasing aggregate size.[21]

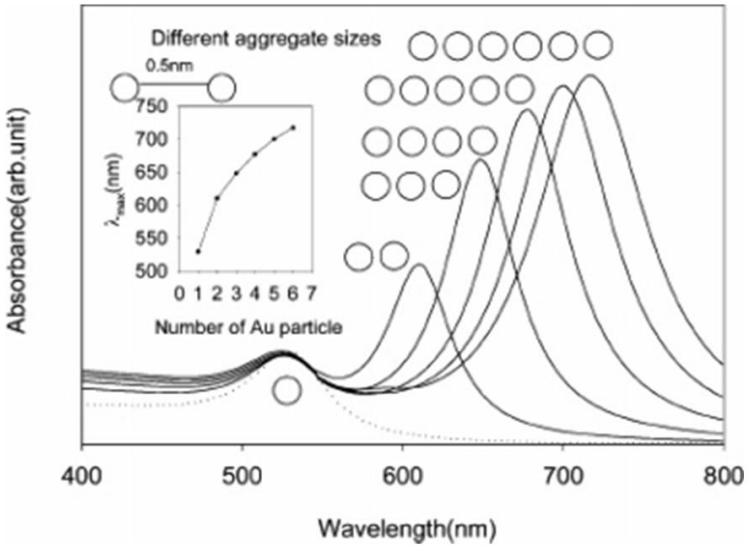

Figure 1-7: Electrodynamic modeling calculations of extinction spectra for AuNP "line aggregates" (d = 40 nm, s = 0.5 nm).

1.2.2 : Surface Plasmon Resonance Scattering of Gold Nanoparticles

In addition to its SPR absorption, AuNP suspensions scatter strongly colored light when illuminated by a white light beam. It was calculated that the scattering coefficient of a 80 nm spherical AuNP is around 3.2×10^{10} M^{-1} cm^{-1} at 560 nm, which is five orders of magnitude higher than the light scattering from fluorescein, a fluorescent molecule commonly used in molecular imaging (emission coefficient: 9.2×10^{4} M^{-1} cm^{-1} at 483 m).[13] The scattering light from the AuNP suspensions has the same appearance as fluorescent solutions as shown in Figure

1-8a.[22] Unlike fluorescent probes, the scattering light generated by AuNPs is not prone to quenching and does not photobleach with repeated or continuous exposure to light. The light scattering is sensitive to the size of the nanoparticles as well. AuNPs with a diameter of 58 nm scatter green light while AuNPs with a core diameter of 78 nm scatter yellow light (Figure 1-8b and c). The scattering light is also tunable by varying the shape, and composition of the nanoparticles as shown in Figure 1-9.[23] The scattering color as observed from dark field imaging changes from green to yellow when the gold particle shape changes from sphere to rod. Different from AuNPs, the scattering light from silver nanoparticles appears to be red.

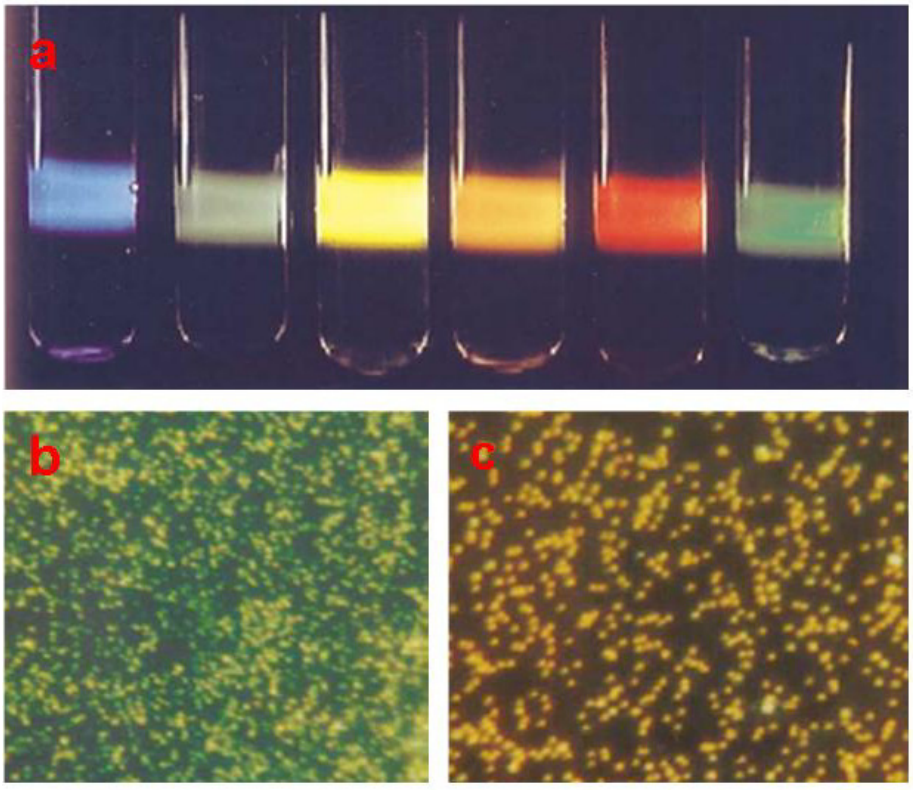

Figure 1-8: AuNPs of different size irradiated by a beam of white light (a), the light scattering imaging of 58 nm AuNPs (b), the light scattering imaging of 78 nm AuNPs (c).

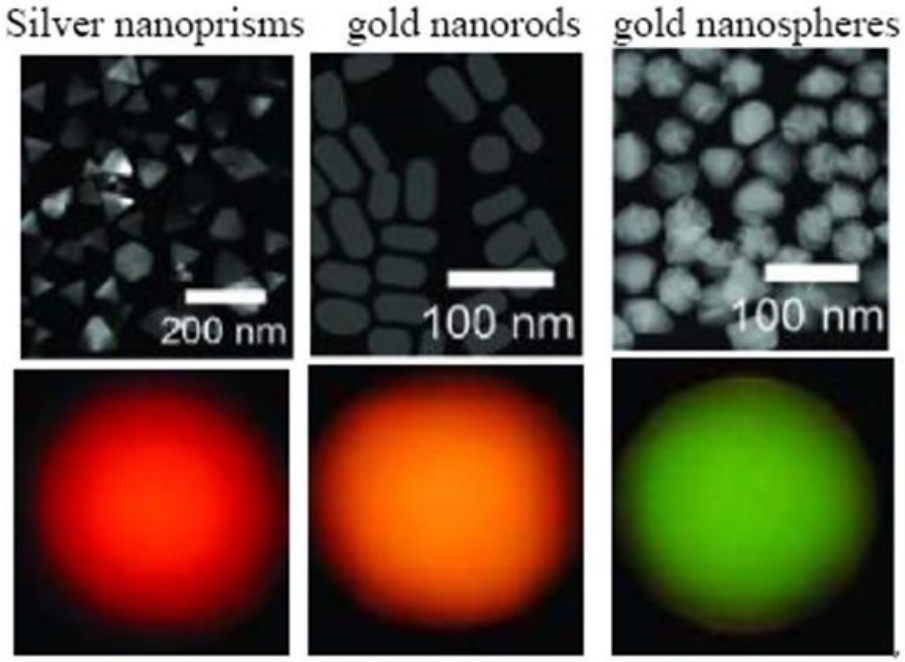

Figure 1-9: TEM and light scattering images of silver nanoprisms, GNRs, and AuNPs.

Juan Yguerabide and others conducted a theoretical study to calculate the scattering intensity and cross-section of AuNPs through Equation 1-5 and 1-6.[22]

$$I = \frac{16\pi^4 a^6 n_{med}^4 I_0}{r^2 \lambda_0^4} \left| \frac{m^2 - 1}{m^2 + 2} \right|^2 \sin^2(\alpha) \tag{1-5}$$

$$C_{sca} = \frac{128\pi^5 a^6 n_{med}^4}{3\lambda_0^4} \left| \frac{m^2 - 1}{m^2 + 2} \right|^2 \tag{1-6}$$

Where a is the particle radius, n_{med} is the refractive index of the medium surrounding the particle, I_0 is the intensity of the incident monochromatic light, m is the relative refractive index of the bulk particle material, α is the angle between the detection direction, λ_0 is the wavelength of the incident beam.

From Equation 1-5 and 1-6, we can see that the light scattering power is proportional to the sixth power of the particle radius. Therefore, the scattering intensity increases drastically with increased particle size. Table 1-1 shows the relative intensity scattered from AuNPs with different sizes. The scattering light intensity of a 100 nm nanoparticle is four orders of magnitude higher than that of a 20 nm nanoparticle.[3]

Table 1-1: Comparison of calculated intensity of light scattered at 90°C by AuNPs illuminated with white unpolarized light ($I_{u,\,INT}$) and monochromatic (I_u)

Diameter (nm)	$I_{U,INT}(90)$	$I_U(90)^a$
20	1	1
40	71.3	72.5
60	859	973
80	4.42×10^3	5×10^3
100	1.33×10^4	1.5×10^4
120	2.74×10^4	3.1×10^4
140	4.34×10^4	4.92×10^4
160	5.79×10^4	6.56×10^4
180	7.15×10^4	8.1×10^4
200	8.3×10^4	9.4×10^4
300	1.76×10^4	2×10^4

According to the above introduction, we know that the peak intensity and position of both SPR absorption and scattering bands are highly dependent on the size and shapes of AuNPs, the refractive index of the surrounding medium, and the interaction with neighboring particles. Since the total extinction efficiency is equal to the sum of the scattering and absorption efficiency, the

absorption and scattering percentage will vary depending on the size and shape of the nanoparticles.

It has been reported that for spherical AuNPs with a diameter of 10 nm, the absorbance is much higher than the scattering, but as the particle size increases, scattering becomes increasingly significant. The ratio of scattering to absorption for 100 nm AuNPs is several hundred times greater than that of a 10 nm nanoparticle.[24] Also, the ratio of scattering to absorption depends on the particle shape as shown in Figure 1-10. The scattering cross-section of gold nanorods increases with increasing aspect ratio.

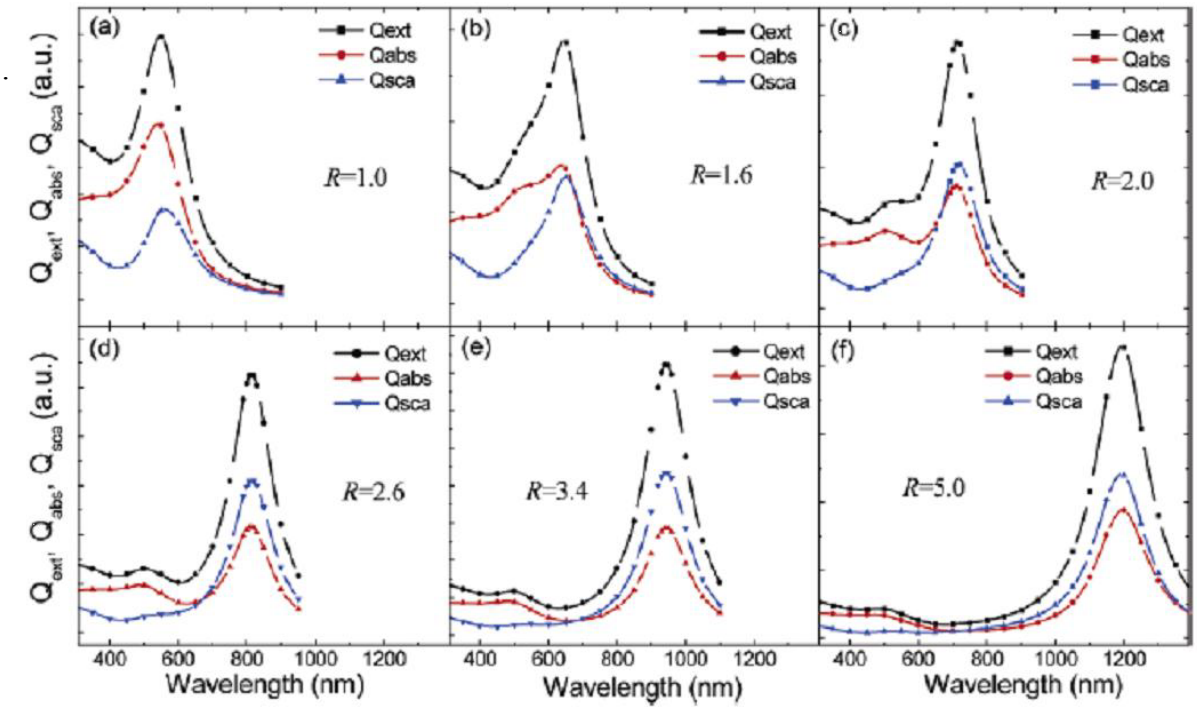

Figure 1-10: A series of calculated spectra for optical extinction, absorption and scattering efficiencies for GNRs with different aspect ratios.

1.3 : Synthesis of Gold Nanoparticles

There are two general strategies to synthesize AuNPs. The first one is a top-down approach. A bulk gold material can be broken into smaller particles using photo or electron beam lithography.[25] However, top-down approach involves the use of complicated instrumentation. Another one is called bottom-up approach, where nanoparticles can be synthesized from the corresponding atoms and molecular species through chemical reactions.[26] The synthesis of AuNPs relies heavily on the bottom up approach. AuNPs with different sizes (1~100s nm) and shapes (spheres, rods, shells, and cages) have been synthesized with various reduction techniques and capping materials.[27]

1.3.1 : Synthesis of Spherical Gold Nanoparticles

The citrate reduction of gold salt, $HAuCl_4$, in aqueous solution developed by Tukevitch et al is among the most extensively used method for wet chemical synthesis of spherical AuNPs (Figure 1-11a).[5] In this reaction, trisodium citrate works as both a reducing and stabilizing agent in the synthesis, and the nanoparticles size can be varied from 5 nm to 150 nm through adjusting the ratio of trisodium citrate to gold salts, and other experimental conditions. The reaction is easy to set up and conduct and the obtained nanoparticles have a relatively good size distribution, typically in the range of 10%. However, this method also suffers several limitations. The citrate-protected nanoparticles become unstable at an environment with relatively high ionic strength or elevated temperature, due to the loose shell coating of citrate molecules on nanoparticles surface through electrostatic interactions.[28] For the same reason, the nanoparticles cannot be dried and recollected from aqueous solution, because the drying process will inevitably destroy the citrate ligand layer. The concentration of AuNPs that can be obtained in solution is also very limited.

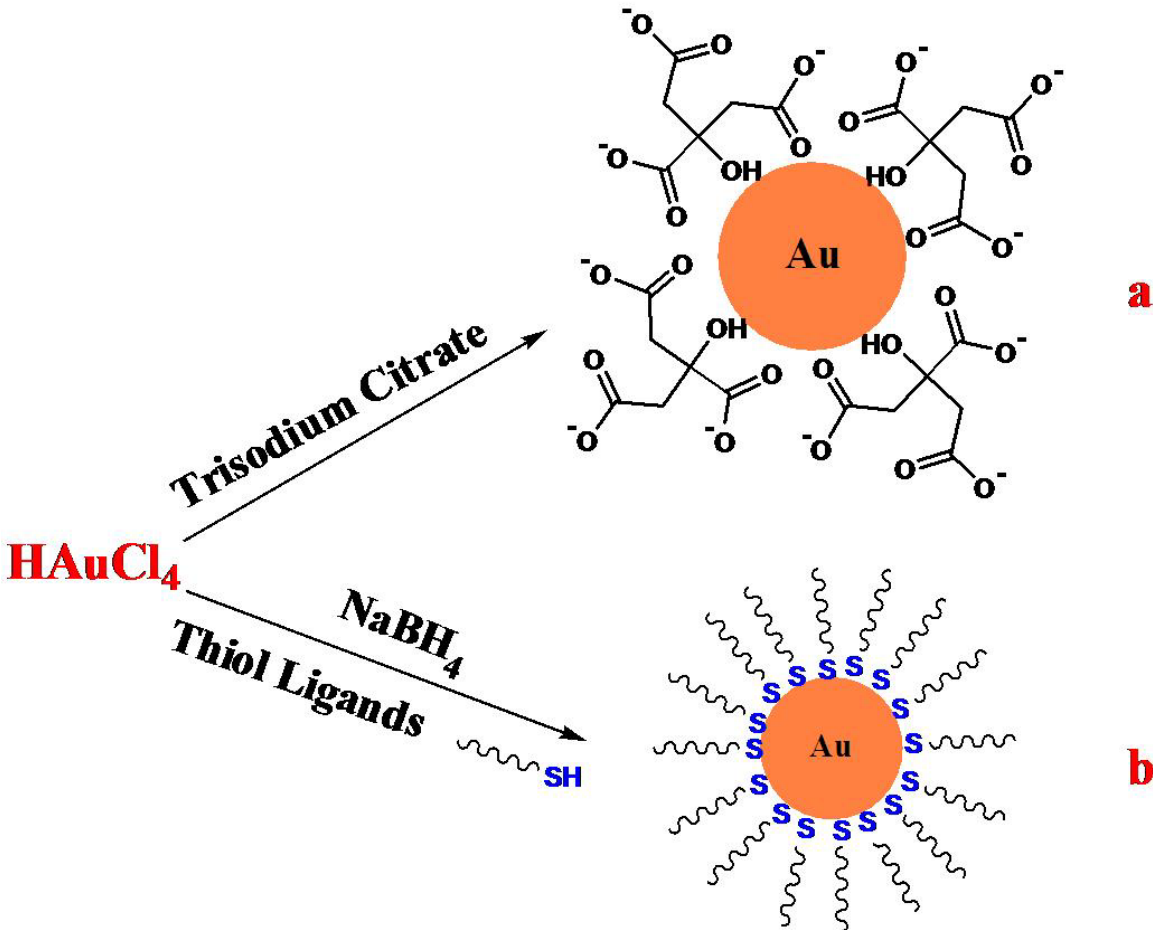

Figure 1-11: Two schematic strategies to synthesize the spherical AuNPs (a: citrate method; b: Brust-Schiffrin method).

Another most extensively used method for spherical AuNP synthesis is Brust-Shiffrin reaction as shown in Figure 1-11b.[8] In contrast to Turkevitch method, the Brust-Shiffrin reaction leads to nanoparticles soluble in organic solvents with a typical size in the range of 1-8 nm. The reaction was conducted in an oil-water two phase environment, with gold salt reduced by sodium borohydride ($NaBH_4$, in aqueous solution) in the presence of thiol capping ligands (oil phase) and a phase transfer agent (tetraoctylammonia bromide). Thiol ligands form a stable monolayer

on nanoparticle surface through a strong Au-S bond, and provide two key functions in this method: shielding the nanoparticles from agglomeration and furnishing a scaffold for the attachment of functional molecular entities. The size of nanoparticles can be controlled through the stoichiometry of the metal salt to thiol capping ligand, other experimental conditions, or post-synthesis annealing process. The advantage of thiol-protected AuNPs is that these particles can be repeatedly isolated and re-dissolved into many organic solvent without irreversible aggregation to occur. The concentration of the nanoparticle solution can be made much higher than citrate-stabilized AuNPs by re-dissolving dried nanoparticles back into solutions. However, the disadvantage of this chemical synthesis is that most AuNPs are insoluble or have poor solubility in aqueous solution, and the size of the nanoparticles is often limited to less than 10 nm, most often, to less than 5 nm. This is a significant limitation for applications based on the surface plasmon resonance (SPR) or SERS effect of AuNPs, as these properties only become obvious on nanoparticles large than 10 nm.[29]

Other than thiol ligands, amine ligands have also been used for spherical AuNP synthesis as both reducing and stabilizing ligands.[30, 31] An alkylamine, oleylamine, has been reported for the synthesis of AuNPs in the size range of 10-20 nm in both organic solvents and mixed water-oil two phase reaction mixture. Phospholipid can be as well used to synthesize and stabilize AuNPs with improved biocompatibility.[32] Although a certain level of understanding has been obtained on the reaction mechanism of amine-induced nanoparticle formation, the mechanism is still yet not as clear as thiol chemistry.

1.3.2 : Synthesis of Gold Nanorods

The synthesis of GNRs with controllable size and aspect ratio has been extensively carried out both chemically and electrochemically.[33] One of the most commonly used method is a template-induced growth of nanorods inside a rod-shaped liposome formed from cetyltrimethylammonium bromide (CTAB) surfactant.[34, 35, 36, 37] A spherical AuNP with a diameter around 5 nm was first synthesized by chemical reduction of gold salts with a strong reducing agent ($NaBH_4$). These seeds, serving as the nucleation sites for nanorods formation, were then added slowly to the growth aqueous solution including gold salts, rod-like CTAB templates, and silver nitrate. Subsequently, the GNRs formed slowly inside CTAB templates upon addition of the weak reducing agent, ascorbic acid. By simply adjusting the amount of gold seeds with respect to the gold precursor, a fine-tuning of the aspect ratio of the nanorods can be achieved as shown in Figure 1-12.[34, 35] The as-synthesized nanorods are protected by a positively charged CTAB bilayer on the surface, which make the nanorods soluble in aqueous solution.

An electrochemical route has also been used to synthesize GNRs.[38] In a typical electrochemical cell, a gold metal plate was used as the sacrificial anode and a platinum plate as the cathode. Both electrodes were immersed into an electrolytic solution containing rod-like CTAB templates. The gold cation generated at the anode was able to form a complex binding with the CTAB templates and thus migrate to the cathode where reduction occurs. A subsequent sonication was followed to shake off the nucleated nanorods from the cathode surface, and dispersed back to the solution.

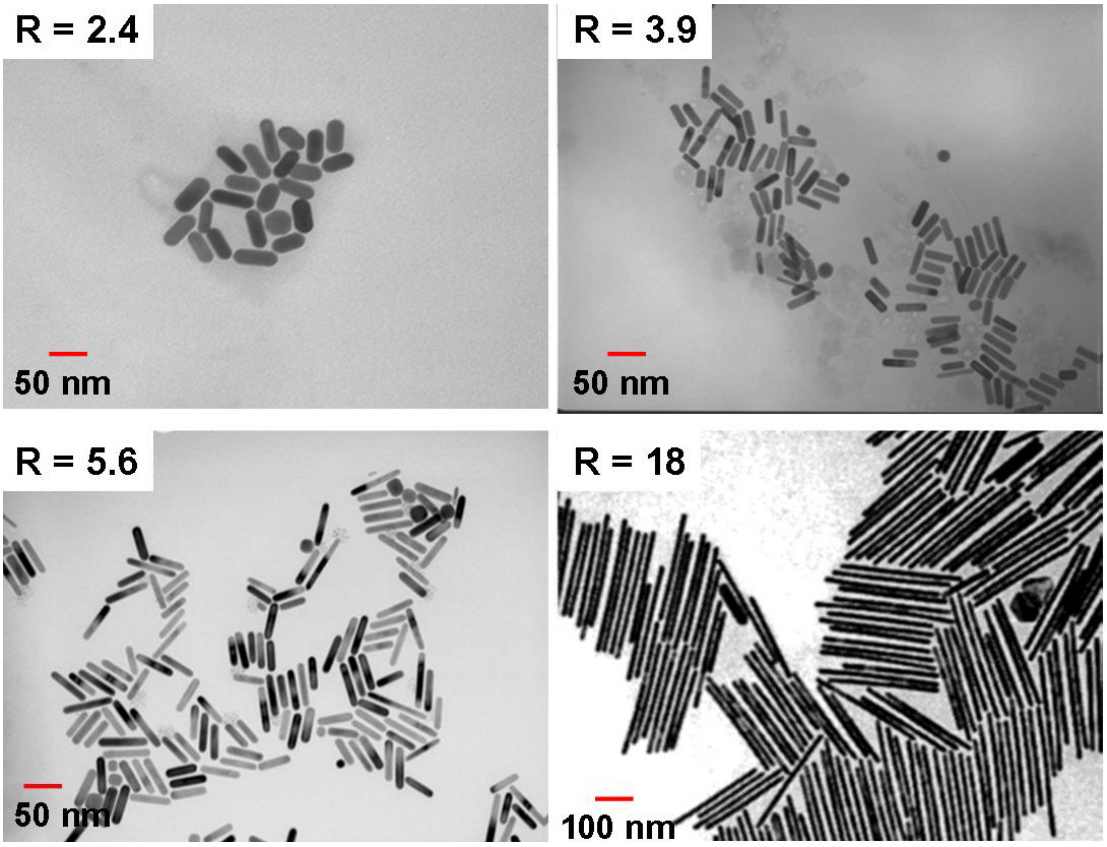

Figure 1-12: TEM images of GNRs with different aspect ratio (2.4, 3.9, 5.6, 18)

Besides these methods mentioned above, several other methods such as electrochemical deposition in hard template have also been investigated for producing GNRs.[39] However, these methods lead to low yields, with poor reproducibility and much difficulty in obtaining long rods in decent yields.

1.3.3 : Synthesis of Gold Nanoparticles with Other Shapes

In addition to spherical and rod-like AuNPs, other types of AuNPs such as shells,[40] cages,[41] and wires[42] have been synthesized recently using different templates and growth conditions.

Gold nanoshells with SPR band in the near infrared region have been developed by coating silica nanoparticle with an ultrathin gold layer.[40] A silica nanoparticle with a diameter of 40 nm was synthesized according to Stöber method and followed by surface functionalization with amine group using amine-terminated silane, 3-aminopropyltrimethoxysilane. 2 nm AuNPs was then exchanged to the particles surface and used as a seed to initiate the gold nanoshell growth. Various stages in the growth of a gold shell on the silica nanoparticles surface are shown in Figure 1-13a.[43] The diameter of the gold shells is largely determined by the diameter of the silica cores, and the shell thickness can be easily controlled through the amount of gold deposited on the silica core surface.

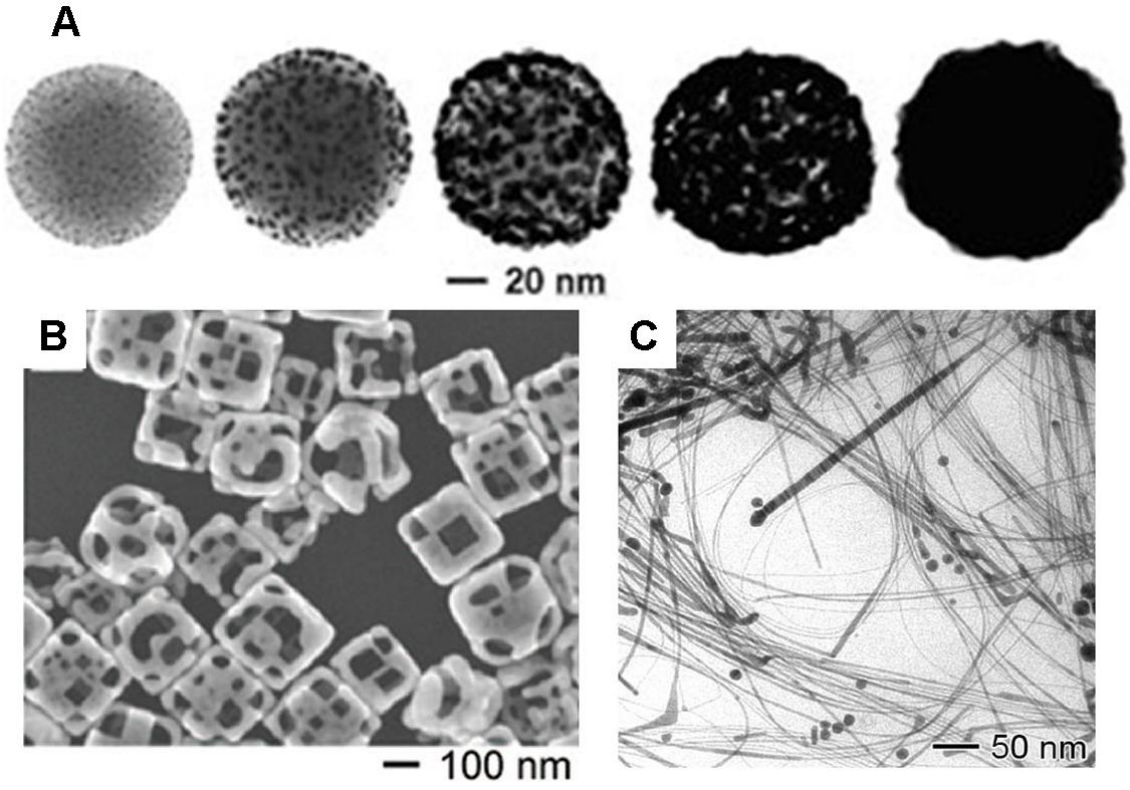

Figure 1-13: (A): TEM images of the gold nanoshell during shell growth having a silica core diameter of 100 nm. (B): SEM image of gold porous nanocages from the galvanic replacement reaction. (C): TEM image of gold nanowires with an average diameter of 1.8 nm and an average length of 2 μm.

Other than nanoshells, gold nanocages with hollow interiors and porous walls have been synthesized via galvanic replacement reaction between truncated silver nanocubes and aqueous $HAuCl_4$ solution as shown in Figure 1-13b.[41] Silver nanostructures with controlled morphologies could be generated through polyol reduction, where silver nitrates was reduced by ethylene glycol to form silver nanoparticle seeds. The silver nanostructures can then be used as a sacrificial template and transformed into gold nanocages via galvanic replacement reaction. It was found that the replacement proceeds through three steps: initiation of silver dissolution by pitting at a specific site on the surface of the silver nanocube, formation of a pin-free nanobox consisting of thin walls through a combination of galvanic replacement; and gold-silver alloying followed by generation of pores in the wall through a dealloying process. The dimension and wall thickness of the resultant gold nanocages could be easily controlled by adjusting the ratio of silver to $HAuCl_4$.

Furthermore, gold nanowires have been synthesized recently using aurophilic attraction interaction.[42] The aurophilic bonding between Au^I halides and coordinating ligands (alkylamine) can lead to the formation of one dimensional polymeric chains. Due to the van der Waals interaction between the side chains, the one dimensional chain can form polymeric strands with backbones of Au^I ions surrounded by alkyl ligands. When the Au^I was converted to Au^0 under slow reduction, the nucleation and growth of Au can be mediated by the one dimensional polymer strands to generate ultrathin nanowires. Figure 1-13c shows the TEM image of gold nanowires with an average diameter of 1.8 nm and an average length diameter of 2 μm obtained via reactions between [(oleylamine)AuCl] and 10 nm Ag nanoparticles in hexane.

Overall, the field of chemical synthesis of AuNPs with controllable sizes and shapes is presently a very active area of research, and the ability to control the size and shapes at the molecular level provides access to a wide variety of AuNPs with unique and tunable optical properties.

1.4 : Surface Functionalization of Gold Nanoparticles

The successful application of AuNPs depends critically on our ability to modify and functionalize their surface to provide stability and specific chemical functionality. Currently there are three major ways for surface functionalization of AuNPs, as summarized in Figure 1-14. The first one is direct synthesis of AuNPs in the presence of desired functional ligand molecules (Figure 1-14a). These ligand molecules are typically small organic or organometallic complex molecules. In order to form a monolayer on nanoparticle surface, the ligands need to have at least one functional group such as thiol with high affinity towards gold. A second requirement is that the molecules used for direct synthesis of AuNPs must be able to form a stable monolayer on nanoparticle surface. For example, mercaptosuccinic acid can serve as a stabilizer during borohydride reduction of $HAuCl_4$ to give 1-3 nm, water-dispersible gold nanoparticles.[43] The resulting carboxylic acid group on the particle surface can be further used as the anchor point to conjugate with molecules, polymers, and biomolecules. Glutathione,[44] trimethyl (mercaptoundecyl) ammonium,[45] and thiolated derivatives of polyethylene glycol (PEG) [46] have also been used as thiol-based stabilizers during the formation of AuNPs with a variety of reducing agents.

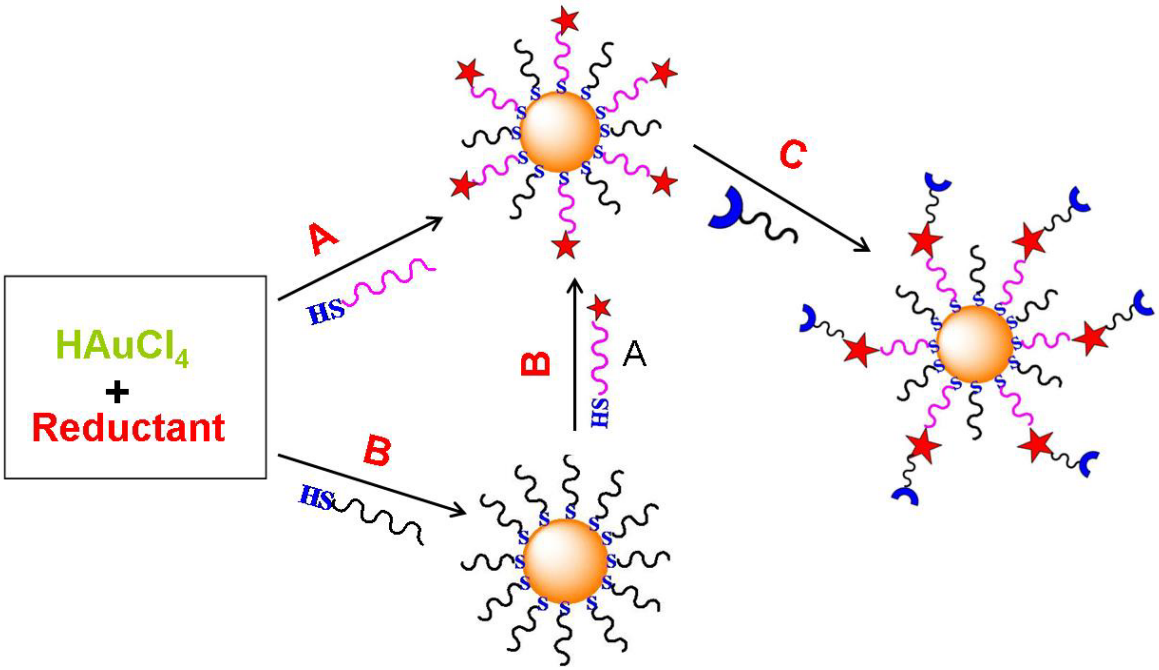

Figure 1-14: A schematic illustration of three common strategies for surface functionalization of AuNPs (A: direct formation of AuNPs in the presence of functional thiol; B: Thiol place exchange method; C: covalent/nocovalent coupling method).

The second approach is a place exchange reaction which was first developed by Murray et al (Figure 1-14b).[9] After the synthesis of AuNPs using a non-functional ligand, most often alkanethiolate ligand,[47, 48, 49] new functional groups or molecules may be attached to the nanoparticles through the place exchange reaction of new incoming ligands with existing alkanethiolate ligands attached to nanoparticle surface. The place exchange reaction can be done in solution or solid phase. The amount of functional ligands versus the nonfunctional alkanethiolate ligands can be conveniently controlled by varying the ligand ratio and kinetics of the place exchange reaction. This approach offers a greater versatility compared to the first approach and is currently one of the most extensively employed method for AuNP surface modification and functionalization with small ligands.

A third approach involves coupling functional moieties directly with existing organic layer on nanoparticle surface via either covalent or noncovalent interactions (Figure 1-14c). Compared to the first and second approach, this approach offers the best flexibility. There is no need for the functional moieties to have gold affinity groups such as thiol, and it is not necessary for the functional moieties to be able to form a stable monolayer on nanoparticle surface. This is another widely used approach for surface functionalization of nanoparticles. Organic molecules[50], polymers[51, 52], biomolecules[53], inorganic materials[54] have all been used to modify AuNPs through this approach. As an example, biomacromolecules such as proteins[55], antibodies[56] and enzymes[57] may be attached to citrate-stabilized AuNPs through electrostatic interactions. For polymers, a "grafting from" approach is a slight variation of this third approach. Polymerization initiators are first immobilized on nanoparticle surface. By placing the nanoparticles in a monomer solution, polymerization leads to nanoparticles functionalized with a layer of polymer brush.[58, 59] If a layer of inorganic precursor moieties is first attached to the nanoparticle such as trimethoxysliane, a sol-gel reaction will lead to the formation of a silica layer on nanoparticle surface.[54]

These three methods provide complementary approaches for surface functionalization of AuNPs. However, none of these approaches can directly lead to a good control over the number and location of chemical functional groups distributed on the nanoparticle surface. This difficulty is caused by the presence of multiple reactive sites of nanoparticles. As an example, for a AuNP with a diameter of 2 nm, there are total about over 100 surface gold atoms,[60] with each gold atom possibly reacting with a thiol or amine functional ligand. When a place exchange reaction is conducted on the nanoparticles, it is inevitable that multiple functional ligands will be attached

simultaneously to the nanoparticle surface. Special techniques as developed in this dissertation are needed to control the chemical functionalization of nanoparticles.

1.5 : Applications of Gold Nanoparticles

AuNPs with unique optical, electric, and catalytic properties have generated much enthusiasm over the last two decades in optical sensing and imaging, nanoelectrics, self-assembly, molecular diagnostic and caner therapy, drug delivery, and catalysis.

1.5.1 : Biological Imaging Applications

AuNPs scatter light very strongly at the surface plasmon resonant frequency, making them very promising for optical imaging and labeling of biological systems.[61, 62, 63] Unlike conventional fluorescent dyes used in biomedical imaging, the scattered light generated by AuNPs is not prone to quenching and does not photobleach with repeated or continuous exposure to light. Also the scattered light color and intensity can be tuned by changing their size and shape. The intense scattered light from AuNP allows AuNPs to be visualized easily by naked eyes or using inexpensive instruments, such as dark-field optical microscopy. As a demonstration, El-Sayed and coworkers reported the use of AuNPs to image cancer cells by conjugating AuNPs with a cancer biomarker, epidermal growth factor receptor (EGFR), which is in significantly higher amounts in cancer cells as shown in Figure 1-15.[64] The cancer cell surface was defined by strong light scattering from AuNPs. Thus, cancer cells could be better distinguished from normal cells, in which case AuNPs were dispersed randomly in the cells due to nonspecific binding.

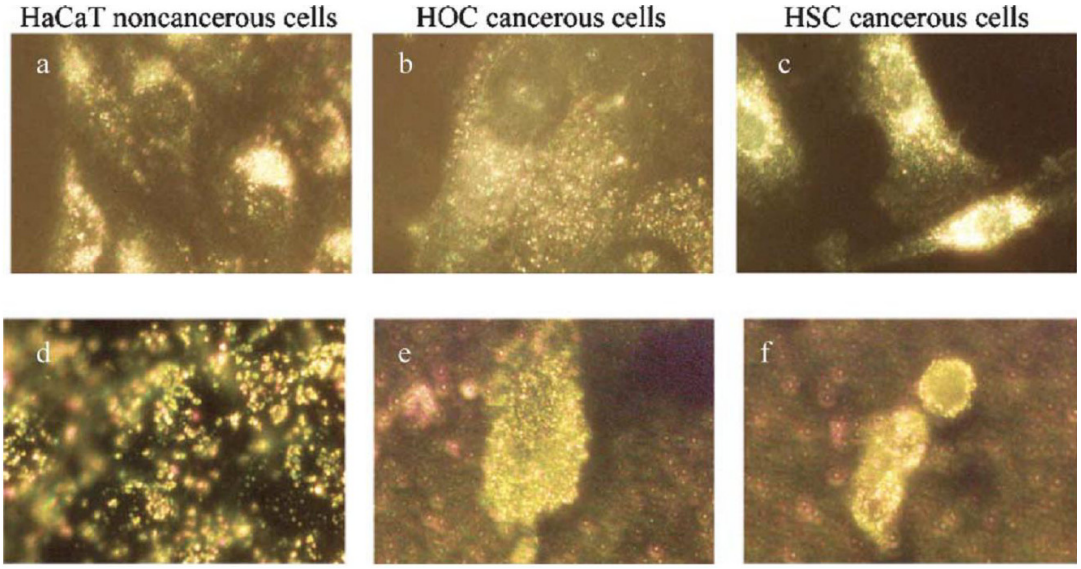

Figure 1-15: Light scattering of cell labeled with (a-c) AuNPs and (d-f) anti-EGFR coated AuNPs. the anti-EGFR coated nanoparticles bind specifically to the cancerous cells, while all AuNPs are non-specifically bound. (a&d) nonmalignant epithelial cell line HaCaT (human keratinocytes), (b&d) malignant epithelial cell lines HOC 313 clone 8 (human oral squamous cell carcinoma), (e&f) malignant epithelial cell lines HSC 3 (human oral squamous cell carcinoma).

So far, most of AuNP-related bioimaging studies were carried out in cell cultures. There have been a few examples of in vivo imaging using AuNPs as the contrast agent. Recently, Nie and coworkers reported an in vivo targeted imaging of cancer using Raman spectroscopy and AuNPs.[65] Malachite green molecules, an SERS reporter, were adsorbed on the surface of 60 nm citrate-stabilized AuNPs following by surface coverage with a polyethylene glycol (PEG) shell. An epidermal growth factor receptor (EGFR), ScFv antibody, was then tethered on the nanoparticle surface through covalent coupling. In the in vivo studies, the bioconjugated AuNPs were systemically administered in mice bearing human head and neck tumor. The nanoparticles were effectively localized at the tumor site and detected by specific SERS bands of malachite green as shown in Figure 1-16. This method has several advantages such as the absence of toxic

heavy metals, and non-invasive detection. However, clearance of such large sized nanoparticles (60 nm) from the body is a matter of concern. Retention of such large nanoparticles in the body may interfere with other imaging techniques at the later stages.

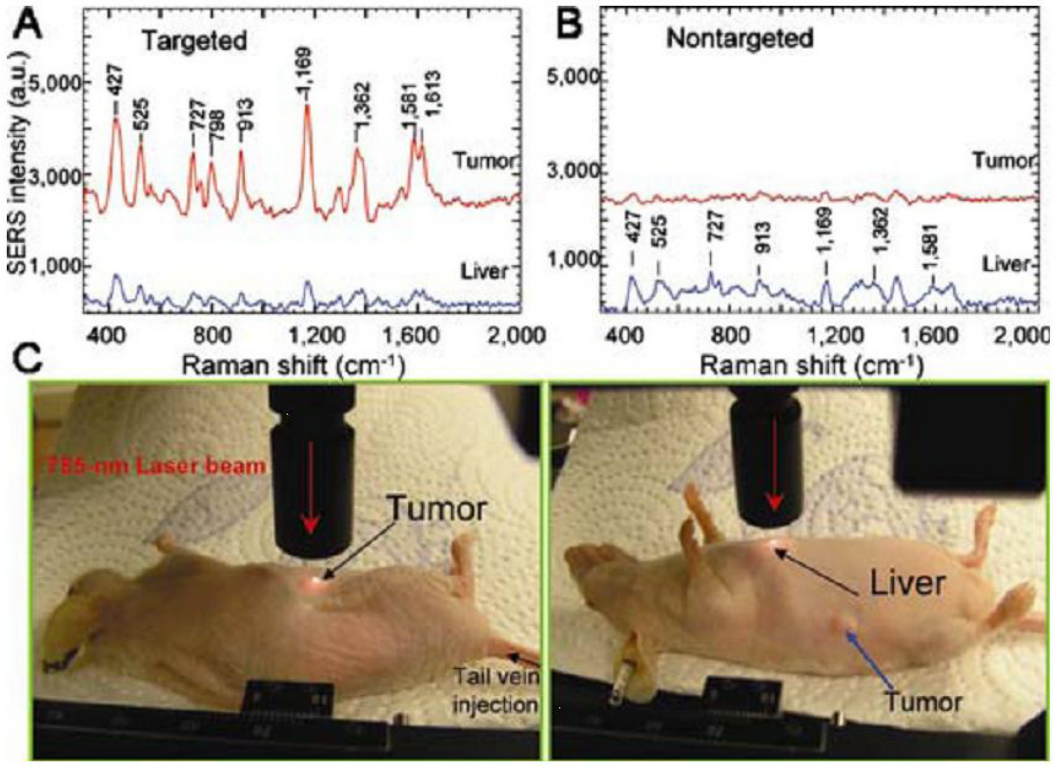

Figure 1-16: In vivo cancer targeting and surface-enhanced Raman detection by using ScFv antibody-conjugated AuNPs that recognize the tumor biomarker EGF receptor. (A&B): SERS spectra obtained from the tumor and the liver locations by using targeted and nontargeted nanoparticles. (C): photographs showing a laser beam focusing on the tumor site and on the anatomical location of the liver.

1.5.2 : Photothermal Therapy Applications

Photothermal therapy is a technique with promising potential for the treatment of cancer and other diseases. It includes two key components. The first one is the light source. Lasers with a spectral range of 650-900 nm for deep tissue penetration are often used in therapy. The second

component is the optical absorber that can transform the optical irradiation into heat to destory the cancer cells.

Due to the strong SPR absorption, AuNPs have demonstrated a great potential in photothermal therapy applications. It has been found that the absorbed photon energy is converted efficiently into heat on a picosecond time domain due to electron-phonon and phonon-phonon relaxation processes.[66] If the nanoparticles are incorporated or incubated with biomolecules, cells or tissues, this heat energy will cause a sharp increase on the local temperature around the nanoparticles and thus cause the damage of the surrounding biomolecules, cells, and tissues. As demonstrated in a work by Hirsch and coworkers,[67] human breast carcinoma cells incubated with gold nanoshells (55 nm silica core, 10 nm thick gold shell) exhibiting an near NIR SPR peak centered at 800 nm undergo photothermal damage on exposure to NIR laser light (wavelength: 820 nm; power: 4 W/cm^2; time:7 min). The in vitro studies of NIR therapy was further extended to in vivo study by injection of thiolated-PEG ligands coated gold nanoshells into mice tumors. Low doses of NIR laser light irradiation (820 nm, 4 W/cm^2, 4-6 min) resulted in a large temperature increase in the tumor regions (ΔT = 37.4 + 6.6°C as revealed by magnetic resonance temperature imaging), enough to induce irreversible tissue damage as shown in Figure 1-17. The laser dose was 10- to 25- fold less when using AuNPs as photon-energy absorbers than the traditional NIR-absorbing dyes. Control tissues exposed to NIR light without gold nanoshell injection showed a much lower temperature increase (ΔT < 10°C) of tumor tissue, and no obvious tissue damage was observed.

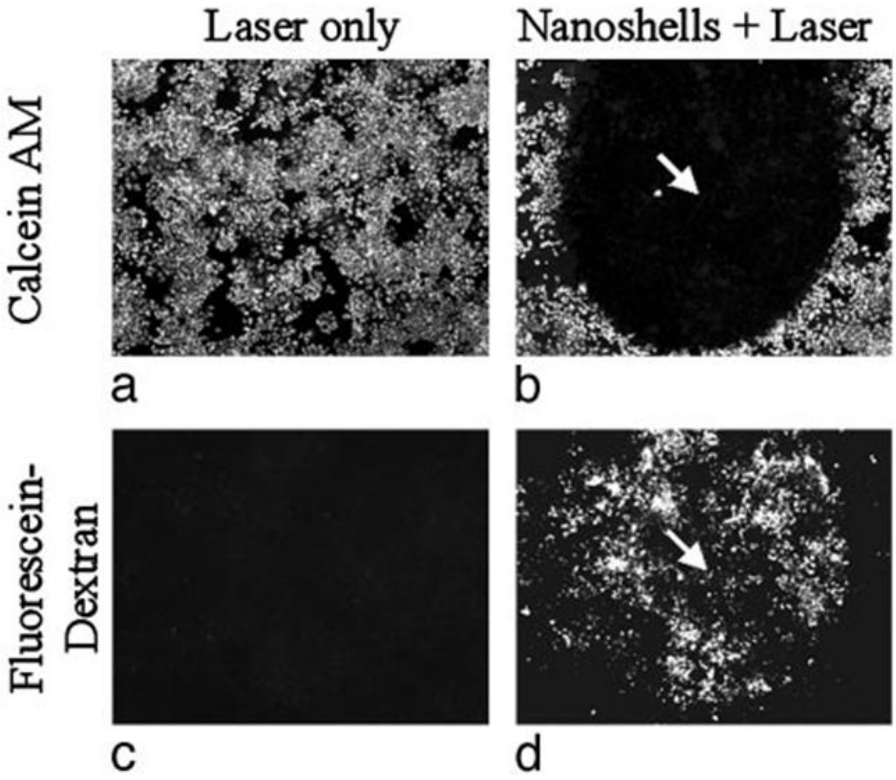

Figure 1-17: cells irradiated in the absence of nanoshells maintain both viability, as depicted by (a) calcein fluorescence, and membrane integrity, as indicated by (c) lack of intracellular fluorescein dextran uptake. Cells irradiated with nanoshells possess well-defined circular zones of cell death, as shown by (b) the calcein fluorescence study and (d) cellular uptake of fluorescein detran resulting from increased membrane permeability.

1.5.3 : Optical Sensing Applications

Another interesting property of the SPR of AuNPs is that its resonant frequency depends not only on the size and shapes of the particles, but also on the refractive index of the surrounding medium.[12] The change of the refractive index of surrounding medium results in a shift of the position and intensity of the SPR peak, which can be detected sensitively by different readout technique such as absorption spectroscopy (for colloidal nanoparticles in solution) and scattering spectroscopy (for nanoparticles deposited on a substrate).[68, 69] In order to sense

chemical/biological species, AuNPs were first deposited on the quartz substrates and then conjugated with recognition molecules, which specifically bind the target analyte as shown in Figure 1-18A.[70] These surface immobilized AuNPs have been recently used to detect the binding of antibody to human serum albumin with a detection limit of nanomolar range (Figure 1-18B). This approach has also been used to immobilize AuNPs on optical fibers, which have demonstrated the ability to detect streptavidin using biotin-avidin interaction and staphylococcal enterotoxin B using the antibody-antigen interaction at picomolar concentration.

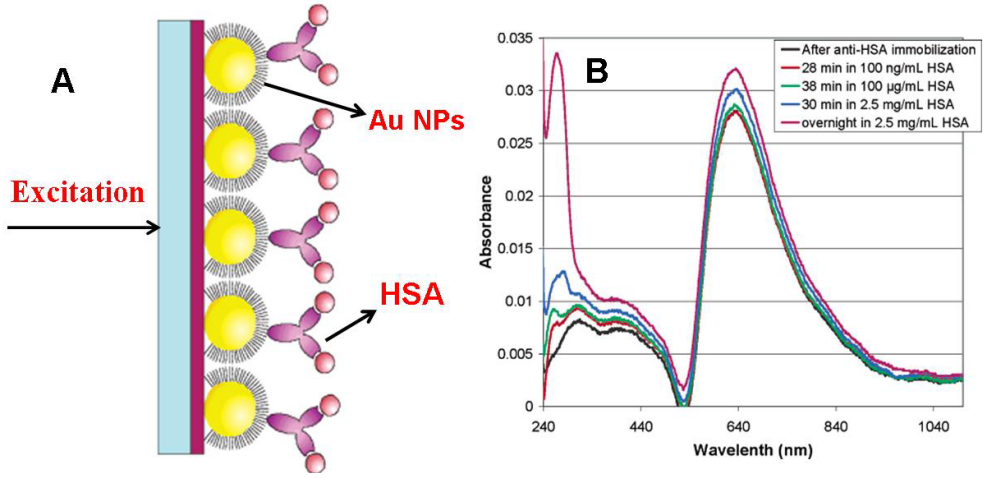

Figure 1-18: (A): A schematic representation of the optical sensing based on AuNPs deposited on a quartz substrate. (B): The absorbance spectra for Human serum albumin immobilized on AuNPs surface and the subsequent recognition of anti- Human serum albumin.

Another type of optical sensing using AuNPs takes advantage of the dependence of SPR band on the interparticle distances.[71, 72,] The SPR band starts to red shift upon nanoparticle aggregation due to the interparticle coupling effect. By using appropriately functional AuNPs that assemble in the presence of analytes, the assembly- induced SPR band shift and color change has enabled sensing of DNA, antibody, and disease biomarkers. In a work done by Mirkin and coworkers,[73, 74] two sets of citrate-stabilized AuNPs were functionalized with two

sets of DNA nucleotides probes. Upon the addition of a complementary target DNA nucleotide, the DNA hybridization between two DNA probes and target DNA induced nanoparticle aggregation and changed the color of the solution from red to blue. The aggregation-induced SPR change can be detected directly by UV-Vis absorption spectroscopy as shown in Figure 1-19.

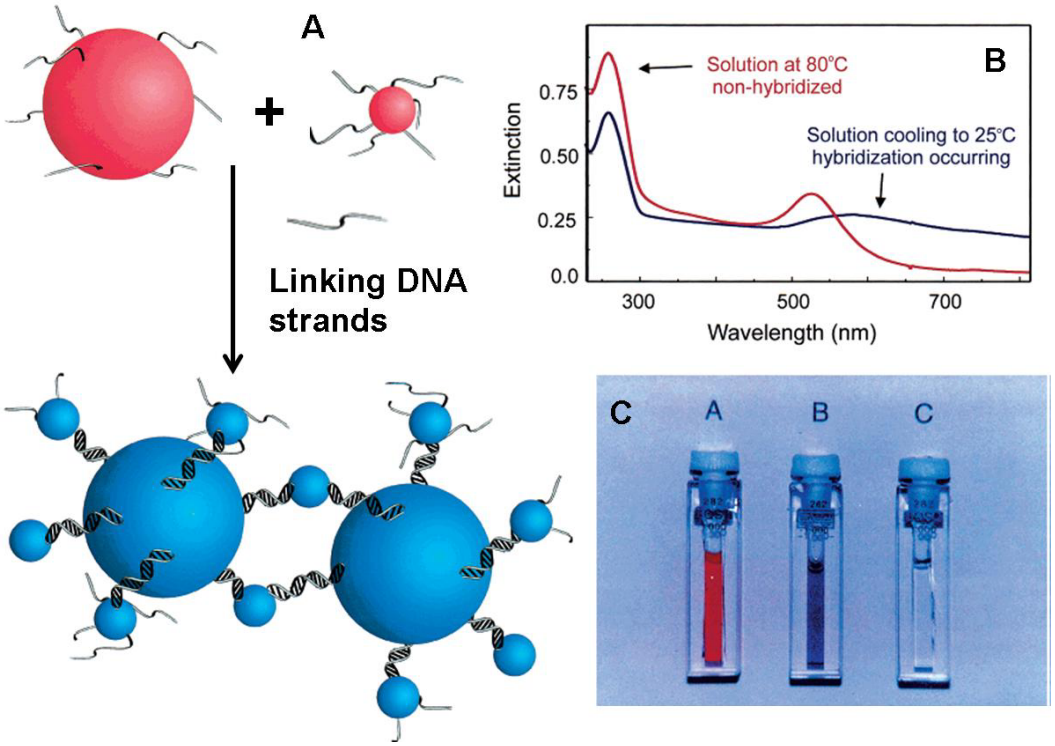

Figure 1-19: (A): A schematic illustration of calorimetric detection method using oligonucleotide-functional AuNP probes. (B): UV-Vis spectrum of oligonucleotide-modified 13 nm AuNPs before (red line) and after (blue line) DNA-induced assembly. (C): Photographs of 13-nm AuNPs solution before (cuvette A) and after (cuvette B) DNA-induced assembly. After extended periods of time nanoparticle precipitate forms and settles to the bottom of the cuvette (cuvette C).

1.5.4 : Catalysis Applications

Nanoscale gold catalysis has attracted increasing interest largely because of Haruta's discovery of unprecedented catalytic activity and specificity of gold at nanometer sizes.[78] Gold in the bulk is chemically inert and has often been regarded as a poor catalyst. However, when the dimension of gold is reduced below 10 nm, it turns out to be surprisingly active for many reactions.

In the heterogeneous catalysis, AuNPs have been utilized in the CO oxidation,[79] propylene epoxidation,[80] and NO_X reduction[81] etc. The activity of AuNPs depends on the size, surface property of the nanoparticles as well as the interaction of the particle with the supported substrates. For example, the high activity of gold catalysts for CO oxidation requires AuNPs to be less than 5 nm.[79] It was found that the decrease of mean surface coordination number and the ready mobility of surface gold atoms, particularly at corner and edges, could lead to a greater chemisorptivity and a stronger interaction with the support.

In the homogeneous catalysis, citrate-stabilized colloidal AuNPs have been shown to be active redox catalyst in the reaction between hexacyanoferrate (III) and thiosulfate ions.[82] It was found that the initial reaction rate is linearly dependent on the concentration of AuNPs. The reaction was surface controlled catalysis, instead of diffusion controlled. Some other reactions such as thiol oxidation under UV radiation were also catalyzed by AuNPs. For the colloidal nanoparticle catalysis, the stabilizer is most important. Weak stabilizer will not keep the nanoparticle stable during reactions while stronger stabilizer will cap the nanoparticle too strongly thus the surface activity is limited. Therefore, AuNPs prepared in different methods and capped by different ligands affect greatly the catalytic activity of the particles. [83]

1.6 : Summary of the Dissertation

The chemical synthesis of AuNPs with tunable size and shapes has been extensively studied over the last two decades. The as-synthesized AuNPs show narrow size distribution, tunable optical properties, a wide range of surface chemistry, and good biocompatibility. It provides an ideal building block in the bottom-up fabrication of more complex nanostructures and offers great potential applications in biosensing, molecular imaging, and cancer medicine. However, there are two remaining challenges in AuNP research. The first one is how to link and organize individual nanoparticles into an actual and functional device, which depends greatly on our ability to control the number and position of the functional groups on the particle surface as precisely as traditional organic synthesis. The second challenge is how to stabilize nanoparticle in the high ionic strength environment, especially under physicological conditions, which is crucial to the successful applications of AuNPs. Motivated by these two challenges, this dissertation is aimed at exploring the chemical synthesis and surface modification with the effort to control the number of functional groups on AuNP surface, and to increase its stability in high ionic strength environments.

In Chapter 2, we developed a solid phase exchange reaction to synthesize AuNPs with a single surface functional group. This approach is based on a “catch” and “release” mechanism to control the number of functional groups attached to the nanoparticle surface. Bifunctional thiol ligands with a carboxylic group were fist immobilized on a solid polymer support with a controlled density. The density was low enough that neighboring thiol ligands were far apart from each other. When the modified polymer support was incubated in a 2 nm AuNP solution, a one-to-one place exchange reaction took place between the polymer-bound thiol ligands and

AuNPs. After cleaving off from the solid support, nanoparticles with a single carboxylic group were obtained. Such monofunctional AuNPs can be treated and used as molecular nanobuilding blocks to form more complex nanomaterials with controllable structures. As an example, polylysine with side amino groups was then chosen to react with the monofunctional AuNPs. It was originally assumed that nanoparticles would covalently attach to polylysine like beads dangling around a string to form nanoparticle chains. In contrast, some very interesting "nanonecklace" structures with a diameter from 60 to 150 nm depending on the molecular weight of polylysine were observed. We believe that the nanonecklace structures were formed by covalent attachment of nanoparticles to the polylysine backbone followed by ring closure of the polylysine chain. We further found that the optical limiting properties of "nanonecklace" AuNP assemblies were enhanced significantly in comparison with the individual nanoparticles. Time-resolved spectroscopy studies showed that the enhancement of nonlinear optical properties was ascribed to the electromagnetic interactions between the nanoparticles in close proximity.

In Chapter 3, we used two biocompatible polymers, polyacrylic acid (PAA) and thiol-functionalized polyethylene glycol (PEG), to surface modify the citrate-stabilized AuNPs to increase their stability and biocompatibility. It was found that the polymers replaced the citrate molecules on the particle surface and prevent the agglomeration of nanoparticles in high ionic strength conditions. The resulting polymer-modified AuNPs with a diameter of 30 nm can be individually dispersed in the aqueous solution with a salt concentration up to 800 mM. In addition, we developed a solid-phase place exchange reaction for surface modification of CTAB-stabilized gold nanorods (GNRs) with bifunctional thiol ligands inside an ionic exchange resin. The GNRs were first loaded into the ionic exchange resin beads suspended in an aqueous

solution. Once trapped inside the resin beads, a bifunctional hydrophobic thiol ligand was added to the resin beads suspended in chloroform solution. The place exchange reaction between the GNRs and the thiol ligands took place inside the resin beads. It was found that the resulting nanorods diffused slowly to the chloroform solution with good stability against aggregation, which resulted from the successful replacement of the CTAB surfactants with the hydrophobic thiol ligand on the nanorod surface. The carboxylic acid group on the nanorods surface could be used to further conjugate with other chemicals, polymer and biomolecules through covalent or no-covalent chemistry.

In Chapter 4, we developed a one-step homogeneous AuNP-based assay to detect proteins and DNAs by monitoring the average particle size change using dynamic light scattering (DLS). To conduct the homogeneous assay, AuNPs were first functionalized with a pair of monocolonal antibody or a pair of DNA probes, which are able to form a sandwich structure upon the addition of analyte solution (protein or target DNA). Both antigen-antibody binding and DNA hybrization introduced the formation of nanoparticle dimer, trimer, and high order aggregates. By measuring the degree of nanoparticle aggregation from DLS analysis, we are able to quantitatively determine the concentration of protein and target DNA analytes in the sample solution. The detection limit of this assay can reach pM range or lower, which is three orders of magnitude greater than that of conventional absorption instruments. This research opened a new possibility in developing rapid and low-cost point-of-care diagnostic products for sensitive detection of protein biomarkers and specific DNA sequences.

In Chapter 5, we used AuNPs as a photothermal ablation agent to break the Amyloid peptide (Aβ) aggregates, which are found commonly in the brain of Alzheimer's disease patient.

AuNPs with a diameter of 5 nm were synthesized and protected with a short ethylene glycol ligand, following by surface functionalization with a single carboxylic acid group using the solid phase exchange method. The nanoparticles were then conjugated with Aβ peptides. The conjugates were mixed with Aβ peptide fragments in solution. The aggregated peptide was then exposed to a continuous laser irradiation. It was found that with AuNP/Aβ peptide conjugates present, the aggregates were destroyed by photothermal ablation. The ablation was selective to the site of irradiation and minimal damage was observed to the surrounding area as a result of thermal diffusion. This demonstrated the potential of AuNPs as a novel photothermal therapy agent for Alzheimer's disease.

1.7 : List of References

1: Faraday, M. *Phil.Trans. Royal. Soc. Lodon* **1857**, 147, 145.

2: Mie, G. *Ann. Phys*. **1908**, 25, 329.

3: Gan, R. *Ann. Phys*. **1915**, 47, 270.

4: Maxwell-Garnett, J. C. *Phil. Trans. Royal. Soc. Lodon* **1904**, 203, 385.

5: Turkevitch, J.; Stevenson, P. C.; Hiller, J. *Discuss. Faraday Soc*. **1951**, 11, 55.

6: Frenz, G. *Nature Phys. Sci*. **1973**, 241, 20.

7: Schmid, G.; Baumle, M.; Pfeil, R.; Bandermann, F.; Meyer, S.; Calis, G. H. M.; VanDer, J. W. A. *Chem. Ber*. **1981**, 114, 3634.

8: Brust, M.; Walker, M.; Bethell, D.; Schiffrin, D. J.; Whyman, R. *Chem. Comm*. **1994**, 801.

9: Hostetler, M. J.; Templeton, A. C.; Murray, R. W.; *Langmuir*, **1999**, 15, 3782.

10: Templeton, A. C.; Wuelfing, W. P.; Murray, R. W. *Acc. Chem. Res.* **2000**, 33, 27.

11: Schmid, G. Nanoparticles: *From Theory to Applications,* Wiley-VCH: New York, **2004**.

12: Link, S.; El-Sayed, M. A. *Annu. Rev. Phys. Chem.* **2003**, 54, 331.

13: Jain, P. K.; El-Sayed, I. H.; El-Sayed, M. A. *Nanotoday* **2007**, 2, 18.

14: Rotello, V. M. *Nanoparticles: Building Blocks for Nanotechnology*, Springer, New York, **2004**.

15: Du, H.; Fuh, R. C. A.; Li, J.; Corkan, A.; Lindsey, J. S. *Photochem. Photobiol*. **1998**, 68, 141.

16: Link, S.; El-Sayed, M. A. *J. Phys. Chem. B* **1999**, 103, 4212.

17: Thomas, K. G.; Barazzouk, S.; Ipe, B. I.; Joseph, S. T. S.; Kamat, P. V. *J. Phys. Chem. B* **2004**, 108, 13066.

18: Huang, X.; El-Sayed, I. H.; Qian, W.; El-Sayed, M. A. *J. Am. Chem. Soc*. **2006**, 128, 2115.

19: Jain, P. K.; Huang, X.; El-Sayed, I. H.; El-Sayed, M. A. *Acc. Chem. Res.* **2008**

20: Ghosh, S. K.; Pal, T. *Chem. Rev*. **2007**, 107, 4797.

21: Zhong, Z.; Patskovskyy, S.; Bouvrette, P.; Luong, J. H. T.; Gedanken, A. *J. Phys. Chem. B* **2004,** 108, 4046.

22: Yguerabide, J.; Yguerabide, E. E. *Anal, Biochem*. **1998**, 262, 137.

23: Freemantle, M. *Science* **2001**, 79, 10.

24: Jain, P. K.; Lee, K. S.; El-Sayed, I. H.; El-Sayed, M. A. *J. Phys. Chem. B* **2006**, 14, 7238.

25: Corbierre, M. K.; Beerens, J.; Lennox, R. B. *Chem. Mater.* **2005**, 17, 5774.

26: Daniel, M. C.; Astruc, D. *Chem. Rev.* **2004**, 104, 293.

27: Eustis, S.; El-Sayed, M. A. *Chem. Soc. Rev*. **2006**, 35, 209.

28: Weisbecker, C. S.; Merritt, M. V.; Whitesides, G. M. *Langmuir* **1996**, 12, 3944.

29: Noguez, C. *J. Phys. Chem. C* **2007**, 111, 3806.

30: Leff, D. V.; Brandt, L.; Heath, J. R. *Langmuir* **1996**, 12, 4723.

31: Liu, X.; Atawter, M.; Wang, J.; Dai, Q.; Zou, J.; Brennan, J. P.; Huo, Q. *J. Nanosci. Nanotech.* **2007**, 7, 3126.

32: He, P.; Urban, M. W. *Biomacromolecules* **2005**, 6, 1224.

33: Perez-Juste, J.; Pastoriza-Santos, I.; Liz-marzan, L. M.; Mulvaney, P. *Coord. Chem. Rev*. **2005**, 249, 1870.

34: Jana, N. R.; Gearheart, L.; Murphy, C. J. *J. Phys. Chem. B* **2001**, 105, 4065.

35: Nikoobakht, B.; El-Sayed, M. A. *Chem. Mater*. **2003**, 15, 1957.

36: Kim, F.; Song, J. H.; Yang, P. *J. Am. Chem. Soc*. **2002**, 124, 14316.

37: Zijlstra, P.; Bullen, C.; Chon, J. W. M.; Gu, M. *J. Phys. Chem. B* **2006**, 110, 19315.

38: Ying, Y.; Yang, S. S.; Lee, C. L.; Wang, C. R. C. *J. Phys. Chem. B* **1997**, 101, 6661.

39: Martin, C. R. *Science* **1994**, 266, 1961.

40: Oldenburg, S. J.; Averitt, R. D.; Westcott, S. L.; Halas, N. J. *Chem. Phys. Lett*. **1998**, 288, 243.

41: Chen, J.; Mclellan, J.; Siekkinen.; Xia, Y. *J. Am. Chem. Soc.* **2006**, 128, 14776.

42: Lu, X.; Yavuz, M. S.; Tuan, H. Y.; Korgel, B. A.; Xia, Y. *J. Am. Chem. Soc.* **2008**, 130, 8900.

43: Chen, S. H.; Kimura, K. *Langmuir* **1999**, 15, 1075.

44: Schaaf, T. G.; Knight, G.; Shafigullin, M. N.; Borkman, R. F.; Whetten, R. L. *J. Phys. Chem. B* **1998**, 102, 10643.

45: Cliffel, D. E.; Zamborini, F. P.; Cross, S. M.; Murray, R. W.; *Langmuir*, **2000**, 16, 9699

46: Zheng, M.; Davidson, F. Huang, X. *J. Am. Chem. Soc*. **2003**, 125, 7790.

47: Song, Y.; Huang, T.; Murray, R. W. *J. Am. Chem. Soc*. **2003**, 125, 11694.

48: Lin, S.; Tsai, Y.; Chen, C.; Lin, C.; Chen, C. *J. Phys. Chem. B* **2004**, 108, 2134.

49: Warner, M. G.; Reed, S. M.; Hutchison, J. E. *Chem. Mater*. **2000**, 12, 3316.

50: Chandrasekharan, N.; Kamat, P. V.; Hu, J.; Gones, G. *J. Phys. Chem. B* **2000**, 104, 11103.

51: Chen, Y.; Cho, J.; Young, A.; Taton, T. A. *Langmuir* **2007**, 23, 7491.

52: Sumerlin, B. S.; Lowe, A. B.; Stround, P. A.; Zhang, P.; Urban, M. W.; McCormick, C. L. *Langmuir* **2003**, 19, 5559.

53: Katz, E.; Willner, I. *Angew. Chem. Int. Ed*. **2004**, 43, 6042

54: Graf, C.; Vossen, D. L. J.; Imhof, A.; Blaaderen, A. *Langmuir* **2003**, 19, 6693.

55: Shenton, W.; Davis, S. A.; Mann, S. *Adv. Mater*. **1999**, 11, 449.

56: Thanh, N. T. K.; Rosenzweig, Z. *Anal. Chem*. **2002**, 74, 1624.

57: Gole, A.; Dash, C.; Soman, C.; Sainkar, S. R.; Rao, M.; Sastry, M. *Bioconjugate Chem*. **2001**, 12, 684.

58: Ohno, K.; Koh, K. M.; Tsuji, Y.; Fukuda, T. *Macromolecules* **2002**, 35, 8989.

59: Shan, J.; Chen, J.; Nuopponen, M.; Tenhu, H. *Langmuir*, **2004**, 20, 4671.

60: Shenhar, R.; Rotello, V. M. *Acc. Chem. Res*. **2003**, 36, 549.

61: Sokolov, K. *Cancer, Res*. **2003**, 63, 1999.

62: Yelin, D.; Oron, D.; Thiberge, S.; Moses, E.; Silberberg, Y. *Optics Express* **2003**, 11, 1385.

63: Raub, C. B.; Orwin, E. J.; Haskell, R. *J. Biomech. Eng*. **2003**, 125, 1.

64: El-Sayed, I. H. *Nano. Lett*. **2005**, 5, 829.

65: Qian, X.; Peng, X.; Ansari, D. Yin-Goen, Q.; Chen, G.; Shin, D.; Yang, L.; Yong, A. Wang. M.; Nie, S. *Nat. Biotechnol*. **2008**, 26, 83.

66: Burda, C.; Chen, X.; Narayanan, R.; El-Sayed, M. A. *Chem. Rev*. **2005**, 105, 1025.

67: Hirsh, L. R. *Proc. Nat. Acad. Sci*. **2003**, 100, 13549.

68: Yu, C.; Irudayaraj, J. *Anal, Chem*. **2007**, 79, 572.

69: Haes, A. J.; Hall, W. P.; Chang, L; Klein, W. L.; Van Duyne, R. P. *Nano. Lett*. **2004**, 4, 1029.

70: Frederix, F.; Friedt, J. M.; Choi, K. H.; Laureyn, W.; Campitelli, A.; Mondelaers, D.; Maes, G.; Borghs, G. *Anal. Chem*. **2003**, 75, 6894.

71: Mirkin, C. A. *Inorg. Chem.* **2000**, 39, 2258.

72: Rosi, N. L.; Mirkin, C. A. *Chem. Rev*. **2005**, 105, 1547.

73: Elghanian, R.; Storhoff, J. J.; Mucic, R. C.; Letsinger, R. L.; Mirkin, C. A. *Science* **1997**, 277, 1078.

74: Mirkin, C. A.; Lestinger, R. L.; Mucic, R. C.; Storhoff, J. J. *Nature* **1996**, 383, 607.

75: Nam, J.; Stoeva, S.; Mirkin, C. A. *J. Am. Chem. Soc.* **2004**, 126, 5932.

76: Taton, T. A.; Mirkin, C. A.; Letsinger, R. L. *Science* **2000**, 289, 1757.

77: Cao, Y. W.; Jin, R. C.; Mirkin, C. A. *Science* **2002**, 297, 1536.

78: Haruta, M. *Catal. Today,* **1997**, 36, 153.

79: Valden, M.; Lai, X.; Goodman, D. W. *Science* **1998**, 281, 1647.

80: Stangland, E. E.; Stavens, K. B.; Andres, R. P.; Delgass, W. N. *J. Catal.* **2000**, 191, 332.

81: Salama, T. M.; Ohnishi, R.; Ichikawa, M. *Chem. Comm*. **1997**, 105.

82: Freund, P. L.; Spiro, M. *J. Phys. Chem.* **1985**, 89, 1074.

83: Meyer, R.; Lemire, C.; Shaikhutdinov, S. K.; Freund, H. J. *Gold Bulletin* **2004**, 37,

CHAPTER 2 : SYNTHESIS AND NONLINEAR OPTICAL PROPERTY STUDIES OF MONOFUNCTIONAL GOLD NANOPARTICLES AND THEIR CONJUGATES WITH POLYMERS

2.1 : Introduction

In the bottom-up approach towards gold nanoparticle (AuNP)-based nanomaterials and nanodevices development, two important aspects need to be addressed clearly: the first one is the synthesis of nanoparticles itself and the second one is how to assemble the nanoparticles together into a material or a device with desired structures, properties, and functions.[1, 2, 3] In the last two or three decades, tremendous success has been achieved in the synthesis of many varieties of nanoparticles with tunable sizes and unique properties using chemical or physical methods.[4, 5] However, the assembling aspect remains as a significant bottleneck of current nanomaterial research.[6, 7] Because of their extremely small sizes, chemical approaches are often used as the most efficient methods for the organization of AuNPs into complex nanomaterials with predefined structures and properties. So far, the organization of AuNPs has been accomplished predominately using a supramolecular chemistry approach such as self- or template- induced assembly.[8, 9, 10, 11] AuNPs are often required to functionalize with chemical functional groups on their surface. Relying on these surface functional groups, nanoparticles can be assembled together into large network structures through noncovalent interactions with other molecules. By selective design of the functional groups and the template, different nanoparticle network structures such as one-dimensional wires, two-dimensional arrays, and three-dimensional crystals can be obtained.[12, 13, 14] Despite the tremendous success of self- and template- induced

assembly in the development of nanoparticles-based functional materials, the level of control on the nanomaterial structures and properties is still very limited. Covalent bond chemistry is an alternative approach which may be used for the assembly of AuNPs into higher order structures. If nanoparticles can be treated as "molecules", which means they possess a well-controlled chemical functionality, then chemical reactions may be used to organize nanoparticles together with precisely defined structures and properties. This approach is similar to the total chemical synthesis of complicated natural products from small molecular units. Due to a much better control on the chemical reactions versus self-assembly and increased stability of covalent bonds versus noncovalent bond interactions, one may expect that nanomaterials constructed from AuNPs using covalent bond chemistry will have improved controllability and stability on nanostructures and provide a wider range of applications.

In order to use covalent bond chemistry to control AuNP assembling into high order nanomaterials, one must first be able to control the chemical functionality of individual AuNPs. Unfortunately, it is extremely challenging to control the number of functional groups attached to each particle because of multiple reactive sites available on the particle surface. Given the example of AuNPs with a core diameter around 2 nm, there are in total about 100 surface gold atoms, and the total number of organic thiol ligands attached on the particles surface is also close to 100.[15] Synthetic methods that are commonly used for monolayer-protected AuNP synthesis including the Schiffrin reaction and place exchange reaction can only lead to a mixture of nanoparticles with either no functional groups or with multiple unknown numbers of functional groups.[16] Due to this lack of a precise control on the number of functional groups, any chemical

reactions conducted on such nanoparticles most likely will lead to the formation of large aggregates with unknown and irreproducible structures and properties.[6]

To overcome this challenge, one needs to be able to synthesize AuNPs with controlled number of chemical functional group attached to the surface. In this chapter, we have developed a solid phase place exchange reaction to synthesize 2 nm AuNPs with a single functional group attached on the surface.[17] We then demonstrated that the covalent bonding chemistry between monofunctional AuNPs and polymer templates can be used to build more complex nanomaterials with controllable structures. A "necklace"-like AuNP/polylysine assembly was obtained by covalently conjugating the monofunctional AuNPs to the side chain of the polylysine following a ring closure of the polymer chain.[18] These necklace AuNP assemblies exhibited enhanced optical limiting properties in comparison to individual AuNPs. Time resolved spectroscopy showed that the strong enhancement of nonlinear optical properties was a result from the electromagnetic interaction between nanoparticles in close proximity.[19] This property can find potential applications as optical power limiters to protect eyes and optical devices from high power laser damage.[20]

2.2 : Experimental Section

2.2.1 : Chemicals and Materials

All solvents and organic chemicals were purchased from Aldrich (Milwaukee, WI) or VWR (West Chester, PA) except the following: The gold salt $HAuCl_4$ was purchased from Strem Chemicals (Newburyport, MA). The acetyl-protected 6-mercaptohexanoic acid was prepared according to the reference.[21] 1% DVB crosslinked Wang Resin with a particle size

around 100~200 meshes and a hydroxyl group density of 0.75 mmol/mg was obtained from AnaSpec Inc (San Jose, CA). The sephadex gel used in gel permeation chromatographic purification of nanoparticles was a lipophilic dextrix gel LH-20 with a separation limit of 7,000 dalton molecular weight (Amersham Biosciences, Sweden). The gel was pre-incubated in dichloromethane/methanol mixed solvent (9/1, V/V) overnight prior use. Polylysine (molecular weight range: M_1: 4,000-15,000; M_2: 30,000-70,000; M_3:7,000-150,000) was purchased from Sigma-Aldrich. Polyamidoamine (PAMAM) dendrimer (Generation 5) was purchased from Aldrich. Poly (acrylic acid) (molecular weigh: 90, 000) was obtained from Polysciences Inc (Warrington, PA).

2.2.2 : Instrumentation and Characterization

UV-absorption spectra were recorded on an Agilent 8453 spectrometer. For Transmission Electron Microscopy (TEM) studies, approximately 5 μL of sample in the appropriate solvent was placed on a 300 mesh Formvar coated grid, and immediately wicked off using filter paper. After drying for about 5 minutes in the air, TEM images were obtained from a FEI Tecnai F30 high resolution TEM at 300 KeV.

The optical limiting measurements were carried out using 4.1 ns pulsed laser at 532 nm. A Q-switched Quantel Brilliant Nd:YAG laser was used as the light source. The repetition rate of the laser was set to 10 Hz. Energies of the incident laser beam were attenuated by a combination of a half-wave plate and a polarizing cube beam splitter. The beam was then split by a wedged beam splitter. One of the reflected beams was used to monitor the incident energy. The diameter of the transmitted beam was reduced to half of the original size by a telescope and was then focused by a 30-cm plano-convex lens (*f*/78.6) to the center of a 2-mm quartz cell. The radius of

the beam waist was approximately 69 μm. The incident energy and the output energy were monitored by two Molectron J4-09 pyroelectric joule meters. The transient difference absorption was investigated using an Edinburgh LP920 laser flash photolysis spectrometer. Samples were degassed with argon for 30 min and were excited by the third harmonic output (355 nm) of a Quantel Brilliant Nd: YAG laser. The laser pulse width (FWHM) was 4.1 ns, and the repetition rate was adjusted to 1 Hz.

Transient absorption measurements have been carried out using ultrafast pump-probe spectrometer detecting in the visible region. 1 mJ, 100 fs pulses at 800 nm with a repetition rate of 1 KHz were obtained from Nd: YLF (Empower) pumped Ti: Sapphire regenerative amplifer (Spitfire®, Spectra-Physics) with the input from Millennia pumped Ti: Sapphire oscillator (Spectraphysics, Tsunami). The output of laser beam was split to generate pump and probe beam pulses with a beam splitter (85% and 15%). The pump beam was produced by an optical parametric amplifier (OPA-800C). The pump beams used in the present investigation, i.e., 375, 430 nm, were obtained from the fourth harmonic of the signal and idler beams respectively. They were focused onto the sample cuvette. The probe beam was delayed with a computer controlled motion controller and then focused into a 2 mm sapphire plate to generate white light continuum. The white light was then overlapped with the pump beam in a 2 mm quartz cuvette containing the sample and the change in absorbance for the signal was collected by a CCD detector (Ocean optics). Data acquisition was controlled by the software from ultrafast systems. Typical power of probe beam was ~ 10 $\mu J/cm^2$ while the pump beam was around 1000 $\mu J/cm^2$. Magic angle polarization was obtained from the nonresonant fitting of the solvent response, which was around

120 fs. The sample was stirred by a rotating magnetic stirrer and little degradation of the sample was observed during the experiments.

2.2.3 : Synthesis

2.2.3.1 : Synthesis of Butanethiol-Protected AuNPs

1-Butanethiol monolayer-protected AuNPs with a diameter around 2 nm were synthesized according to the Brust-Schiffrin reaction. Briefly, tetraoctylammonium bromide (2.5 equivalents) was stirred vigorously in toluene in a 500 mL round bottom flask. $HAuCl_4$ (1 equivalent) in 100 mL of deionized water was added. As the $AuCl_4^-$ salt was transferred from the aqueous phase to the organic phase, the solution color was changed from a bright yellow to a red-brown. The organic phase was then separated, and the desired amount of 1-butanethiol was added to the above solution. The solution was stirred for 30 min followed by the addition of $NaBH_4$ (10 equivalents) in deionized water. The resulting solution quickly turned dark black. The solution continued to stir at room temperature for 3~4 hours. The black organic phase was isolated and the toluene solvent removed using a rotary evaporator. The crude product was washed with ethanol and acetone and finally dried in vacuum.

2.2.3.2 : Synthesis of Monofunctional AuNPs

The bifunctional 6-meraptohexanoic acid with the thiol group protected by an acetyl group was immobilized on Wang resin beads in 5:1 mole ratio (-OH: -SH) through ester bond formation. A typical loading recipe was as follows: to 2 gram Wang resin suspended in 15 mL dichloromethane, 6-mercaptohexnoic acid (0.3 mmol), 4-hydroxybenzotriazole (HOBT, 0.3 mmol), and 4-(dimethylamino) pyridine (DMAP, 0.06 mmol) dissolved in 450 μL of N,N'-

dimethylformamide were added followed by the addition of 1,2-diisopropylcarbodiimide (DIPCDI, 46 μL). The reaction suspension was gently shaken at room temperature for 5-8 hours. After washing with dimethylformamide, dichloromethane and methanol, the acetyl group was deprotected using 33% piperidine in dimethylformamide solution for 1 hour. Ellman's agent, 5,5'-dithio-bisnitrobenzoic acid, was used to monitor the deprotection reaction. If the acetyl groups were deprotected successfully, the Wang resin beads turned bright yellow after mixing with 5,5'-dithio-bisnitrobenzoic acid solution. After washing/drying cycle again, a 2 nm butanethiol monolayer-protected AuNP solution in mixed dichloromethane/hexane (1/2, V/V) was added to the beads. The place exchange reaction was allowed to proceed for 5 hours in 40° C water bath followed by 12 hours shaking at room temperature. During this time the beads turned into black and the nanoparticle solution became clear. The beads were then washed with dichloromethane until this solution became clear. The dark beads were dried and then suspended in 12 mL dichloromethane for 30 minutes. The AuNPs were then cleaved from the beads by adding 3 mL trifluoroacetic acid solution (TFA) (20% TFA in dichloromethane) and gentle shaking at room temperature for 3 hours. At the end of the reaction, solvent was evaporated off to leave behind the crude product. The crude product was then washed with petroleum ether for 5 times with occasional sonication followed by centrifugation. Each time the washing solution was tested for organic impurities by thin layer chromatography (TLC). The nanoparticles were then re-dissolved in a mixture solvent of dichloromethane/methanol (9/1), and purified by gel permeation chromatography using the same solvent. Two bands eluted out the gel column, and the first band was collected as the monofunctional AuNPs. The yield of the final product was around 0.8 mg per gram resin.

2.2.3.3 : Synthesis of "Necklace"-like AuNP/Polylysine Conjugates

Polylysine solution (0.5 mg/mL, 100 μL in methanol) was mixed with the as-synthesized monofunctional AuNPs (1.0 mg/mL, 400 μL in dichloromethane/methanol, 1/1) solution followed by the addition of 50 μL DIPCDI, The reaction mixture was shaken at room temperature for 2 hours and sonicated occasionally to increase the coupling efficiency. The solution was centrifuged and washed with methanol for several times to remove the unreacted polylysine and nanoparticles. The precipitates were then dissolved in a mixed dichloromethane/methanol solvent with a trace amount of TFA and then subjected to TEM analysis.

2.2.3.4 : Synthesis of AuNP/PAMAM 5 Dendrimer Conjugates

400 μL of monofunctional AuNPs solution (0.75 mg/mL) in a 1:1 dichloromethane/methanol solvent was mixed with 30 μL of 1% generation 5 PAMAM dendrimer solution in methanol. To the solution, 20 μL DIPCDI was added and the mixture solution was allowed to react at room temperature for 24 hours with gentle shaking. The coupling product was subjected to TEM analysis without further purification.

2.3 : Results and Discussions

2.3.1 : Synthesis of Monofunctional Gold Nanoparticles

The synthesis and study of AuNPs is a major area of current nanoparticle and nanomaterial research. However, controlling the number of functional groups on the nanoparticle surface remains a significant challenge. Hainfeld et al reported the first example of stoichiometrically controlled functionalization of a triphenylphosphine-protected gold

nanocluster Au_{11} with a single amino group.[22] In this method, a mixture of non-functionalized and functionalized triphenylphosphine ligands were used to control the number of functional groups attached to the particle surface. For example, in the case of Au_{11} nanocluster, it is known that there are total of 7 ligands bound on the nanocluster surface. If a ratio of 6:1 of non-functionalized and functionalized ligand was used during the nanocluster synthesis, one could expect that statistically, there will be six non-functionalized ligands and one-functionalized ligand attached to each nanoparticle surface. Although a mixture of products were obtained at the end of the reaction, monofunctional nanoclusters could be readily separated from non-functional and multifunctional particles using ion exchange chromatography technique. Later this method was further extended to the synthesis of monofunctional Au_{55} nanoclusters with a core diameter of 1.4 nm.[23] However, it is clear that this method is not suitable for larger particles, as the ratio of monofunctional nanoparticles in the mixture product will decrease substantially with increased core diameter of the nanoparticles. Other than the synthetic challenges, there are other problems associated with the triphenylphosphine-stabilized gold nanoclusters. For example the triphenylphosphine ligands are immobilized on the particle surface by electrostatic interactions. Such interactions can be easily destroyed at elevated temperature or high ionic strength of the media. This disadvantage significantly limits the applications of these gold nanoclusters.

Alivisatos et al reported the separation of 5 and 10 nm AuNPs with a discrete number of DNA strands using gel electrophoresis.[24] In this method, different amount of charged DNA was attached onto AuNP surface by adjusting the DNA/nanoparticles ratio, and then transferred to a gel column. Charged nanoparticles migrate in the porous gel under an electric field, and nanoparticle mobility depends mainly on their surface charge density. Therefore nanoparticles

with discrete number of DNA strands attached to the surface could be separated using gel electrophoresis. It was found that the length of DNA strands should be at least 30-base pair long in order to obtain an efficient separation in gel electrophoresis. In a similar approach, Lèvy et al recently reported the use of metal ion affinity chromatography to separate peptide-labeled 6 nm AuNPs according to the number of peptides on nanoparticles surface.[25] AuNP/peptide conjugates were prepared by mixing AuNPs with peptide in solution. The peptides used in this method compose two functional entities: the His-tag (a sequence of 6 histidines), which is able to complex with chelated transition metal ions such as nickel and the label. After removing the excess peptide by size exclusion chromatography, the mixture of labeled and unlabeled nanoparticles was transferred to metal ion affinity chromatography. The unlabelled nanoparticles were then washed off and the labeled nanoparticles were immobilized into the gel through metal ion/His-tag complex interaction. Finally the peptide labeled nanoparticles was eluted successively from the gel column depending on the number of peptides attached on nanoparticles surface using imidazole as a competitor. The metal ion affinity chromatography could differentiate AuNPs with discrete number of peptide molecules. However, for the separation-based approach, the biggest limit is that a relatively large molecule (DNA, polymer, or peptides) which can be either separated by gel electrophoresis or affinity chromatography needs to be attached to the nanoparticle surface. Essentially this is a separation method leading to nanoparticles modified with discrete number of molecules, instead of discrete number of functional groups for more general uses. Chromatographic and other separation methods are typically time-consuming and difficult to scale-up with reasonable cost.

Wilson et al reported the synthesis of a 15 nm AuNP with a single biotin functional group attached on the surface through polymer capping ligand with a single functional group.[26] In this approach, both pyridyldithio propionate and biotin were first functionalized onto the side chain of aminodextran polymer in the presence of an amide coupling agent, N-hydroxysuccinimide (NHS). One biotin molecule was able to attach to one aminodextran polymer chain by adjusting carefully the stoichiometric loading ratio of PDP and biotin onto the polymer. The monobiotin functionalized aminodextran polymers were then mixed with AuNPs. The polymer chain formed a protecting layer by wrapping around the nanoparticles surface through the multiple Au-S bonds. The length of the polymer was designed in such a way that one polymer chain was enough to protect one nanoparticle. As a result, a single biotin functional group was attached on each AuNP. The monobiotin functionalized AuNP was confirmed by a titration experiment based on the flocculation of unprotected AuNPs. As seen from the whole process, the monofunctionalization of nanoparticles is essentially achieved through the controlled functionalization of polymer capping ligands. However, a key challenge is to make sure the size of the particle and the size of the polymer chain are compatible and there will be only one polymer chain protecting one particle.

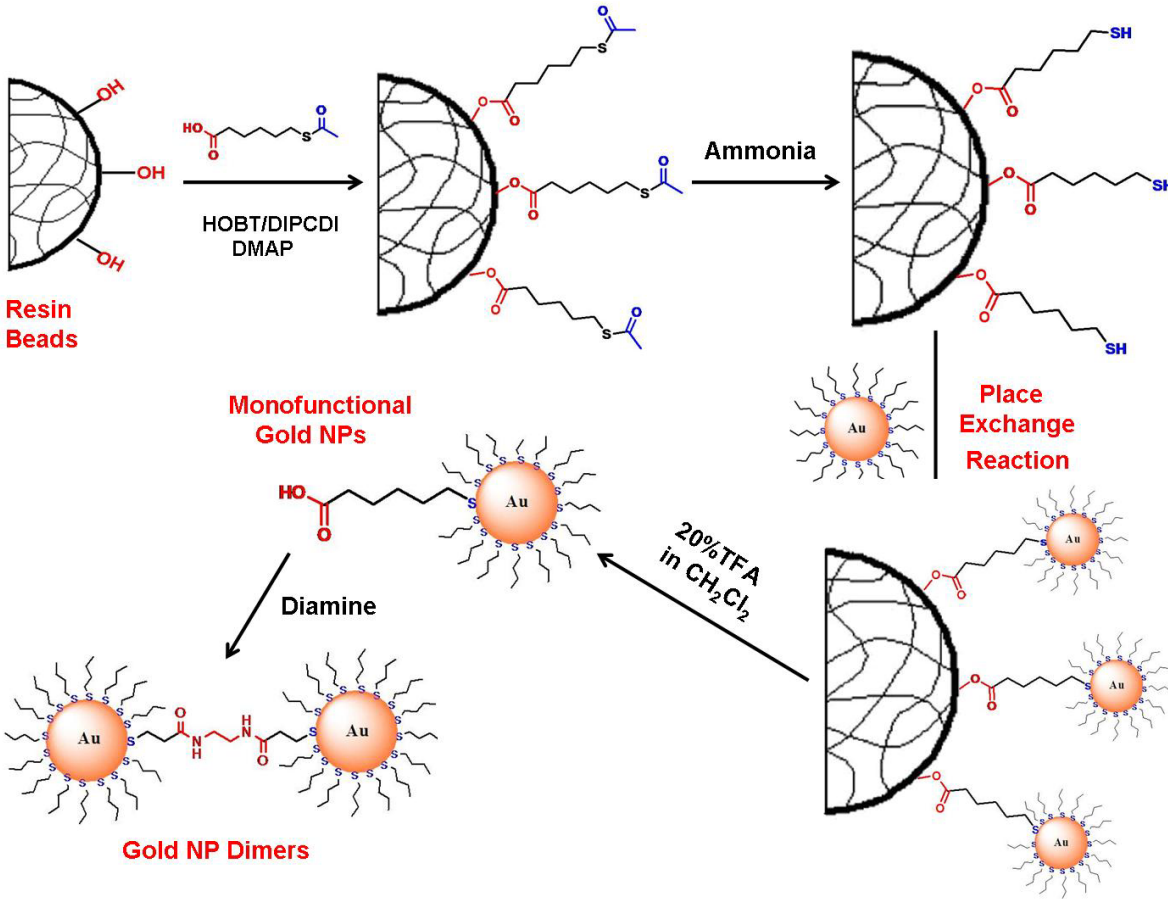

Figure 2-1: A schematic illustration of solid phase place exchange method to synthesize the monofunctional AuNPs

In contrast to the previous approaches that are all based on solution reactions and processes, we developed a solid phase place exchange reaction method for controlling the number of functional groups attached on AuNP surface.[17, 27] Solid phase synthesis is a synthetic strategy in which chemical reactions are conducted on a polymer support and has been extensively used in peptide synthesis and combinatorial chemistry. In our work, we used a solid phase synthesis technique to control the number of bifunctional thiol ligands attached to nanoparticles during the place exchange reaction as shown in Figure 2-1. The bifunctional alkanethiol ligands, 6-mercaptohexanoic acid, were first immobilized on a solid support such as

the crosslinked polystyrene Wang resin through an ester bond formation. The loading density of the thiol ligands on the solid support was controlled to be low enough to ensure that neighboring thiol ligands attached to the solid support were sufficiently far apart after swelling of the polymer beads with appropriate solvents. After deprotected the acetyl group using ammonia, the thiol groups were allowed to undergo a place exchange reaction with butanethiol-protected AuNPs, which were prepared according to the Shiffrin reaction with an average diameter of 2.2 nm. Since the bifunctional thiol ligands were sufficiently far apart from each other, statistically, one can expect that one thiol ligand would react with one nanoparticle. The effective place exchange reaction between resin-bound thiol ligands and AuNPs was clearly observed from the darkening of the resin beads after 12 hours of incubation of nanoparticles with resin beads in solution as shown in Figure 2-2. After washing off any unexchanged nanoparticles, the resin-bound nanoparticles were cleaved from the resin using 20% TFA in dichloromethane solution. After further washing and purification, AuNP with a single carboxylic group attached on the surface was obtained as the major product.

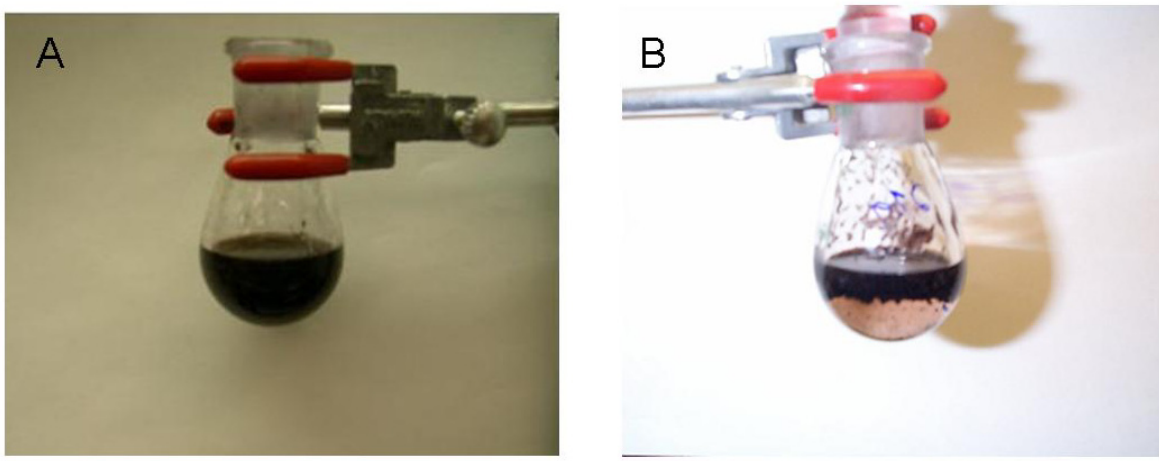

Figure 2-2: Photographs of the mixtures of resin polymer beads and AuNP solution. A: mixing after 10 mins; B: mixing after 24 hours.

TEM image in Figure 2-3A shows that the monofunctional AuNPs are randomly distributed on the carbon grid, and has the same average diameter of 2.2 nm as the original AuNPs, indicating that the structure of the nanoparticles remained intact during the solid phase exchange reaction.

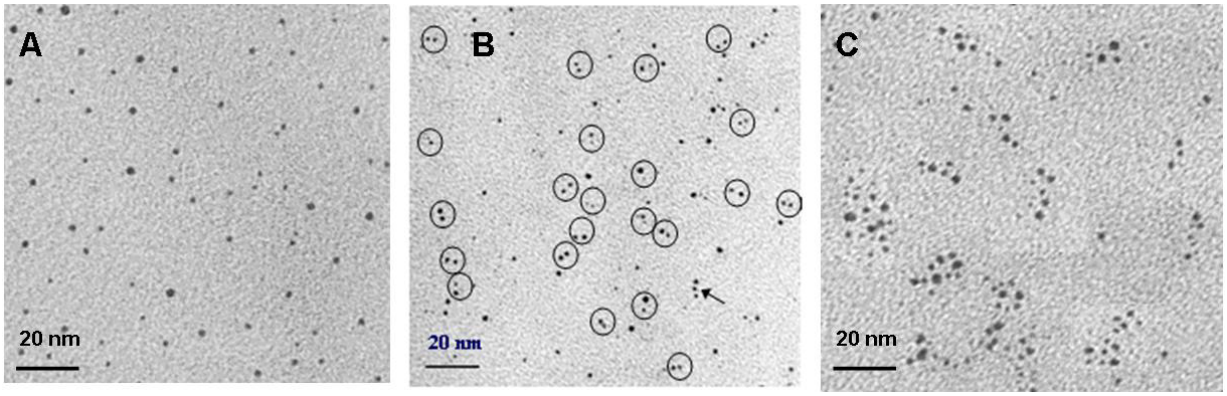

Figure 2-3: A: TEM image of the monofunctional AuNPs obtained from solid phase place exchange reaction; B: TEM image of diamine coupling product of monofunctional AuNPs; C: TEM image of diamine coupling product of multifunctional AuNPs obtained from solution phase place exchange reaction.

Although the synthesis of monofunctional AuNPs using the solid phase place exchange method is quite straightforward, the characterization has been a significant challenge for a long time. For an AuNP with a core diameter in the range of 2 nm, the nanoparticle is surface protected with around 100 thiol ligands.[16] Most spectroscopic techniques, including NMR, FT-IR, or X-ray photoelectron spectroscopy (XPS), are not sensitive enough to give quantitative analysis to distinguish one functional group among 100 nonfunctional ligands. To overcome this challenge, we introduced a simple diamine-coupling reaction to analyze the monofunctional AuNP product from the solid phase place exchange reaction. An aliphatic diamine was used to couple the monofunctional AuNPs together in the presence of an amide coupling agent, DIPCDI. It was assumed that if there was only one carboxylic group attached on the particle surface, it

was expected that statistically, nanoparticles dimers instead of trimers, tetramers and large aggregates should appear as the major component in the coupled product. Figure 2-3B shows the TEM image of monofunctional AuNP product after coupling with diamine. From this image, one can clearly see that a large number of particle pairs appear on the grids. The distance between the two nanoparticle cores in the pairs is around 1.0 – 1.5 nm, which corresponds to the length of the organic ligand bridge between the two nanoparticles. By counting the number of nanoparticle pairs that appeared in several TEM images of this sample, it is estimated that about 60% of the solid phase synthesis product is single functional group-modified nanoparticles. At a close look, a very small fraction (less than 5%) of nanoparticle trimers and aggregates are also present along with some individual nanoparticles. the individual nanoparticles are likely non-functionalized nanoparticles or nanoparticles not coupled with diamine. The nanoparticle trimers and large aggregates correspond to nanoparticles with more than one functional group.[28]

Theoretically, one could also prepare AuNPs with a single or other controlled numbers of functional groups through place exchange reaction in solution by using a very small ratio of the incoming thiol ligands versus the replaced thiol ligand. To compare the solid phase place exchange with the solution phase place exchange approaches, in a control experiment, we prepared two solution phase place exchange reaction products using 11-mercaptoundecanoic acid as the incoming ligand: one is less than 5% exchange ratio and another sample is aimed for 40% exchange ratio. The two solution place exchange reaction products were also coupled with diamine for TEM analysis. It was noticed that while the coupling product of 5% exchange ratio remained soluble in dichloromethane, the coupling product of 40% exchange ratio was insoluble in most organic solvents, indicating the formation of large aggregates due to the existence of

multiple functional groups on the particle surface. A TEM image of the 5% exchange product coupled by diamine shows the presence of large aggregates in Figure 2-3C. This result indicates that the solid phase place exchange modification is a much better approach in preparing nanoparticles with controlled functionality. In order to limit the number of functional groups attached to the nanoparticles surface during the solution place exchange reaction, the concentration of the incoming thiol ligands has to be very low. As a result, the chance for the incoming ligands to collide with nanoparticles is extremely low, which inevitably leads to a low efficiency of ligand exchange. In contrast, in solid phase synthesis, the incoming ligands are immobilized on the polymer bead and by increasing the reaction temperature nanoparticles have a much better chance for collision with the ligands to allow place exchange reaction to occur. More importantly, once the nanoparticle is attached to the beads, this nanoparticle will not react further with other ligands to allow attachment of multiple surface functional groups. It should be pointed out that the solid phase place exchange method is not only limited to AuNPs, but can be adapted to any other types of nanoparticles with appropriate solid phase reactions.

2.3.2 : Monofunctional Gold Nanoparticle/Polymer Conjugates

Self assembly process has been used extensively to organize individual nanoparticle building block together into bulk material and structures relying largely on the noncovalent chemical interactions between these functional particles and templates.[29, 30] However, these noncovalent interactions can be easily disrupted due to changes in pH, temperature, ionic strength or solvent polarity of the environment. This lack of stability and robusticity limits how the material may be processed into a final product, since a slight change in the chemical environment has a dramatic effect on the assembled nanomaterial architectures. As mentioned

above, if a nanoparticle has a well controlled chemical functionality and can be treated similarly as typical organic molecules, a simple chemical reaction may be used to covalently link nanoparticles together into well-defined and robust architectures, bulk materials, and devices.

To demonstrate this possibility, we conducted a simple chemical reaction between monocarboxyl functionalized AuNPs synthesized using the solid phase place exchange reaction and a polymer, polylysine, as shown in Figure 2-4.[18] Polylysine is a linear polypeptide and has one amino group in each lysine residue. Therefore, it was expected that the single carboxylic acid-functionalized nanoparticles would attach to the side chains of polylysine through the formation of amide bond like beads dangling around a string to form nanoparticle chains. polylysine with three different molecular weight range, namely, 4,000-15,000 (M_1), 30,000-70,000 (M_2), and 70,000-150,000 (M_3) Da were used in the coupling reactions with the monofunctional AuNPs.

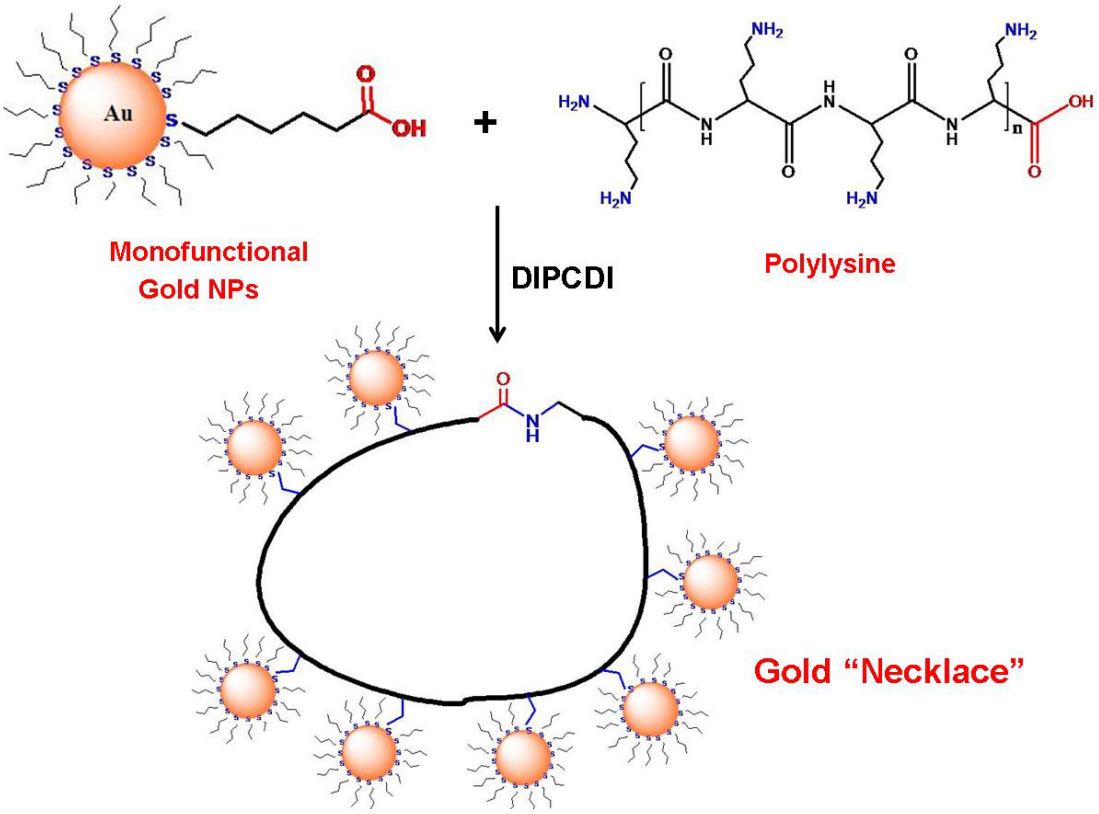

Figure 2-4: A "necklace"-like AuNP assemblies synthesized from amide coupling of the monofunctional AuNPs with polylysine template.

During the reaction, it was noticed that after the addition of the activation agent, DIPCDI, to the solution, nanoparticle precipitates were formed within about 30 min. The reaction mixture was then sonicated occasionally to obtain more complete coupling. After 2h of reaction time, the precipitates were separated from the solution and further purified by centrifugation and washing with methanol to remove the free polymers. The coupled product was found to be soluble in a mixed dichloromethane and methanol solution with the addition of a trace amount of trifluoroacetic acid (TFA ~ 1%).

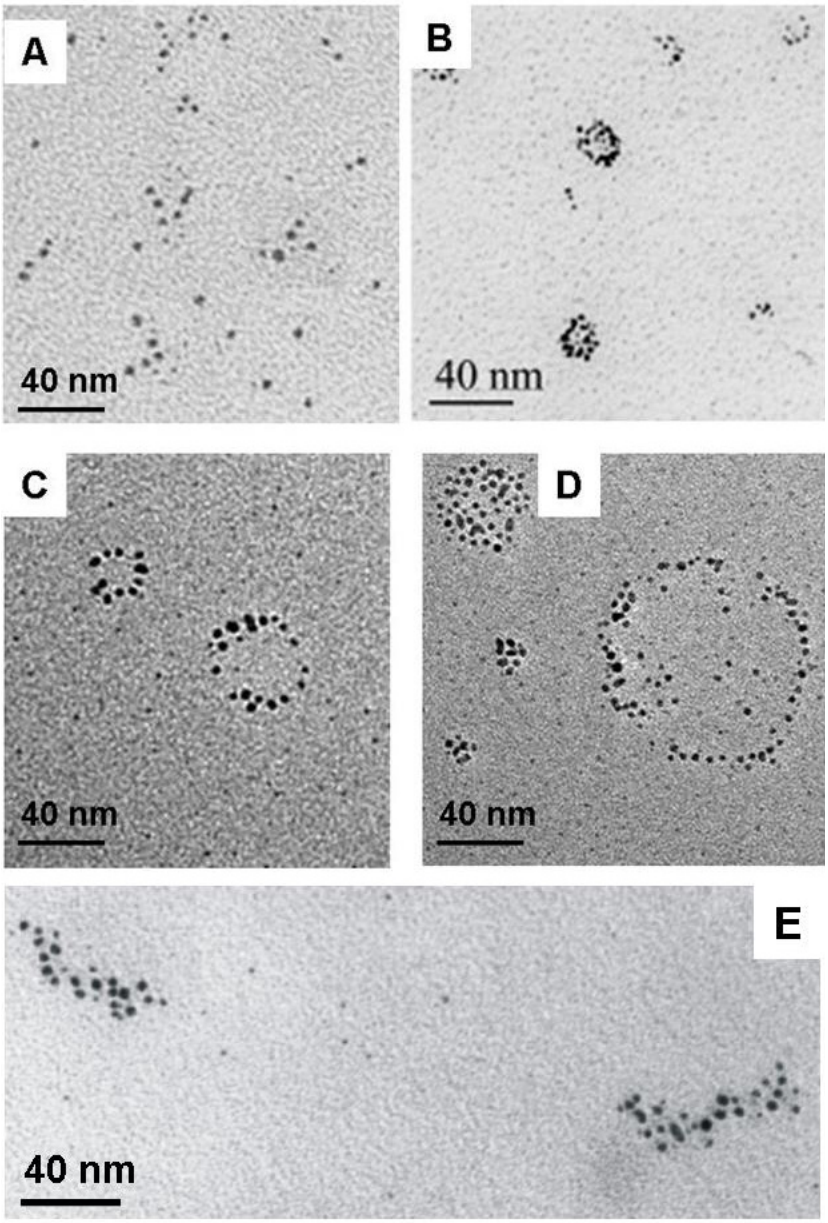

Figure 2-5: A: TEM image of the coupling product of monofunctional AuNPs with polylysine in solution. B-D: TEM images of the "necklace"-like AuNP/polylysine assemblies. E: TEM image of the coupling product of monofunctional AuNPs with carboxylic acid-blocked polylysine in solution.

Figure 2-5 shows the TEM images of both solution and precipitate portions of samples M_1 through M_3. The nanoparticles in solution appear mostly as individual nanoparticles along with a small aggregate as shown in Figure 2-5A. This suggests that the solution mainly contains unreacted nanoparticles or nanoparticle-polymer conjugates with a few particles attached. In contrast, some very interesting "nanonecklace" structures are observed from the precipitate portion samples as shown in Figure 2-5B-D. The average length of the necklace increases with increased molecular weight of polymer. We believe that the nanonecklace structures are formed by covalent attachment of nanoparticle to the polylysine backbone, followed by ring closure of the polylysine chain. Because each polylysine chain has a carboxylic acid end group, in the presence of amide coupling agent, the carboxylic end group could have reacted with the end or one of the side amino groups from the same polylysine to form a cyclic polypeptide.

To further confirm this result, we conducted the following control experiment. We used a Boc-protected ethylenediamine molecule to block the carboxyl group of the polylysine in the presence of DIPCDI. The block polylysine was then coupled with monocarboxylic AuNPs under the same reaction conditions. TEM analysis of this coupled product dissolved in the same solvent only show some linear nanoparticle chains and random aggregates as shown in Figure 2-5E. The control experimental results demonstrate reliably that the necklace structures observed from the monofunctional AuNP/polylysine coupling product are due to the ring closure of the polylysine chain by covalent bonding rather than by any self-assembling or solvent drying process. It is worth to point out that the monocarboxyl functionalized AuNPs are critical for the successful formation of the necklace structures. If a nanoparticle contains multiple functional groups, even

if it is only a limited few, the multiple functional groups will cause crosslinking of the polymers, leading to insoluble nanoparticle networks.

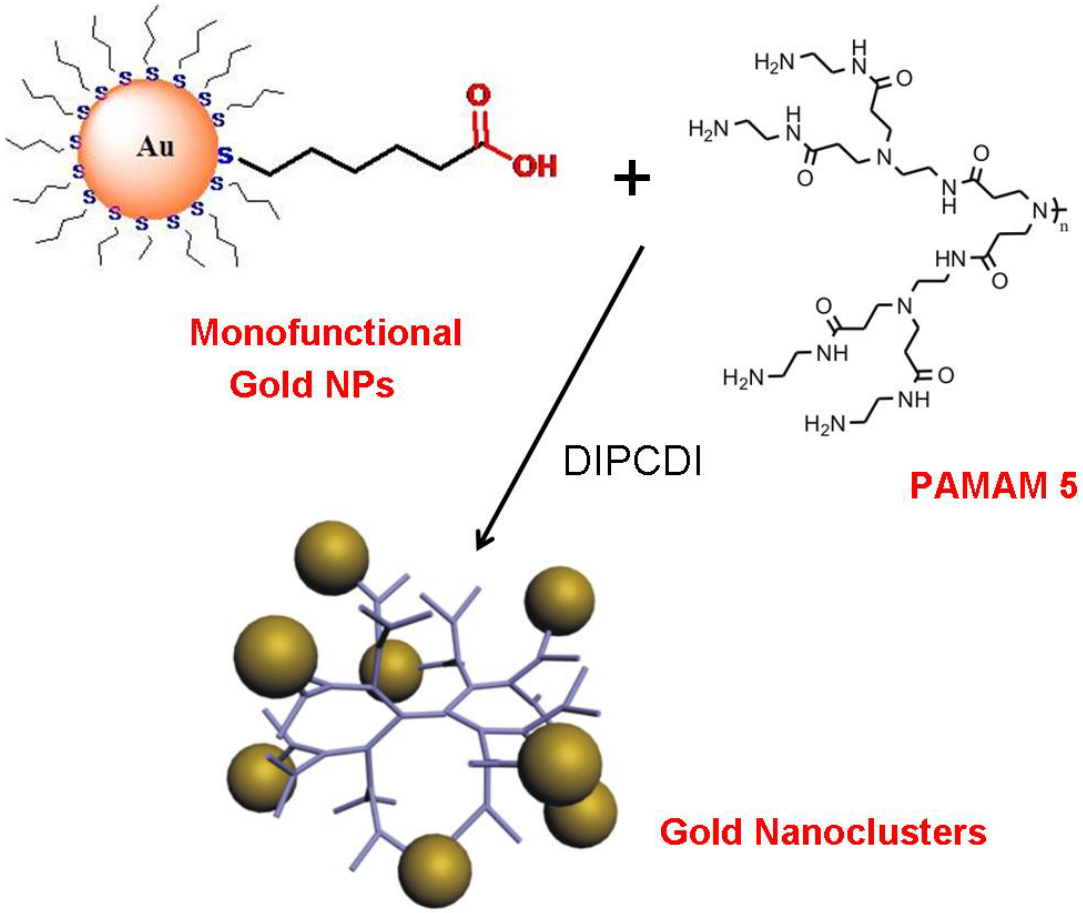

Figure 2-6: A schematic representation to prepare AuNP/dendrimer conjugate from the monofunctional AuNPs and a generation 5 PAMAM dendrimer.

The possibility of using simple chemical reactions to organize the monofunctional AuNPs into well-defined aggregate structures was further demonstrated by the synthesis of a AuNP/PAMAM dendrimer conjugate as shown in Figure 2-6.[31] A generation 5 PAMAM dendrimer has 128 amino groups on the periphery, which are available for reacting with single carboxylic functionalized AuNPs in the presence of DIPCDI activated agent. The coupling

reaction product was then subjected to TEM analysis without further purification. As you can see from Figure 2-7A, nanoparticles are not randomly distributed in the TEM grid, with many of them appearing as clusters ranging in size from 4-10 nanoparticles per cluster and with a diameter of 10-13 nm. This cluster size is reasonable, considering the diameter of the nanoparticles plus the nanoparticle protective monolayer and the estimated diameter of a generation of 5 PAMAM dendrimer. A statistical analysis of over 3600 nanoparticles from multiple samples is shown in Figure 2-7B. the histogram indicates that the majority of the nanoparticles (55%) appear in clusters with size ranging from 4-10 nanoparticles per cluster, and that much smaller percentages are in the form of single particles, dimers/trimers or larger aggregates. The single nanoparticle could be those which did not react with the dendrimer. The dimers/trimers may be dendrimers with two or three nanoparticles attached. The larger clusters (> 10 particles per cluster) may be resulted from the two or more nanoparticle/dendrimer conjugates in close proximity.

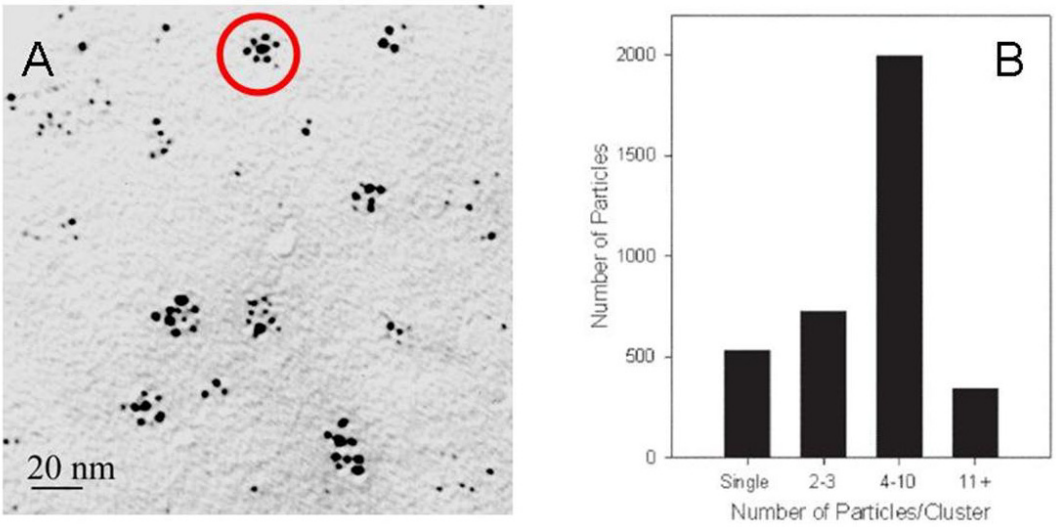

Figure 2-7: A: TEM image of the monofunctional AuNP/PAMAM dendrimer conjugates. B: Histogram showing the number of particles per cluster for various cluster sizes of nanoparticle/PAMAM dendrimer conjugates.

2.3.3 : Optical Limiting Properties of "necklace"-like Assemblies

It has been demonstrated that the properties of AuNPs are not only related to the size and characteristics of individual nanoparticles but also are affected profoundly by the interparticle distance and interaction.[32, 33] Following our synthesis of "necklace"-like AuNP/polylysine assemblies using covalent bonding chemistry, we investigated the nonlinear optical properties of the necklace AuNP assemblies for application in optical limiting. Nonlinear optical power limiters have generated much interest due to their potential applications for human eye and optical sensor protection from being damaged by high power lasers.[34] It is well known that for optical limiting application, the material is required to exhibit high linear transmittance at low incident energy, but low transmittance when the incident energy is above the limiting threshold.

Recently, the nonlinear optical properties of AuNPs in solution, solid state, and assemblies have been studied.[35, 36, 37] There are three major mechanisms that account for the optical limiting properties of AuNPs: nonlinear scattering, free-carrier absorption, and reverse saturable absorption. Mostafavi and co-workers reported that the optical limiting performance of AuNPs for nanosecond laser pulses exhibited size dependence when the particle size was smaller than 9 nm, no optical limiting was observed, and the optical limiting mechanism for large nanoparticles was ascribed to nonlinear scattering effect.[38] In contrast, Philip and co-workers discovered that AuNPs with an average core size of 3 nm exhibited optical limiting for both 7 ns and 35 ps laser pulses which was attributed to free-carrier absorption.[39, 40]

To verify the feasibility of the necklace AuNP/polylysine assemblies for optical limiting applications, the nonlinear transmission of the necklace AuNP/polylysine assemblies have been investigated using a 4.1 ns Q-switched Quantel Brilliant Nd:YAG pulse laser at 532 nm with a

repetition rate of 10 Hz. Energies of the incident laser beam were attenuated by a combination of a half-wave plate and a polarizable cubic beam splitter. The beam was then split by a wedged beam splitter. One of the reflected beams was used to monitor the incident energy. The diameter of the transmitted beam was reduced to the half of the original size by a telescope and was focused by a 30-cm plano-convex lens (*f*/78.6) to the center of a 2-mm sample cell. The radius of the beam waist was approximately 69 μm. The incident energy and the output energy were monitored by two Molectron J4-09 pyroelectric joule meters. As shown in Figure 2-8A, the necklace AuNP/polylysine assemblies exhibit significant optical limiting performance in comparison with the individual AuNP. The limiting threshold, defined as the incident fluence at which the transmittance begins to deviate from the linear transmission line, is as low as ~ 0.04 J/cm^2, and the transmission drops to 25% when the incident fluence is increased to ~ 1.7 J/cm^2, corresponding to a transmission decrease of 67% comparing to the linear transmission. In contrast, the limiting threshold for the individual AuNP is approximate 0.3 J/cm^2, the transmittance drops to 50% at incident fluence of 1.7 J/cm^2, a 33% of transmission decrease. It is obvious that the necklace AuNP assemblies exhibit much stronger optical limiting performance than that of the individual nanoparticles. Due to the fact that the polylysine backbone does not show any optical limiting effect, it is reasonable to believe that the enhanced optical limiting behavior for the necklace AuNP/polylysine assemblies is related to the interactions between AuNPs in proximity, probably a dipole-dipole interaction.[41] Such interactions can change the electron distribution on the particle surface, and thus, influence the polarizability of the nanoparticles which in turn gives rise to enhanced optical limiting properties.

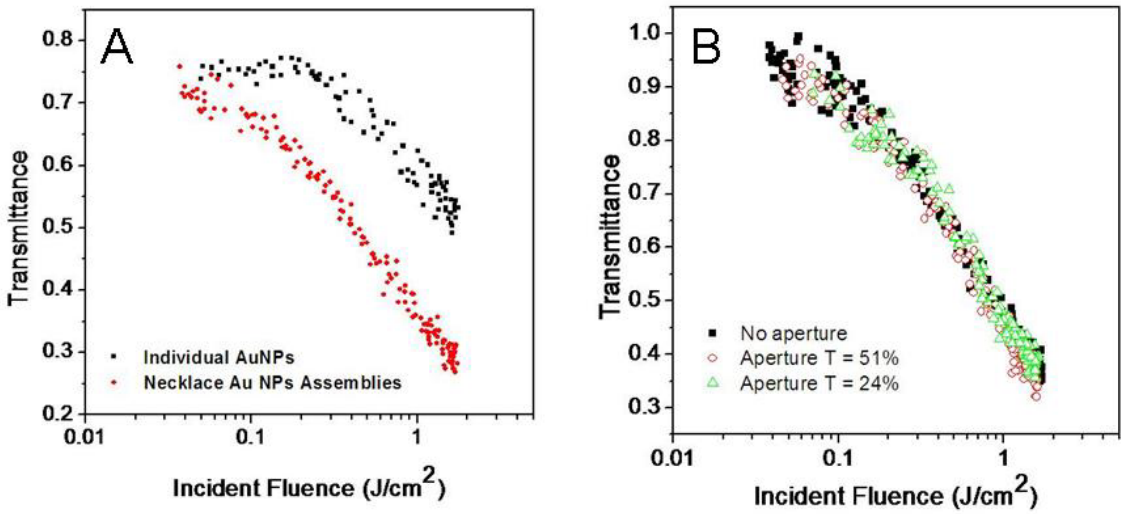

Figure 2-8: A: Optical limiting curves of the individual AuNP (black line) and the necklace AuNP assemblies in dichloromethane/methanol (1/1, with ~ 1% trifluoroacetic acid). B: Aperture size effect on the optical limiting curves of the necklace AuNP assemblies.

To determine whether the optical limiting of the necklace AuNP/polylysine assemblies also emanates from nonlinear scattering, an aperture was placed in front of the detector that monitors the output energy after the sample. The size of the aperture was adjusted to allow for different amount of light to pass through. It was expected that if the optical limiting was dominated by nonlinear scattering, the limiting performance would be influenced by the size of the aperture. A smaller aperture (*i.e.* a lower transmission ratio of the aperture) would give rise to a better optical limiting performance. However, the results shown in Figure 2-8B suggest that negligible scattering was found from the solution of the necklace AuNP/polylysine assemblies. This strongly suggests that nonlinear scattering is not the dominant contributor to the strong optical limiting of the AuNP/polylysine assemblies. Other nonlinear optical effects, such as nonlinear absorption, may contribute to the optical limiting.

Recently, the excited state absorption has been considered as the reason for the optical limiting of AuNPs smaller than 3 nm.[40] In the case of excited state absorption cross-section higher than that of the ground state absorption, the reverse saturable absorption will occur, which in turn will give rise to optical limiting effect. To determine whether the necklace AuNP/polylysine assemblies exhibit reverse saturable absorption, transient difference absorption spectrum was measured, from which the excited state absorption characteristics could be identified. It has been known that a positive absorption band in the transient difference absorption spectrum generally indicates a stronger excited state absorption than that of the ground state absorption in those wavelengths and reverse saturable absorption can occur at the corresponding wavelengths. As shown in Figure 2-9A, the transient absorption at 532 nm is positive indicating that reverse saturable absorption should occur around the SPR peak. Therefore, the optical limiting behavior of the necklace AuNP/polylysine assemblies at 532 nm can be attributed to reverse saturable absorption. To gain insight into the time scale of the optical limiting mechanism, the dependence of the optical limiting on laser repetition rate has been investigated. 1 Hz and 10 Hz repetition rates were employed in our study. As displayed in Figure 2-9B, no significant difference is observed at different laser repetition rate. This further suggests that the mechanism that governs the optical limiting is relatively fast, which cannot be thermally assisted nonlinear scattering that usually occurs at a millisecond time scale. Instead, excited state absorption induced reverse saturable absorption that occurs in a nanosecond time scale can be accountable for the independence of the optical limiting on the laser repetition rates.

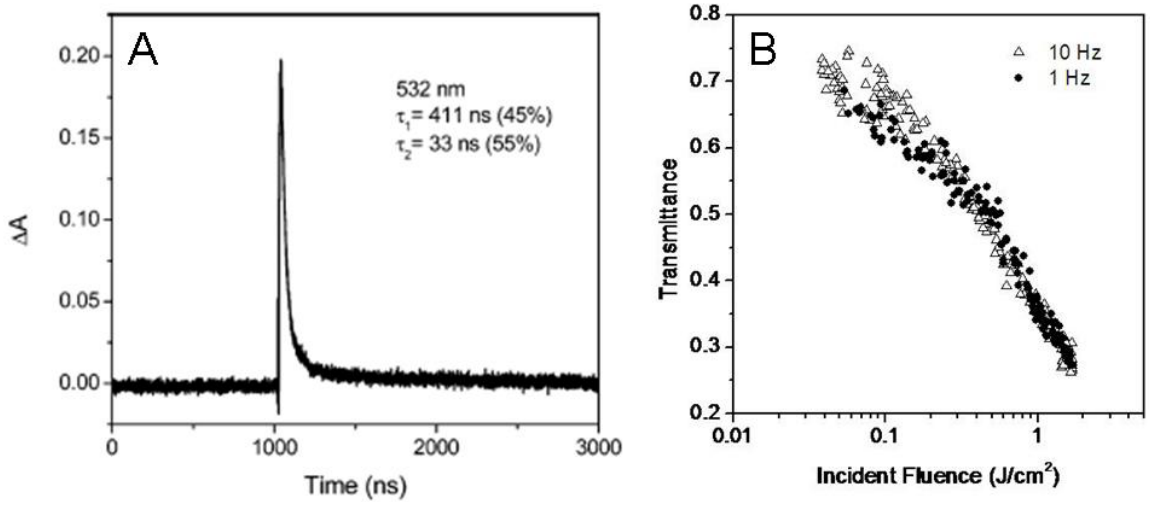

Figure 2-9: A: Transient absorption decay profile of the necklace AuNP/polylysine assemblies. B: Optical limiting curves of the necklace AuNP/polylysine assemblies at different laser repetition rates.

2.3.4 : Electron Dynamic Studies of "Necklace"-like Assemblies

In order to gain a better understanding of the optical limiting mechanism, the nature of the electromagnetic coupling interaction from the necklace AuNP/polylysine assemblies was further investigated with the aid of time-resolved spectroscopy.[20] Figure 2-10A shows the optical absorption spectra of individual AuNPs and necklace AuNP/polylysine assemblies dispersed in dichloromethane/methanol (2/1 v/v) solution. It can be observed that the individual nanoparticles show a typical SPR peak at 520 nm which is common to AuNPs of this size. Interestingly, the necklace AuNP/polylysine assemblies show a slightly red shifted and broader plasmon absorption compared with the individual AuNPs, suggesting electromagnetic interaction with close lying AuNPs. A similar absorption spectrum has been observed for DNA-induced AuNPs assemblies and has also been ascribed to static electromagnetic coupling between the neighboring nanoparticles.[42]

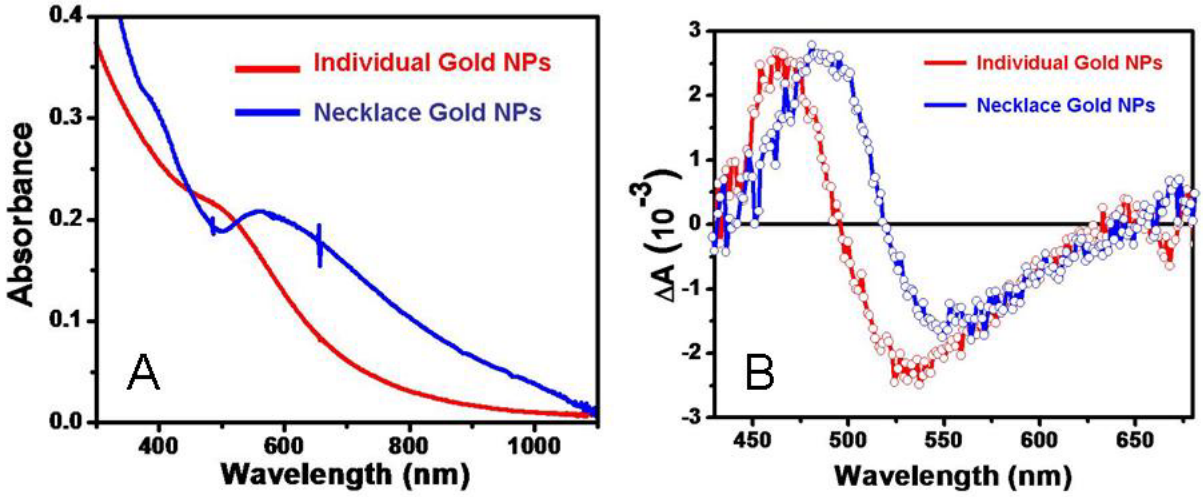

Figure 2-10: UV-Vis absorption spectra (A) and transient absorption spectra (B) of the individual AuNP and the necklace AuNP/polylysine assemblies.

To gain insight into the electron dynamics of necklace AuNP/polylysine assemblies, two color pump-probe measurements have been carried out and compared with that of individual nanoparticles.[43] Figure 2-10B is the transient absorption spectra of both individual AuNPs and necklace AuNP/polylysine assemblies at a time delay of 500 fs after excitation at 390 nm. Similar to what has been observed in the reported literature,[44] the individual AuNPs have shown a negative absorption in the region of 480 to 600 nm region with a maximum at 530 nm and a positive absorption with a maximum at 470 nm. Similar transient absorption features are observed for necklace AuNP/polylysine assemblies except that both the bleach maximum and absorption maximum are shifted to longer wavelengths to 550 nm and 500 nm respectively. This shift to longer wavelengths is consistent with the optical absorption maximum and most likely is arising from the electromagnetic interaction between the neighboring particles. It has been observed that, as the time delay is increased from 100 fs to 800 fs as shown in Figure 2-11 for the case of necklace AuNP/polylysine assemblies, both positive absorption and bleach have

increased in amplitude, while a decay of surface plasmon bleach is observed in case of the individual nanoparticles. the growth of surface plasmon bleach has been ascribed to the electron-electron scattering which occurs on a time scale of 100-500 fs.[45] after the electron-electron scattering, the hot electron relax with a decay profile which has two components related to electron-phonon and phonon-phonon relaxation processes.[46]

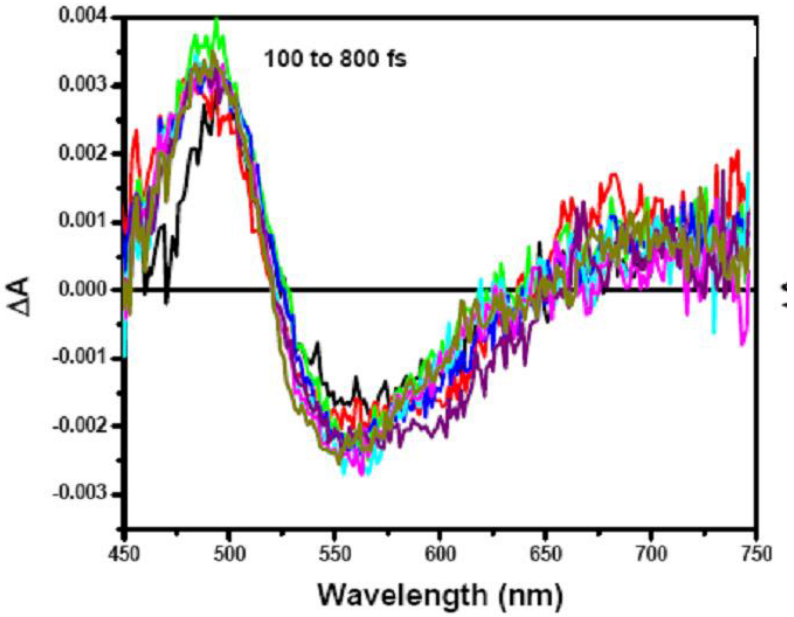

Figure 2-11: Transient absorption spectra of the necklace AuNP/polylysine assemblies with a time delay from 100 fs to 800 fs.

Figure 2-12 shows the kinetic traces of surface plasmon bleach at the peak wavelength of 550 nm for necklace AuNP/polylysine assemblies and 530 nm for individual AuNPs in the same solvent at the same pump power. The kinetics in the Figure 2-12A shows the electron-electron scattering, which is distinguishably slower for the necklace AuNP/polylysine assemblies than the individual AuNP. This could arise from the efficient dipolar coupling between the plasmons of two neighboring particles. In addition to this, the recovery of bleach as shown in Figure 2-12B is

also found to be substantially slower for the necklace AuNP/polylysine assemblies over the individual AuNPs. Pump-power dependent measurements on the necklace AuNP/polylysine assemblies and the individual AuNP have shown that the electron-electron scattering is weakly dependent on pump-power for the necklace AuNP/polylysine assemblies in Figure 2-13A while electron-phonon relaxation dynamics is very much dependent on pump-power as shown in Figure 2-13B.

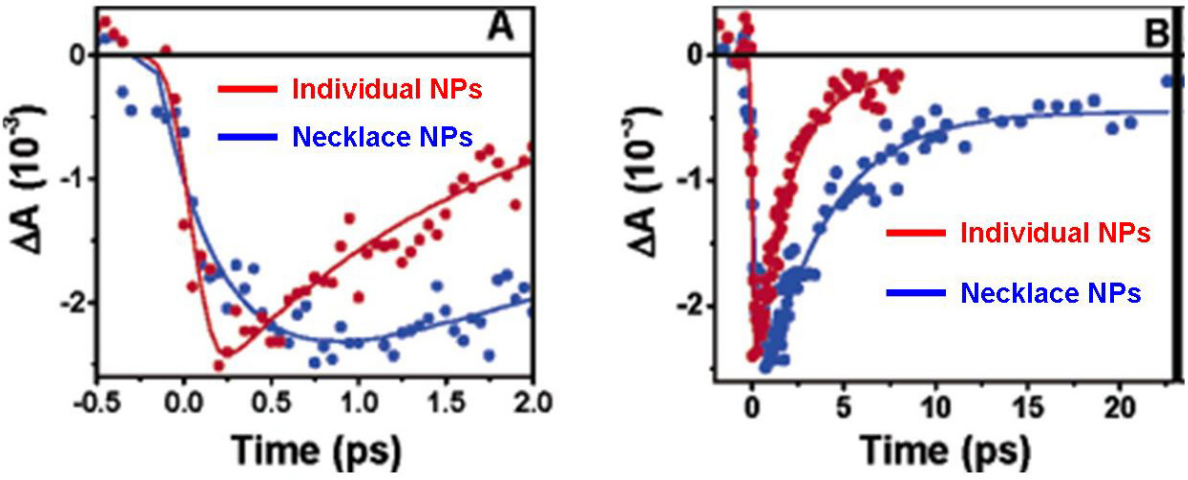

Figure 2-12: Kinetics decay profiles of AuNPs at the peak of their bleach wavelengths (A): in short time window; (B): long time window after excitation at 390 nm.

The zero pump-power electron-phonon relaxation time has been obtained by extrapolating the decay time constants obtained at different pump powers as shown in Figure 2-13B. A time constant of 2.01 ps has been observed for the necklace AuNP/polylysine assemblies, which is significantly longer than what has been obtained for the individual AuNPs with the same sizes (~ 0.7 ps).[46] The corresponding electron-phonon coupling obtained from the two-temperature model are 9.4 x 10^{15}, 2.4 x 10^{16} W m^{-3} K^{-1} for the necklace AuNP/polylysine assemblies and the individual AuNP respectively.

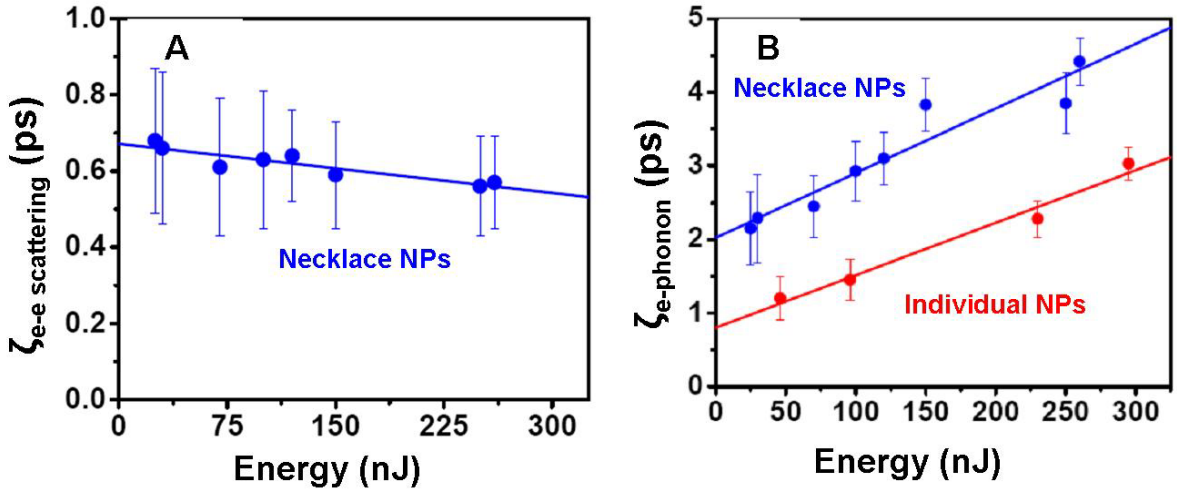

Figure 2-13: A: electron-electron scattering time plot of the necklace AuNP/polylysine assemblies. B: power dependent electron-phonon relaxation times of the individual AuNP and the necklace AuNP/polylysine assemblies.

The present results of slower electron-electron scattering (~580 fs) for the necklace AuNP/polylysine assemblies are quite unexpected. Normally, electron-electron scattering for AuNPs with pump-probe spectroscopy is on the order of ~ 250 fs for this particle size and increases with decreasing pump power.[47] We observed a weak pump power dependence on the electron-electron scattering time in Figure 2-13A. As the particle sizes of the isolated nanoparticles in the necklace assemblies and the individual AuNP are similar, the observed slower internal thermalization in necklace nanoparticle assemblies may be due to the specific arrangement of AuNPs in a necklace fashion. Indeed, the slower electron-phonon relaxation for the necklace AuNP/polylysine assemblies is not expected as well. El-Sayed and co-workers have observed slower electron-phonon relaxation in case of metal nanoparticles dispersed in $MgSO_4$ powder and has attributed it to low thermal conductivity of the surrounding environment.[48] In the present case, we compared the individual AuNP and necklace AuNP/polylysine assemblies consisting of the same size particles and in the same solvent environment. Thus, the effect of

particle size and surrounding environment were ruled out here. In the light above discussions of electron dynamics, the observed results can be explained on the basis of qualitative and phenomenological model of dipole-dipole interaction between the neighboring particles arranged in circular geometry. Upon photoexcitation of necklace AuNP/polylysine assemblies, the electron temperature increases and internal thermalization takes place not only between the electrons in the same nanoparticles but also with electrons in the neighboring particle due to strong electromagnetic coupling between neighboring particles. In this way, electron-electron scattering takes place in the necklace; thus it takes longer than it would normally for the isolated AuNPs. Since this involves an interparticles phenomenon, very weak pump-power dependence is observed in Figure 2-13A. The electron-phonon relaxation in the case of the present small AuNP is dominated by electron-surface scattering. As the electrons are entirely coupled in the spherical geometrical surface, the electron-phonon coupling is decreased due to the weaker electron-surface scattering. Hence one can observe slower electron-phonon relaxation. This is analogous to that of excitation dynamics in molecular J-aggregates, where the exciton-phonon relaxation is slower in aggregates.

2.4 : Conclusions

In summary, we have demonstrated that the covalent bonding chemistry between monocarboxyl functionalized AuNPs and polymer templates could be used for the preparation of AuNP/polymer conjugates with controlled nanostructures. More complex nanostructures can be prepared by tuning the functional groups, shapes, and molecular weight of the polymers. It was found that the AuNP/polylysine assemblies with necklace structure have significant optical

limiting properties for nanosecond laser pulses at 532 nm in comparison with the individual nanoparticle. The enhanced optical limiting properties are probably related to the dipole-dipole interaction between nanoparticles in close proximity, which may influence the distribution of electrons on the particle surface and enhance the polarizability of the AuNP/polylysine assemblies. Time-resolved spectroscopy further confirmed that there have strong electromagnetic coupling over the whole necklace of particle which have great potential applications in linear and nonlinear optics.

2.5 : List of References

1: Nalwa, H. S. *Nanostructured Materials and Nanotechnology:* Academic Press, London, **2002**.

2: Schmid, G. Nanoparticles: *From Theory to Applications,* Wiley-VCH: New York, **2004**.

3: Rotello, V. M. *Nanoparticles: Building Blocks for Nanotechnology*, Springer, New York, **2004**.

4: Burda, C.; Chen, X.; Narayanan, R.; El-Sayed, M. A. *Chem. Rev*. **2005**, 105, 1025.

5: Daniel, M. C.; Astruc, D. *Chem. Rev*. **2004**, 104, 293.

6: Shenhar, R.; Rotello, V. M. *Acc. Chem. Res*. **2003**, 36, 549.

7: Pileni, M. *Acc. Chem. Res*. **2007**, 40, 685.

8: Hamley, I. W. *Angew. Chem. Int. Ed*. **2003**, 42, 1692.

9: Cheng, J. Y.; Ross, C. A.; Smith, H. I.; Thomas, E. L. *Adv. Mater*. **2006**, 18, 2505.

10: Yin, Y.; Xia, Y. *J. Am. Chem. Soc*. **2003**, 125, 2048.

11: Feldheim, D. L.; Keating, C. D. *Chem. Soc. Rev*. **1998**, 27, 1.

12: Lin, S.; Li, M.; Dujardin, E.; Girard, C.; Mann, S. *Adv. Mater*. **2005**, 17, 2553.

13: Sharma, J.; Chhabra, R.; Liu, Y.; Ke, Y.; Yan, H. *Adv. Mater*. **2005**, 45, 730.

14: Boal, A. K.; Ilhan, F.; DeRouchey, J. E.; Thurn-Albrecht, T.; Russel, T. P.; Rotello, V. M. *Nature* **2000**, 404, 746.

15: Templeton, A. C.; Wuelfing, M. P.; Murray, R. W. *Acc. Chem. Res*. **2000**, 33, 27.

16: Hostetler, M. J.; Templeton, A. C.; Murray, R. W. *Langmuir*, **1999**, 15, 3782.

17: Worden, J. G.; Shaffer, A. W.; Huo, Q. *Chem. Comm*. **2004**, 518.

18: Dai, Q.; Worden, J. G.; Trullinger, J.; Huo, Q. *J. Am. Chem. Soc*. **2005**, 127, 8008.

19: Ramakrishna, G.; Dai, Q.; Zou, J.; Huo, Q.; Goodson, T. *J. Am. Chem. Soc*. **2007**, 129, 1848.

20: Sun, W.; Dai, Q.; Worden, J. G.; Huo, Q. *J. Phys. Chem. B* **2005**, 109, 20854.

21: Svedhem, S.; Hollander, C. A.; Shi, J.; Konradsson, P.; Liedberg, B.; Svensson, C. T. *J. Org. Chem*. **2001**, 66, 4494.

22: Hainfeld, J. F.; Furuya, F. R. *J. Histochem. Cytochem*. **1992**, 40, 177.

23: Hainfeld, J. F.; Powell, R. D. *J. Histochem. Cytochem*. **2000**, 48, 471.

24: Zanchet, D.; Micheel, C. M.; Parak, W. J.; Gerion, D.; Alivisatos, A. P. *Nano. Lett*. **2001**, 1, 32.

25: Levy, R.; Wang, Z.; Duchesne, L.; Doty, R. C.; Cooper, A.; Brust, M.; Fernig, D. G. *ChemBioChem*. **2006**, 7, 592.

26: Wilson, R.; Chen, Y.; Averard, J. *Chem. Comm*. **2004**, 1156.

27: Worden, J. G.; Dai, Q.; Shaffer, A. W.; Huo, Q. *Chem. Mater*. **2004**, 16, 3746.

28: Shaffer, A. W.; Worden, J. G.; Huo, Q. *Langmuir*, **2004**, 20, 8343.

29: Elena, V. S.; Dmitri, V. T.; Nicholas, A. K.; Stephen, B.; Christopher, B. M. *Nature* **2006**, 439, 55.

30: Drechsler, U.; Erdogan, B.; Rotello, V. M. *Chem. Eur. J*. **2004**, 10, 5570.

31: Worden, J. G.; Dai, Q.; Huo, Q. *Chem. Comm*. **2006**, 1536.

32: Link, S.; El-Sayed, M. A. *Annu. Rev. Phys. Chem.* **2003**, 54, 331.

33: Ghosh, S. K.; Pal. T. *Chem. Rev*. **2007**, 107, 4797.

34: Nalwa, H. S.; Miyate, S. *Nonlinear Optics of Organic Molecules and Polymer*, CRC press, **1997**.

35: Novak, J. P.; Brousseau, L. C.; Vance, F. W.; Johnson, R. C.; Lemon, B. I.; Hupp, J. T.; Feldheim, D. L. *J. Am. Chem. Soc*. **2000**, 122, 12029.

36: Francois, L.; Mostafavi, M.; Belloni, J.; Delouis, J. F.; Delaire, J.; Feneyrou, P. *J. Phys. Chem. B* **2000**, 104, 6133.

37: Zhan, C.; Li, D.; Zhang, D.; Xu, W.; Nie, Y.; Zhu, D. *Opt. Mater*. **2004**, 26, 11.

38: Francois, L.; Mostafavi, M.; Belloni, J.; Delaire, J. A. *Phys. Chem. Chem. Phys*. **2001**, 3, 4965.

39: Philips, R.; Kumar, G. R.; Sandhyarani, N.; Pradeep, T. *Phys. Rev. B* **2000**, 62, 13160.

40: Philips. R.; Mujumdar, S.; Ramachandran, H.; Kumar, G. R.; Sandhyarani, N.; Pradeep, T. *Mol. Cryst. Liq. Cryst. Sci. Technol. B: Nonlinear Opt*. **2001**, 27, 357.

41: Atay, T.; Song, J. H.; Nurmikko, A. V. *Nano. Lett*. **2004**, 4, 1627.

42: Lazarides, A. A.; Schatz, G. C. *J. Phys. Chem. B* **2000**, 104, 460.

43: Bhaskar, A.; Ramakrishna, G.; Lu, Z.; Tweig, R.; Hales, J. M.; Hagan, D.J.; Van Stryland, E.; Goodson, T. *J. Am. Chem. Soc*. **2006**, 128, 11840.

44: Hodak, J. H.; Martini, I.; Hartland, G. V. *J. Phys. Chem. B* **1998**, 102, 6958.

45: Link, S. A.; El-Sayed, M. A. *Annu. Rev. Phys. Chem*. **2003**, 54, 331.

46: Voisin, C.; Del Fatti, N.; Christofilos, D.; Vallee, F. *J. Phys. Chem. B* **2001**, 105, 2264.

47: Voisin, C.; Christofilos, D.; Del Fatti, N.; Vallee, F.; Prevel, B.; Cottancin, E.; Lerme,

J.; Pellanin, M.; Broyer, M. *Phys. Rev. Lett.* **2000**, 85, 2200,

48: Link, S.; Hathcock, D. J.; Nikoobakth, B.; El-Sayed, M. A. *Adv. Mater*. **2003**, 15, 393.

CHAPTER 3 : SYNTHESIS, SURFACE MODIFICATION AND STABILIZATION OF GOLD NANOPARTICLES

3.1 : Introduction

The successful application of AuNPs depends greatly on our ability to modify and functionalize the particle surface. This typically involves tailoring the surface properties of particles, often accomplished by coating or encapsulating them within a shell of a preferred material.[1, 2] The shell can serve to alter the charge, chemical functional groups, and reactivity of the surface, and also to enhance the colloidal stability and dispersibility of AuNPs under different conditions. In addition, optical, magnetic, and catalytic properties may be readily imparted to the dispersed nanoparticles depending on the nature of the surface coating.[3, 4]

The effective wet chemical synthesis methods for AuNPs with different shapes and size have been extensively studied over the last two decades. One of the most widely used methods to synthesize AuNPs is through reduction of tetrachloroaurate ions ($AuCl_4^-$) in aqueous medium using sodium citrate to generate nanoparticles with typical diameters ranging from 10 to 100 nm.[5] This method has good control over particle size distribution and provides AuNPs with good solubility in aqueous solution. The application of such nanoparticles in biological systems, however, will require much more than just water solubility. Unfortunately, the stability of citrate-protected AuNPs in high ionic strength environment remains as a significant challenge. The high salt concentration screens the electrostatic repulsion interaction between AuNPs and brings them close together to form particle aggregates.[6, 7] Therefore, the successful applications of AuNPs in

biological fluids require further chemical modification and functionalization to improve the colloidal stability in high ionic strength solution. It should be noted that the surface modification of AuNPs with a mean diameter below 10 nm are easily accessible by following the thiol place exchange method developed by Murray.[8, 9] However, this method is not suitable to modify AuNPs with a size above this limit. So far, only a few limited examples have been reported on the surface modification of citrate-stabilized AuNPs with size larger than 10 nm.[10, 11, 12, 13, 14, 15, 16] For example, block copolymers have recently been used to encapsulate citrate-stabilized AuNPs to improve the colloidal stability at harsh conditions. These cross-linked polymer shells provide a protective layer against chemical etching and improve the stability of nanoparticles in organic solvents, at elevated temperatures and in physiological buffer conditions.[17] Kimura et al reported the use of 2-mercaptosuccinic acid (MSA) to modify citrate-stabilized AuNPs in aqueous solution. This study used the MSA-modified AuNPs as a model system to compare theoretically calculated surface potentials to experimental results by taking advantage of the molecularly defined particle surface. However, less attention was paid to the characterization of the colloidal stability of the MSA-modified AuNPs under different conditions.[18]

In this work, we used two biocompatible polymers, polyacrylic acid (PAA) and polyethylene glycol (PEG) respectively, to surface coat the 30 nm citrate-stabilized AuNPs as a way to improve their colloidal stability in high ionic strength environments. These polymer-modified AuNPs can be individually stabilized in high salt solutions and in human serum matrices. The significantly improved stability of AuNPs is critical for their applications as optical probes for biomolecular detection and imaging.

Gold nanorods (GNRs) are another interesting class of gold nanoparticle materials. It shows two distinct SPR bands. The transverse SPR band around 520 nm is due to the excitation across the short dimension of the nanorods, and the longitudinal SPR band is a result of excitation along the long axis of the nanorods. The longitudinal SPR band of the nanorods can be tuned from visible to near infrared (NIR) wavelength range by changing the aspect ratio of nanorods.[19] Recently, the synthesis of GNRs with a controllable size and aspect ratio has been extensively carried out both chemically and electrochemically.[20, 21] One of the most commonly used methods is a template-induced growth of GNRs inside a rod-shaped liposome formed from cetyltrimethylammonium bromide (CTAB) surfactant.[22, 23] The as-synthesized nanorods are protected by a positively charged CTAB bilayer on the surface, which makes the nanorods soluble in aqueous solution.

However, the bilayer structure of GNRs has been a major problem that limits the further applications of GNRs. Similar to other biomembranes, the self-assembled bilayer structure is not robust and can be easily disrupted at high ionic strength or other conditions. This problem is detrimental to the biological application development of GNRs, which almost exclusively requires nanoparticles be used in high salt content buffer solutions. Also, it has been reported that CTAB cationic surfactant shows high cytotoxity at a concentration of ~ 0.1 M.[24] Thus, the replacement of CTAB surfactant with biocompatible stabilizing agents is essential for the biological applications of GNR probes. The surface chemistry modification of GNRs has remained as a significant challenge. So far, only a very limited few examples have been reported on the surface modification of GNRs, such as silica shell coating.[25, 26, 27, 28] In this chapter, we used a solid phase thiol place exchange reaction for surface modification of GNRs inside an

ionic exchange resin beads. 11-Mercaptoundecanoic acid (MUA) ligands were used to replace the CTAB surfactant on the GNR surface inside the pores of ionic exchange polymer beads. The MUA-modified GNRs show a good solubility and stability against particle aggregation in organic solvents, and may be used to build more sophisticated nanomaterials through self-assembly or covalent bond chemistry.

3.2 : Experimental Section

3.2.1 : Chemicals and Materials

All the chemicals and solvent except the few following were purchased from Sigm-Aldrich (Milwaukee, WI) and used without further purification. Hydrogen tetrachloroaurate (III) hydrate ($HAuCl_4$) was purchased from Strem Chemicals (Newburyport, MA). Tetraethylorthosilicate (TEOS) and silver nitrate were purchased from Fluka (Germany). Polyacrylic Acid (PAA) (MW: 90,000; 25 wt% aqueous solution) was obtained from Polysciences Inc (Warrington, PA). Thiol-functionalized Polyethylene Glycol (MW: 5000) was purchased from RAPP Polymere (Germany). Ultrapure water (18.3 MΩ cm^-) was used throughout the work. The human serum samples were obtained from Innovative Research Inc (Southfield, MI).

3.2.2 : Instrumentation and Characterization

UV-vis absorption spectroscopy was recorded on a Cary 300 Bio UV-Visible spectrophotometer from Varian Inc. (Palo Alto, CA). A PD2000DLS^{PLUS} Dynamic Light Scattering Detector and a PDDLS/CoolBatch 4oT Dynamic Light Scattering detector system from Precision Detectors Inc. (Bellingham, MA) were used for dynamic light scattering (DLS)

measurements of particle size. The DLS instrument was operated under the following conditions: temperature 20^{o}C, detector angle 90^{o}, incident laser wavelength 683 nm, laser power 100 mW. The DLS data without molecular normalization was processed using the Precision Deconvolve software. TEM images were obtained from a FEI Tecnai F30 high resolution TEM at 300 Kev. For sample preparation, the 400 mesh carbon/formvar coated copper grids were pretreated with a polylysine methanol solution and then dried at room temperature. 5 μL sample solution was then pipeted on the TEM grids followed by vacuum drying for 30 min. ^{1}H-NMR spectrum was obtained from a Varian 300 MHz instrument. XPS spectrum was recorded on a VG ESCALAB 220i XPS system, which was equipped with a monochromted Al K_{α} source ($h\gamma$ = 1486.6 Ev) and semi-spherical energy analyzer.

3.2.3 : Synthesis

3.2.3.1 : Synthesis of Citrate-stabilized AuNPs

All glassware was cleaned with 1% HCl diluted solution three times, rinsed with Nanopure H_2O, and then oven dried prior to use. Citrate-protected AuNPs with an average diameter of 30 nm were prepared by rapidly injecting a sodium citrate solution (1.5 mL, 38.8 mM) into a boiling aqueous solution of $HAuCl_4$ (100 mL, 0.35 mM) under vigorous stirring. After boiling for 20 min, heat was removed to allow the reaction solution to cool to room temperature. The average particle size was 30 nm determining from DLS measurement. The molar concentration of AuNPs was measured by UV-vis absorption spectroscopy using a molar extinction coefficient of 3.7×10^{-9} M^{-1} cm^{-1} according to a reported literature.[29]

3.2.3.2 : Synthesis of CTAB-stabilized Gold Nanorods (GNRs)

Gold nanorods (GNRs) with an aspect ratio of 4:1 were synthesized using a seed-mediated growth method in the presence of a shape-directing surfactant, cetyltrimethylammonium bromide (CTAB). AuNP seeds were first prepared by adding 250 μL of 4 mM $HAuCl_4 \cdot 3H_2O$ to 9 mL of 0.1 M CTAB surfactant, 600 μL of ice-cold 0.01 M $NaBH_4$ was then added with vigorous stirring for 2 hours at room temperature. To prepare the GNRs, 5 mL of 4 mM $HAuCl_4 \cdot 3H_2O$ and 400 μL of 8 mM silver nitrate were added to 35 mL of 0.1 M CTAB solution at 25°C. To this solution 280 μL of 0.0788 M ascorbic acid was then added, which changed the solution color from dark yellow to colorless. To initiate growth of GNRs, 100 μL of the seed solution was added to the growth solution, and the reaction was stirred at 28°C for 12 hours. The resulting solution of GNRs was centrifuged twice at 8500 rpm for 30 minutes to remove excessive CTAB surfactants. The GNRs were then re-dispersed in distilled water with an approximate concentration of 1 mg/mL.

3.2.3.3 : Silica Surface Coating of Citrate-stabilized AuNPs

1 mL of 40 g/L polyvinylpyrrolidone (PVP) (molecular weight: 10,000) aqueous solution was added dropwise to 10 mL of 0.07 mg/mL citrate-stabilized AuNP solution with vigorous stirring. The PVP was sonicated for 30 min to dissolve in the solution before mixing with AuNP solution. To ensure a complete adsorption of PVP on AuNP surface, the mixture was allowed to stir for 24 hours at room temperature in the dark. The solution was then centrifuged at 6000 rpm for 10 minutes and the supernatant was discarded. The AuNPs after PVP adsorption were redispersed in 10 mL of 5 vol% ammonia solution in ethanol (ammonia: 28 ~ 30 wt% NH_3 in water), and 20 μL TEOS solution (10 vol% in ethanol) was then added dropwise and the mixture

was stirred for 24 hours at room temperature. The reaction mixture was centrifuged and washed with methanol several times, and finally redispersed into the aqueous solution.

3.2.3.4 : Polymer Surface Modification of Citrate-stabilized AuNPs

Citrate-stabilized AuNPs with a diameter of 30 nm were prepared first by rapidly adding 1.5 mL of 38.8 mM sodium citrate solutions into a boiling aqueous $HAuCl_4$ solution (0.35 M, 100 mL) under vigorous stirring. After boiling for 15 min, 2 mL of 27 mg/mL polyacrylic acid (PAA) aqueous solution (pH: ~ 3) was added dropwise to the above solution. The mixture was allowed to boil for 4 hours. Heat was then removed to allow the reaction solution to cool down at room temperature. The reaction mixture was centrifuged and washed with deionized water twice, followed by washing with diluted NaOH solution (pH: 10) twice. The PAA-modified AuNPs were finally redispersed into deionized water.

Polyethylene glycol (PEG)-modified AuNPs were prepared via place exchange reaction between thiol bifunctional PEG and citrate-stabilized AuNPs. 2 mL of PEG aqueous solution (MW: 5,000; 2×10^{-3} M) was added dropwise to 10 mL of the citrate-stabilized AuNPs solution. The mixture was gently shaken at room temperature overnight. The solution was centrifuged at 8500 rpm for 15 mins, and the nanoparticles were redispersed into DI-water and passed through a 0.22 μm filter to remove any large insoluble aggregates.

3.2.3.5 : Surface Modification of GNRs inside an Ionic Exchange Polymer Resin

1.1 gram dry ionic exchange polymer beads (Amberlite IR-67; bead size: 16-50 mesh) were suspended in 2 mL distilled water, and then 2 mL of ~ 1 mg/mL GNRs aqueous solution was added. The suspension was gently shaken at room temperature for 3 hours. The effective

loading of GNRs inside the pore of ionic exchange polymer beads was clearly observed from the darkening of the polymer beads and the clearance of the aqueous solution color. After washing with water to remove the unloaded GNRs and drying with methanol, the GNRs-containning ionic exchange polymer beads were suspend in 5 mL of 11-mercaptoundecanoic acid (MUA) chloroform solution (1 mg/mL). The place exchange reaction between the MUA ligands and GNRs was allowed to proceed for 2 hour with gentle shaking at room temperature with occasional sonication. During this time, the chloroform solution turned into dark red gradually, which indicate the diffusion of GNRs into the chloroform phase. At the end of the reaction, the chloroform solution was collected. The crude product was then washed with methanol and chloroform for 4~5 times with occasional sonication followed by centrifugation. The GNRs were then redissolved in chloroform. The yield of the purified GNRs product was around 0.5 mg per gram resin.

3.3 : Results and Discussions

3.3.1 : Silica Modification of Citrate-stabilized Gold Nanoparticles

Silica coating has become a very popular and convenient approach for surface modification of AuNPs. First, the silica layer offers the possibility to produce nanocomposite with tailored physical properties. Second, the silica shell formed on the particle surface can enhance the colloidal stability and make it possible to be dispersed in a wide range of solvents from very polar to apolar. Third, due to the existence of abundant silanol groups on the silica layer, silica-coated AuNPs can be easily activated to provide the surface with various functional

groups. Finally, the silica shell layer on AuNP surface is a relatively inert coating that provides a good biocompatibility and protects the AuNPs from potential degradation.

The most widely used silica coating method is to add the silica precursor, TEOS, to solutions of seed particles in an ethanol/ammonia mixture to grow a smooth silica shell on the seed particle surface.[30] Therefore, a good affinity between the particle and the silica precursor is extremely important to the successful growth of a uniform silica layer on the particle surface. However, it is well known that gold metal has very little affinity for silica because unlike most other metals, it does not form a passivating oxide film in solution. Furthermore, there are usually adsorbed carboxylic acids or other organic anions present on the surface to stabilize the particles against aggregation. These stabilizers also prevent the adsorption of the TEOS precursor onto particle surface. To overcome this challenge, Mulvaney and co-workers reported the use of a silane coupling agent, 3-aminopropyltrimethoxysilane, to improve the affinity of the citrate-protected AuNPs with the silica precursor. After the formation of a thin layer of sodium silicate in aqueous solution, the particles could be transferred into ethanol for further growth using the Stöber method.[31] However, a disadvantage of this method is that the growth of the initial shell with sodium silicate is strongly pH dependent and difficult to control. The formation of such an initial silica coating on the AuNP surface required a reaction time between 24 h to several weeks before a sufficiently thick silica can be achieved.

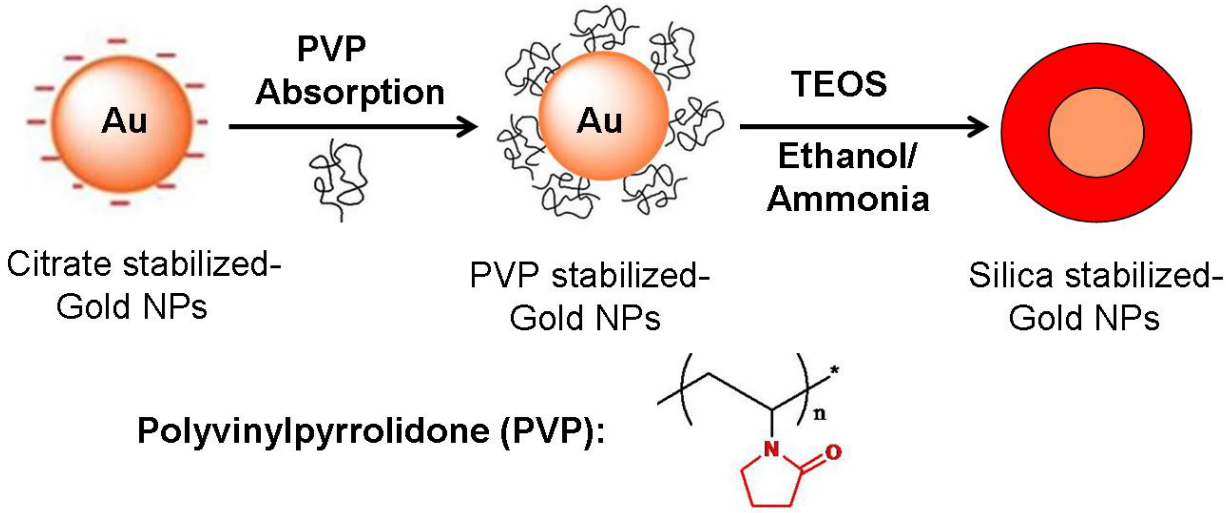

Figure 3-1: A schematic illustration of silica surface coating of citrate-stabilized AuNPs.

We presented a general, simple, and fast method to coat AuNPs with silica shell as shown in Figure 3-1. This method was based on the use of PVP as a stabilizing agent to improve the affinity between AuNPs and TEOS. This amphiphilic, nonionic polymer has been used to adsorb efficiently onto a variety of materials such as metal oxides (TiO_2),[32] silica,[33] graphite,[34] and cellulose [35] to stabilize colloidal particles in water and many nonaqueous solvents. A critical step in the silica surface coating procedure is the transfer of AuNPs that are only stable in aqueous solution to an ethanol/ammonia mixture where the classical Stöber process is performed. For citrate-stabilized AuNPs, we found that it is not possible to transfer the citrate-stabilized AuNPs directly into ethanol solution. The nanoparticles formed an irreversible aggregation and finally precipitated out from the ethanol/water mixture. To stabilize AuNPs during the silica shell growth and increase the affinity of the gold surface to silica precursor, PVP with a molecular weight of 10,000 g/mol were absorbed physically onto the particles surface. PVP is an amphiphilic polymer that is soluble in water and many nonaqueous solvents. This behavior arises

from the presence of a highly polar amide group within the pyrrolidone ring and apolar methylene and methane groups in the ring and along its backbone. After 24 hours of stirring in the presence of PVP, it was observed that the particles had no visible change. The redispersion of the PVP-coated AuNPs in a mixture of ethanol/ammonia also gave no loss of particle stability in contrast to the citrate-stabilized AuNPs.

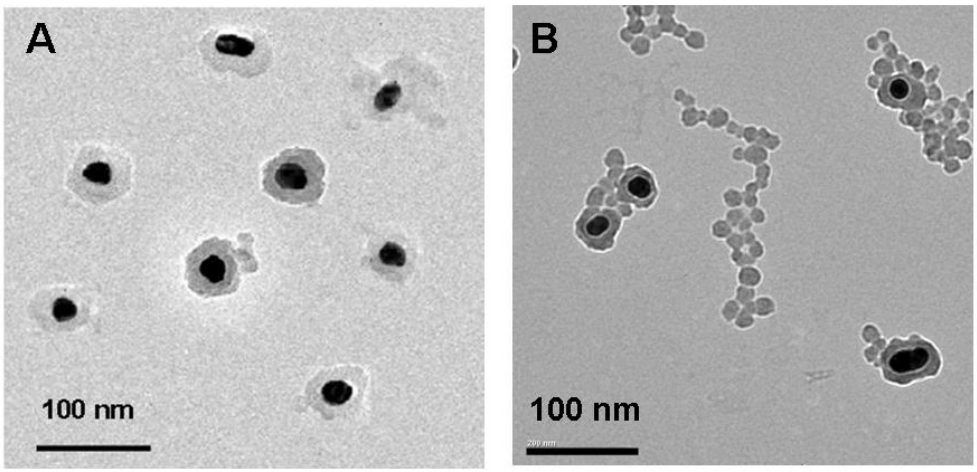

Figure 3-2: TEM images of silica-coated AuNPs with PVP ultrasonification (A) and without PVP ultrasonification (B).

Figure 3-2A shows a typical TEM image of silica-coated AuNPs. The silica layer with an average thickness of 20-40 nm is coated uniformly on the AuNP surface. The core diameter of AuNPs is 30 nm, which is the same as the original citrate-stabilized AuNPs, indicating that the structures of the nanoparticles remained intact during silica coating. It should be mentioned that the homogenization of the PVP polymer solution by ultrasonification before it was added to AuNP solution was critical to the formaton of smooth and uniform silica shells on the particle surfaces. Otherwise, the silica coatings were observed to be less uniform. Additionally, some pure silica nanoparticles with an average diameter of 20 nm were also produced as shown in

Figure 3-2B. This is probably due to the desorption of the PVP chain from the particle surface to the silica growth solution. As a result, some silica precursors nucleate around the free PVP chain in solution and grew into pure silica nanoparticles.

Dynamic light scattering (DLS) measurement has been used extensively to analyze the colloidal particle size and size distribution in solution. It is expected from DLS measurement that the particle size of AuNPs should increase with the growth of silica layer on particle surface. Indeed, as shown in Figure 3-3A, the hydrodynamic diameter of the nanoparticles increased slightly from 30.4 nm to 42.2 nm due to the adsorption of PVP polymer layer on the particle surface. The hydrodynamic diameter of AuNPs increased to 126.4 nm after silica coating. It has been reported that the thickness of silica layer on the particle surface could be further increased by repeated additions of TEOS precursors to the silica-coated AuNP solution.[31] The size distribution of the particles in Figure 3-3A before and after silica shell coating was very narrow, which indicated that the silica-coated AuNPs remained to be individually dispersed in the solution. The effect of silica coating on the optical properties of the AuNPs was revealed from UV-vis absorption spectra as shown in Figure 3-3B. A clear red-shift in the maximum SPR absorption peak of AuNPs from 526 nm to 545 nm after silica coating was observed. This shift is due to an increased local refractive index of the surrounding medium. A similar SPR band shift has been observed on the growth of silica layer on the surface of gold nanorods.[36] In addition, the SPR band of AuNPs did not broaden after silica coating. This further confirmed the AuNPs remained to be well-dispersed in solution during and after silica coating, which agrees well with TEM and DLS studies.

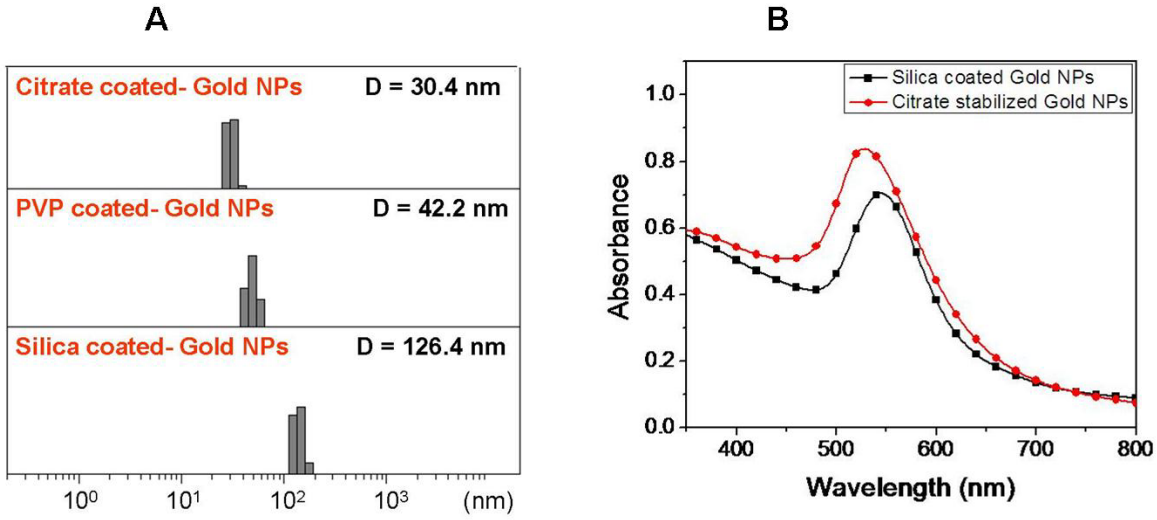

Figure 3-3: DLS measurement (A) and UV-Vis absorption spectra (B) of citrate-stabilized AuNPs before and after silica coating.

3.3.2 : Modification of Citrate-stabilized Gold Nanoparticles using PAA

To improve the stability of citrate-stabilized AuNP in high ionic strength environment, we further used polyacrylic acid (PAA) to replace the citrate molecules on the surface of AuNPs. Figure 3-4 shows the schematic illustration of surface modification of citrate-stabilized AuNPs using PAA at an elevated temperature. In a typical process, a PAA aqueous solution was rapidly injected into a heated and freshly formed citrate-stabilized AuNP solution. Upon continued heating at a temperature close to the boiling point of the solvent, some carboxyl groups on the PAA replaced the citrate molecules on AuNP surface, and the AuNPs were stabilized by the remaining carboxyl groups on the PAA. Followed by centrifuge and washing with deionized water three times to eliminate excessive PAA, and the purified AuNPs can then be well dispersed in water by ionizing the carboxylic groups with a dilute NaOH solution.

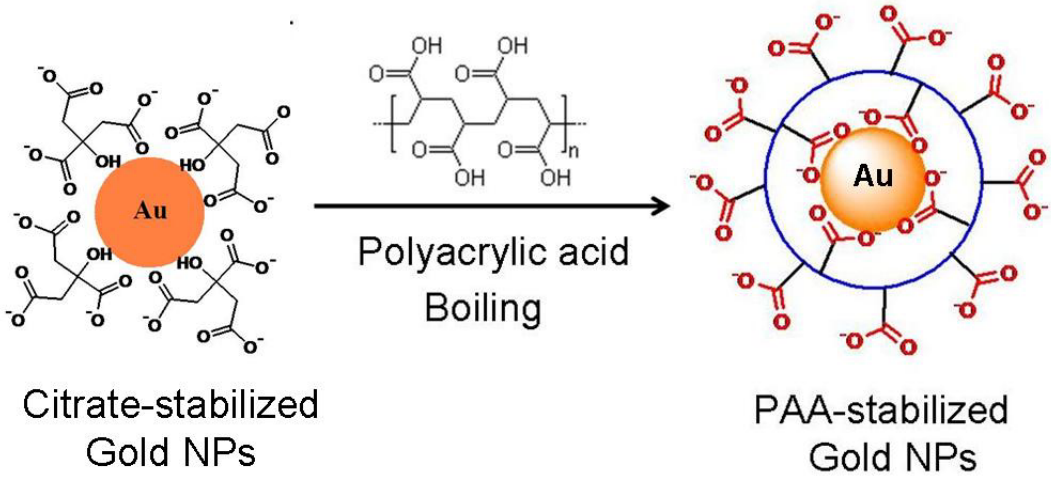

Figure 3-4: A schematic illustration of PAA modification of citrate-stabilized Au NPs.

Compared to the reported ligand exchange processes,[10, 12,] this method has several advantages. First, the exchange reaction between PAA and citrate molecules was performed at relatively high temperatures so that the dynamic solvation of the ligands favors the exchange of original molecules with new ones. Second, each PAA chain binds to AuNP surface through multiple anchoring points, providing a more robust surface adhesion than that is achievable with a small molecule. The strong binding also prevents desorption of ligands from the particle surface, which has been one of the main reasons for decreased colloidal stability in high ionic strength environments. Third, the abundant carboxyl groups on each PAA polymer chain extend into water, making the particles highly soluble in aqueous solutions. In addition, these remaining carboxylic functional groups are available for further surface modification or coupling to bioactive molecules.

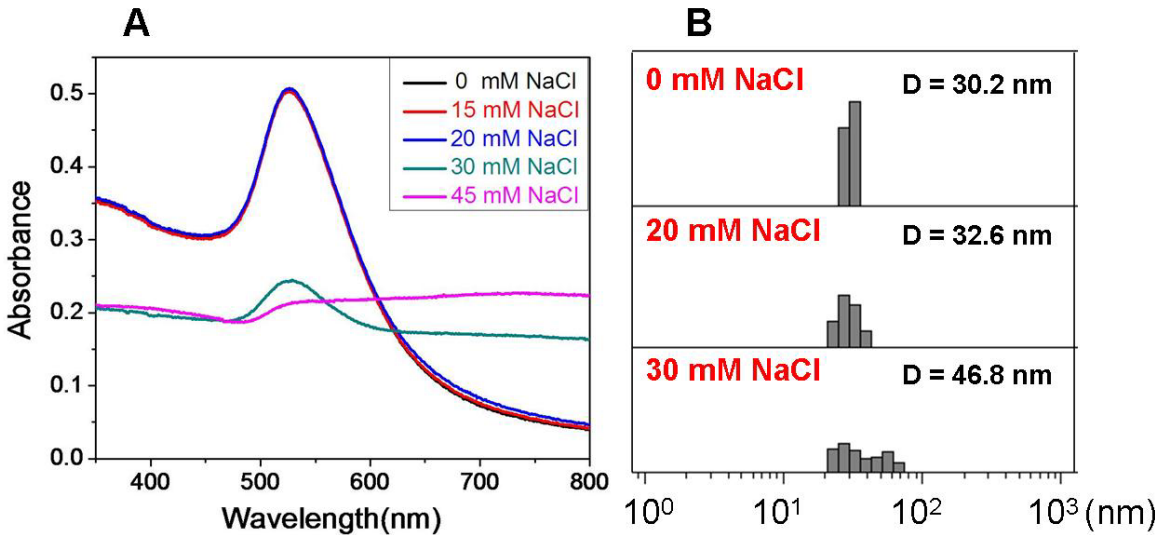

Figure 3-5: UV-Vis absorption spectra (A) and DLS particle size analysis (B) of citrate-stabilized AuNPs at different NaCl concentration.

The colloidal stability of PAA-protected AuNPs in solution was evaluated by monitoring the UV-vis absorption spectrum and DLS particle size analysis. The particle aggregation would expect to shift and broaden the SPR band of AuNPs in the UV-vis absorption spectrum and increase the average particle size, which can be determined from DLS measurement. As a comparison study, the colloidal stability of citrate-stabilized AuNPs with a diameter of 30 nm at different salt concentrations was first studied using UV-vis absorption spectroscopy. Upon addition of NaCl, the color of the nanoparticle solution changed gradually from pink to blue. It is known that an increasing of the ionic strength would decrease the Debye length of colloidal particles in solution.[37] As a result, the average distance of closest approach between particles would decrease, and the nanoparticle aggregation would occur. The solution color change was a result of the screening of the electrostatic repulsion interaction between the surface-charged nanoparticles. In addition, it was found recently that the specific ion adsorption from salt solution

onto AuNP surface play an important role to the color change from red to blue. It has been demonstrated that ion adsorption would affect the surface plasmon state as this would change in the dielectric constant around the particle surface.[38] As shown in Figure 3-5A, up to a NaCl concentration of 20 mM, the SPR spectra of citrate-stabilized AuNPs are indistinguishable. At 30 mM NaCl, there is a significant increase in the absorbance between 600 and 800 nm, which is an indication of the onset of nanoparticle aggregation and is a result of surface plasmon coupling between aggregated nanoparticles. At 45 mM NaCl concentration, the SPR peak centered at 520 nm disappeared into a very broad band, and the nanoparticle aggregates started to precipitate from the solution. DLS measurement in Figure 3-5B further confirmed the formation of particles aggregates in the presence of different NaCl concentrations. The hydrodynamic diameter of AuNP remained at 32 nm with a narrow size distribution at a NaCl concentration of 20 mM. When the NaCl concentration reaches to 30 mM, the salt screening effect not only caused the increase of average particle size to 46.8 nm, but also resulted in a wider size distribution of particle population. Both UV-Vis absorption and DLS measurement indicate that the citrate-stabilized AuNPs started to aggregate together and precipitated out of the aqueous solution at a NaCl concentration of 30 mM. Therefore, the citrate-stabilized AuNPs are not suitable for use at physiological conditions because biofluids typically have a high salt concentration (~ 150 mM).

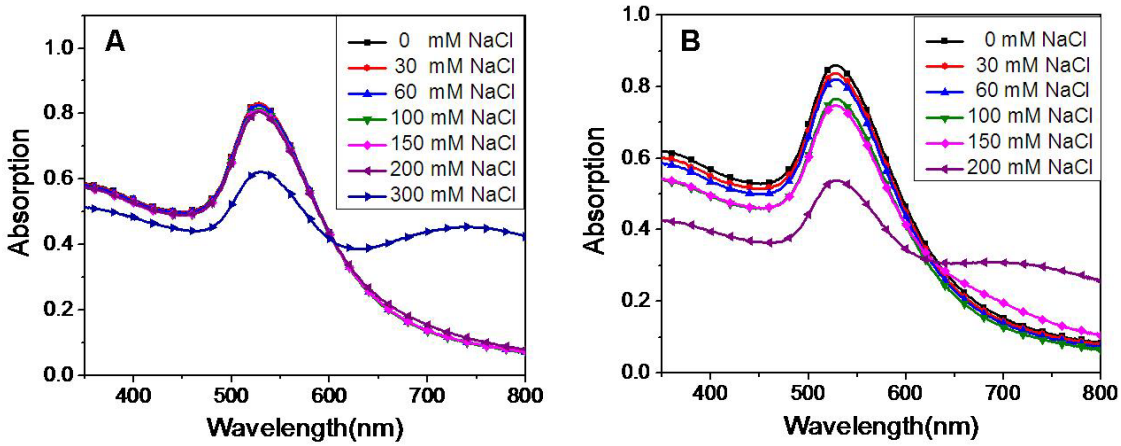

Figure 3-6: UV-Vis absorption spectra of PAA-stabilized AuNPs at different NaCl concentration. A: 10 mins after adding salts; B: 24 hours after adding salts.

Figure 3-6A shows the UV-Vis absorption spectra of PAA-protected AuNPs at different NaCl concentrations. The spectra were taken 10 min after adding the salt. One can see that the colloidal stability of PAA-protected AuNPs was improved significantly in comparison with that of the citrate-stabilized AuNPs. The SPR band of AuNPs did not change even at a NaCl concentration of 200 mM. When the salt concentration reaches to 300 mM, a new broad SPR peak appeared at around 750 nm indicating the formation of particle aggregates. The long term colloidal stability of PAA-protected AuNPs at high salt concentrations was also improved as shown in Figure 3-6B. After 24 hours, the SPR band of AuNPs remained the same at NaCl concentration lower than 150 mM. The stability of PAA-protected AuNPs at different NaCl concentrations was further monitored by DLS particle size measurements. The particle size remained around 30 nm with a narrow size distribution even at a NaCl concentration of 200 mM (Figure 3-7). From both UV-Vis absorption and DLS measurement, it is revealed that the PAA-

protected AuNPs exhibit much enhanced colloidal solubility and stability against salt-induced particle aggregation compared to the citrate-stabilized AuNPs.

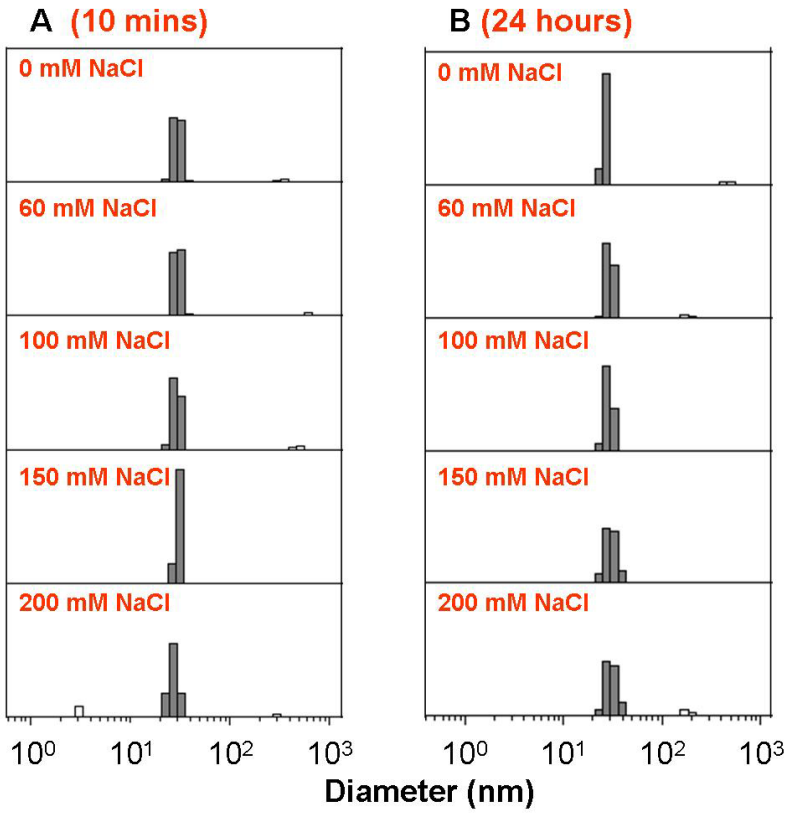

Figure 3-7: DLS particle size measurement of PAA-stabilized AuNPs at different NaCl concentration. A: 10 mins after adding NaCl; B: 24 hours after adding NaCl.

3.3.3 : Modification of Citrate-stabilized Gold Nanoparticles using PEG

Polyethylene glycol (PEG) has been known for its good biocompatibility, its ability to stabilize the particles in the presence of high ionic strength environments and its resistance to protein adsorption.[39] To conduct the surface modification of citrate-stabilized AuNPs as shown in Figure 3-8, the thiol bifunctional PEG was added dropwise into citrate-stabilized AuNP solution, and the mixture was gently shaken at room temperature overnight. The solution was

centrifuged at 8500 rpm for 15 mins, and the nanoparticles were then redispersed into the deionized water. The PEG-modified AuNPs were first characterized by FT-IR. Figure 3-9 is the FT-IR spectra of the citrate-stabilized AuNPs and PEG-modified AuNPs. A band at 1592 cm^{-1} associated with the antisymmetric vibration mode of the $–COO^-$ group suggests the presence of citrate molecules on the particle surface. After ligand exchange with PEG, a new strong band related to the symmetric vibration mode of –C-O-C- appears at 1090 cm^{-1}. A weak peak at 1716 cm^{-1} can be assigned to the stretching mode of –COOH group. The broad band over 3000 cm^{-1} should be resulted from those of trapped water and methanol molecules. On the basis of these observations, it is reasonable to believe that PEG has replaced the citrate molecules on the nanoparticle surface, although the spectra of FT-IR cannot provide quantitative information on the amount of PEG on the particle surface.

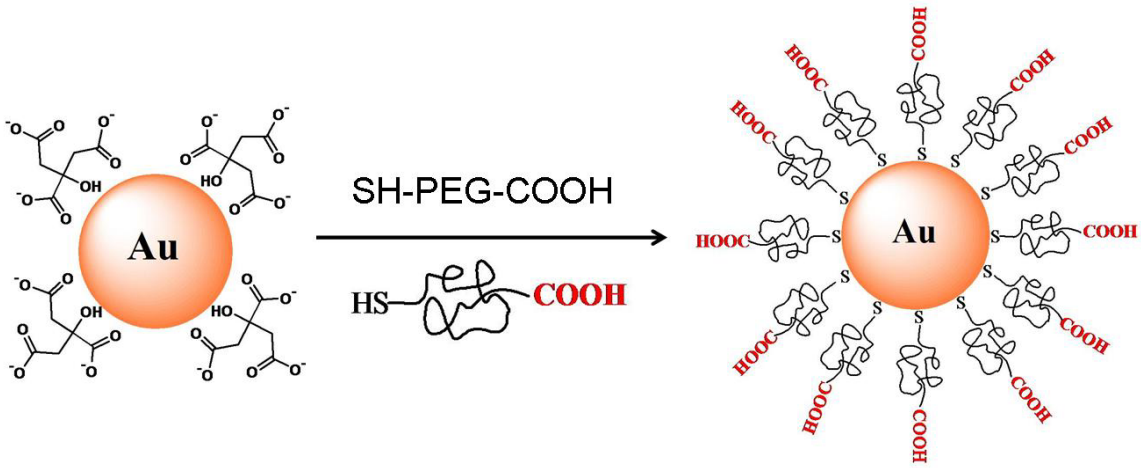

Figure 3-8: A schematic illustration of PEG modification of citrate-stabilized AuNPs

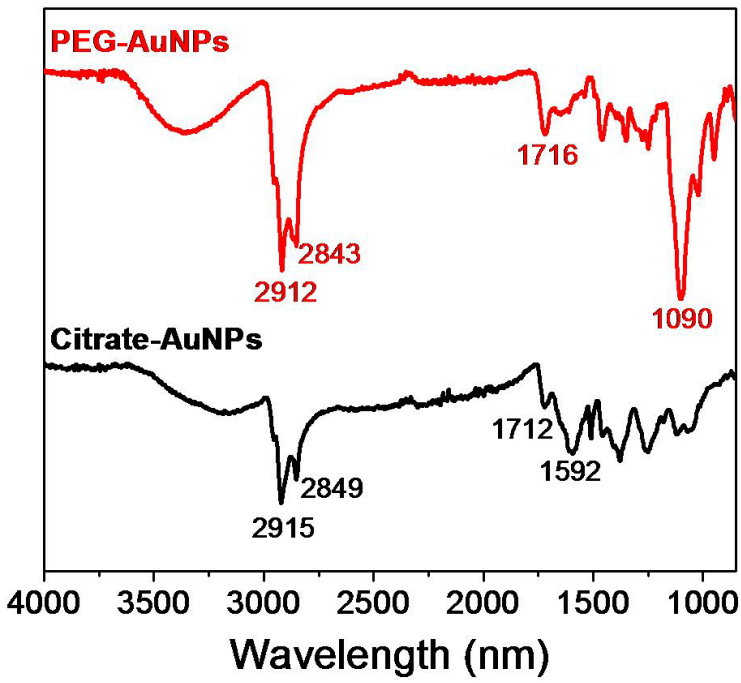

Figure 3-9: FT-IR spectra of citrate-stabilized AuNPs and PEG-modified AuNPs.

The colloidal stability of PEG-modified AuNPs at different NaCl concentrations and pH was then evulated by UV-vis absorption spectroscopy and DLS measurement, which is similar to the study of PAA-protected AuNPs. The UV-vis absorption spectra of PEG-modified AuNPs at various concentrations of NaCl are shown in Figure 3-10A. The characteristic SPR band of AuNP appears at 520 nm. Up to a NaCl concentration of 800 mM, the spectra taken at different NaCl concentration are indistinguishable from each other. No SPR peak shift or boardening was observed. The colloidal stability as a function of pH is shown in Figure 3-10B. There was no indication of particle aggregation with a pH ranging from 2 to 12. DLS particle size analysis as shown in Figure 3-11 further confirmed that the average particle size remained the same at high salt concentrations and pH values between 2 to 10.

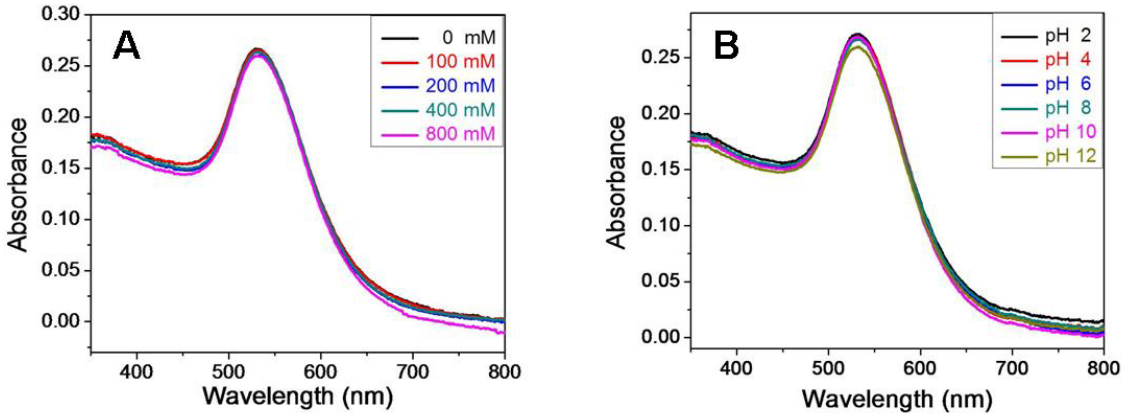

Figure 3-10: UV-Vis absorption spectra of PEG-stabilized AuNPs at different NaCl concentration (A) and pH value (B).

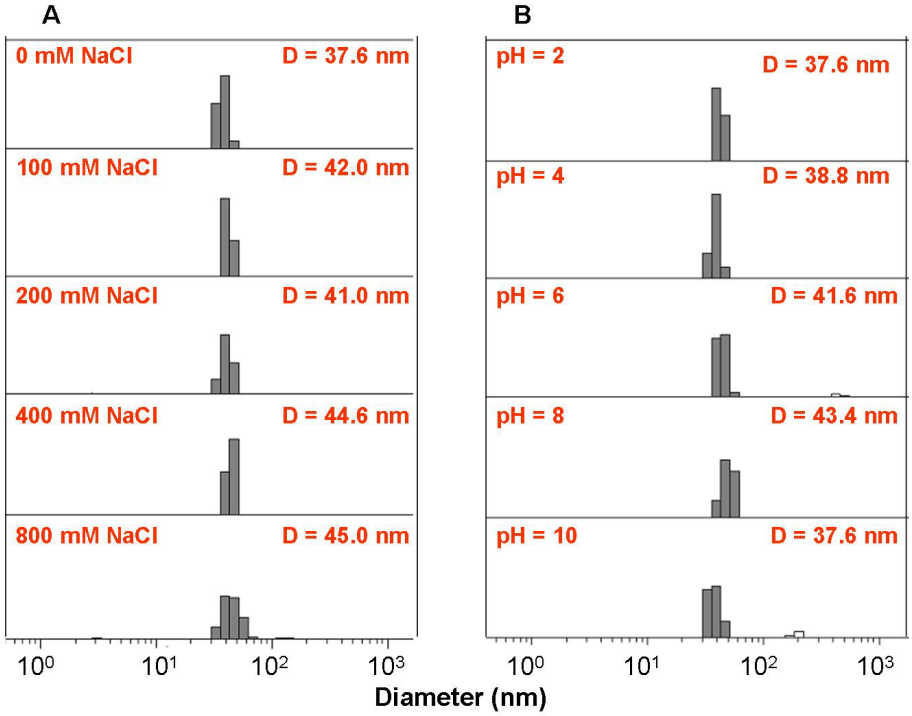

Figure 3-11: DLS particle size measurement of PEG-stabilized AuNPs at different NaCl concentration and pH value.

Both UV-Vis absorption and DLS measurements indicated that the PEG-modified AuNPs were very stable in solutions with high ionic strength and a wide range of pH values. We

attribute this substantial increase of particle stability to three main factors. First, the strong Au-S binding made it more difficult for PEG ligands to detach from the nanoparticle surface. Second, the neutral PEG has good affinity with water, and the charge screening affect of salt is not applicable to the PEG-modified AuNPs solution. Third, the long PEG polymer chain provided an increased steric barrier to prevent nanoparticles from aggregation. It was further observed as shown in Figure 3-12 that the SPR band of AuNP did not shift or broaden even when dispersed into human serum matrices. The absorbance increase was due to the background absorption from human serum matrices. This excellent stability of PEG-protected AuNPs in biological fluids is extremely important and valuable for their applications for biomolecular detection and imaging. The carboxylic acid groups on the particle surface provide a convenient site for conjugating with biomolecules.

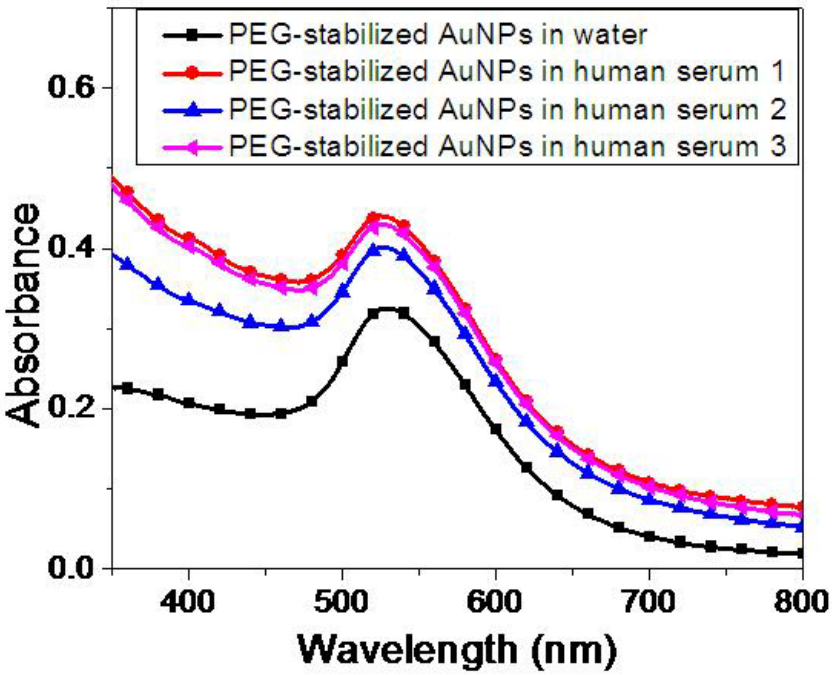

Figure 3-12: UV-Vis absorption spectrum of PEG-stabilized AuNPs before and after diluting into different human serum sample matrix.

3.3.4 : Thiol Ligand Modification of Gold Nanorods inside Polymer Beads

Thiol ligand place exchange reaction in solution developed by Murray has been used extensively for surface modification and functionalization of AuNPs.[9] There have been several reports on surface modification of GNRs with thiol derivatives.[40] However, such modification is often problematic for GNRs. The addition of a small amount of thiol liands to a GNR aqueous solution will first replace the CTAB ligands located at the two poles of GNRs due to a relative high reactivity of surface gold atoms around these polar regions.[41, 42] However, further increase of thiol ligands in solution failed to lead to successful and complete exchange of CTAB ligands with thiol ligands. Instead, this often results in an irreversible agglomeration of GNRs.[43]

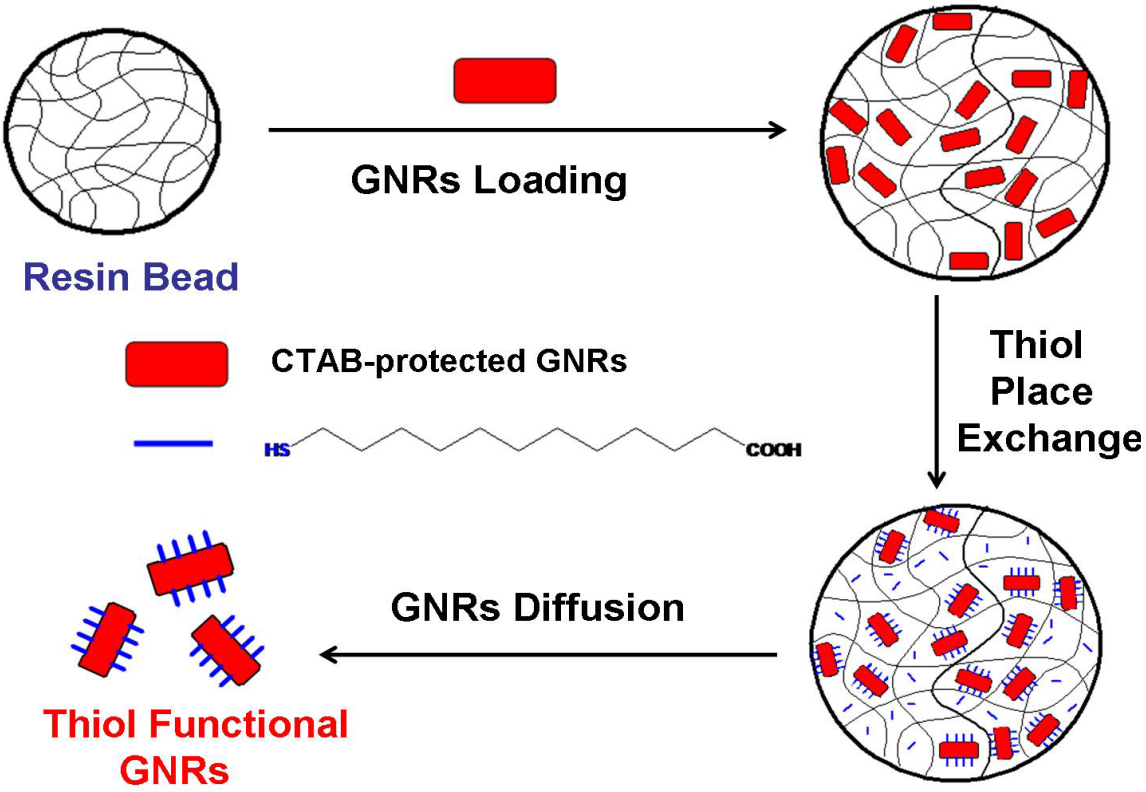

Figure 3-13: A schematic illustration of surface modification of GNRs using thiol place exchange reaction inside ionic exchange polymer beads.

A solid phase place exchange reaction was developed for surface modification of GNRs with bifunctional thiol ligands inside an ionic exchange resin, Amberlite IRA-67. This resin contains positively charged ammonium groups. As illustrated in Figure 3-13, CTAB-protected GNRs were first loaded into the polymer resin beads suspended in an aqueous solution. Once trapped inside the polymer resin, a bifunctional thiol ligand such as 11-mercaptoundecanoic acid (MUA) was added to the polymer beads suspension. A place exchange reaction then took place between nanorods and MUA ligands inside the polymer beads. The successfully modified nanorods were then eluted from the polymer beads to the solution with good solubility against particle aggregation.

During the solid phase place exchange reaction, one can observe clearly a color change of the ionic exchange resin beads from white to black as shown in Figure 3-14A, which indicated a successful loading of GNRs into the pores of ionic exchange polymer beads. Although both GNRs and the ionic exchange resin are positively charged on the surface, we believe the capillary effect is the driving force for nanorods to enter into the pores of resin beads. After washing the beads with a copious amount of water to remove the unloaded GNRs, the beads were washed with methanol and vacuum dried. The dried polymer beads were then suspended in a chloroform solution of MUA ligands. During the place exchange reaction, the nanorods slowly diffused out of the beads to the chloroform solution. The modified nanorods product were then dried and re-dispersed in chloroform. Figure 3-14B shows the GNRs before and after thiol exchange reaction inside the polymer beads. The GNRs were successfully transfered from water to chloroform phase due to the change of surface environment from hydrophilic to hydrophobic.

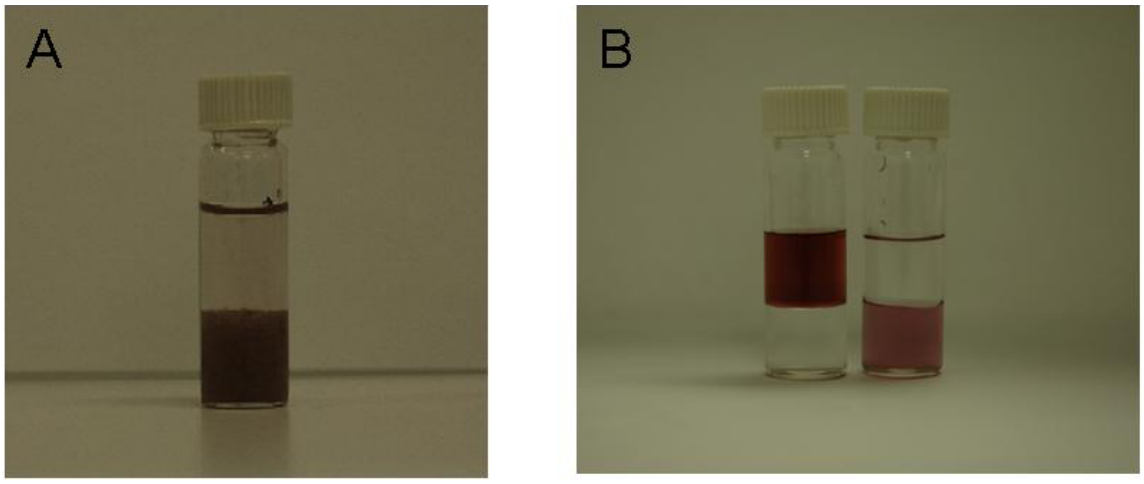

Figure 3-14: A: Photograph of GNRs absorbed into the ionic exchange polymer beads; B: Photograph of GNRs before (left) and after (right) thiol place exchange reaction inside ionic exchange polymer beads.

The MUA-modified GNRs were then characterized by UV-Vis absorption spectroscopy and transmission electron microscopy. Figure 3-15A and B are the UV-Vis absorption spectra of GNRs before and after thiol modification inside the resin polymer beads. After solid phase place exchange reaction, the transverse SPR band of the nanorods remained at 525 nm, and the longitudinal SPR band red shifted from 740 nm to 770 nm. It has been reported that the longitudinal SPR band is more sensitive to the dielectric constant change of the environment than the transverse SPR band.[44] We believe that the red shift of the longitudinal SPR band is a result of solvent change of GNRs from water to chloroform. As a comparison study, we also conducted a place exchange reaction on CTAB-protected GNRs with a mercaptosuccinic acid (MSA) ligand in aqueous solution. During the reaction, it was observed clearly that the color of the solution changed from a dark burgundy to blue with increased amount of MSA ligands. Figure 3-15C is the UV-Vis absorption spectrum of MSA-modifed GNRs obtained from the solution place exchange reaction. The transverse SPR band of the nanorods red shifted to 530 nm, and the

longitudinal SPR band disappeared into a very broad band, a clear indication of nanorod aggregation. A similar spectral change has been observed when an alkanethiol was added to the GNR aqueous solution.[45]

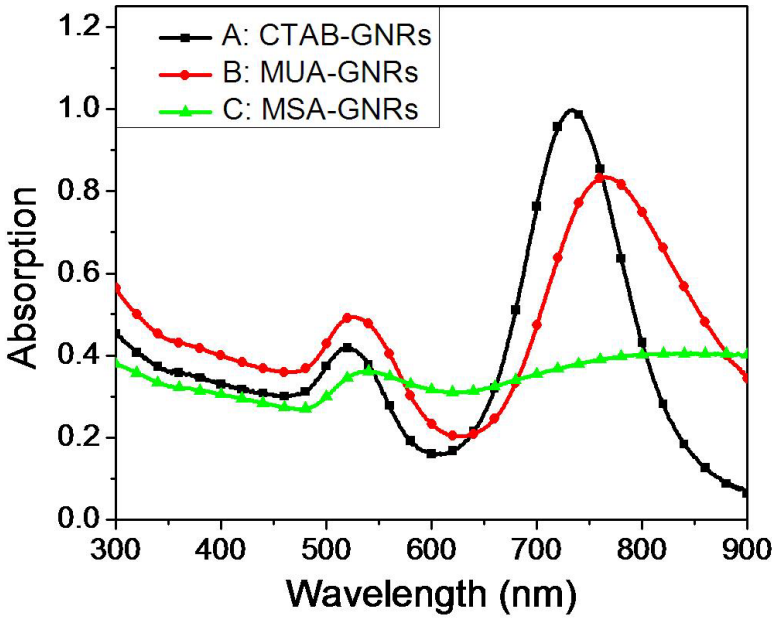

Figure 3-15: UV-Vis absorption spectra of GNRs solution before and after thiol exchange reaction.

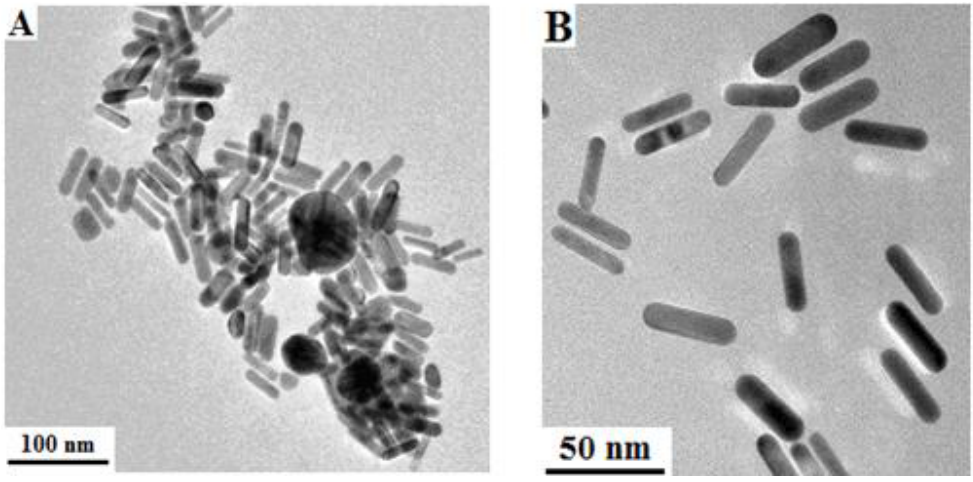

Figure 3-16: A: TEM image of the GNRs after solution thiol place exchange reaction with MSA; B: TEM image of the GNRs after thiol place exchange reaction with MUA inside ionic exchange polymer beads.

TEM analysis further confirmed what was observed from UV-Vis spectroscopic study. As shown in Figure 3-16A, a severe aggregation occured among the MSA-modified GNRs obtained from solution phase place exchange reaction. A certain level of nanrods fusion into larger irregular shaped nanoparticles was also observed. In contrast, the MUA-modified GNRs as obtained from the solid phase place exchange reaction remained well-dispersed with the same aspect ratio as the original CTAB-protected GNRs (Figure 3-16B).

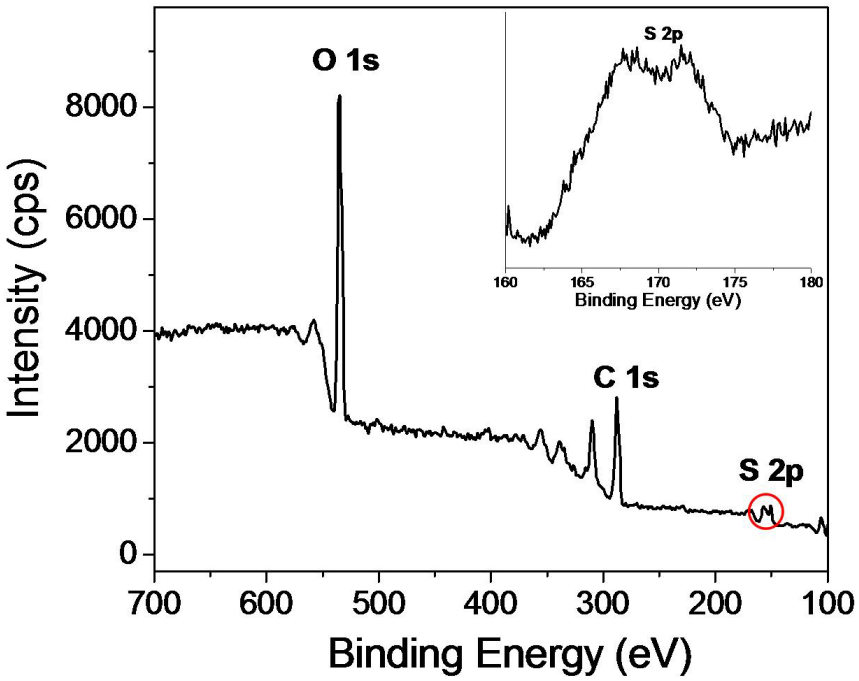

Figure 3-17: XPS spectrum of MUA-modified GNRs

The composition of the MUA-modified GNRs was analyzed by X-ray photoelectron spectroscopy (XPS) and NMR spectroscopy. XPS spectrum of MUA- modified GNRs in Figure 3-17 revealed the presence of sulfur from MUA ligands and the absence of nitrogen and bromine from CTAB ligands. This further confirmed the successful replacement of CTAB with MUA on the surface. The ^{1}H-NMR spectrum of MUA-modified GNRs in *d*-chloroform is shown in Figure

3-18. The assignments of four peaks were 1.2-1.4 ppm (methylene protons at C3-C9), 1.5-1.7 ppm (methylene protons at C2&C10), 2.3 ppm (methylene proton at C11), 2.5 ppm (methylene proton at C1). From both XPS and ^{1}H-NMR analysis, it is revealed that the CTAB ligand has been replaced completely with the MUA on the nanorods surface.

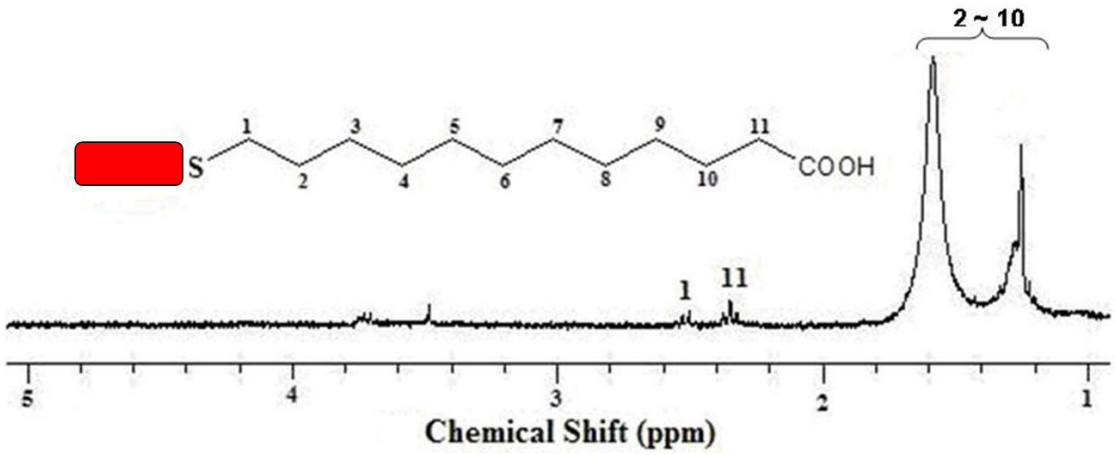

Figure 3-18: ^{1}H-NMR spectrum of MUA-modified GNRs.

The mechanism for the successful place exchange reaction between functional thiol ligands and CTAB-protected GNRs in an ionic exchange resin is rather intriguing. In a free solution, we believe that the failed place exchange reaction between thiol ligands and CTAB-protected GNRs is due to the disruption of the charged surfactant bilayer structure during partial place exchange reaction. It has been reported by Hostetler et al that the place exchange reaction between thiol ligands and AuNPs takes at least 30 min to hours to complete.[46] After the nanorods are partially modified by the thiol ligands, the bilayer structure becomes unstable, however, the thiol ligands have yet to form a stable protecting layer on the nanorod surface. Before this stable monolayer can be formed, the free movement of nanorods in solution results in an irreversible aggregation of the nanorods. In an ionic exchange resin, due to the same charge of the nanorods

and the resin (both are positively charged), the nanorods are confined into the pores of the resin to form a meta-stable self-assembled structure, similar to what has been observed from charged colloidal arrays.[47] The screening effect of the counter ions between the positively charged nanorods as well as the anionic exchange resin prevents the nanorods from aggregation and irreversible adsorption of nanorods to the exchange resin. When a bifunctional thiol ligand such as MUA was loaded to the resin, the MUA ligands can gradually replace the CTAB ligands on the nanorods until a stable monolayer is formed on the nanorod surface.

As an additional support to this proposed mechanism, we conducted the following two control experiments. In the first experiment, the ionic exchange polymer beads without GNRs being loaded were added and incubated in the MUA chloroform solution. After washing the polymer beads with chloroform and drying with N_2, the presence of MUA ligand inside the polymer beads was confirmed by the Ellman's agent (5,5'-dithio-bisnitrobenzoic acid) test.[48] In the second control experiment, polymer beads loaded with CTAB-protected GNRs were added to a pure chloroform solution. It was clear that no GNRs diffused out of the polymer beads into the chloroform solution without MUA ligands in the solution. These two experiments complementarily confirmed that a place exchange reaction between the MUA ligands and CTAB protected- GNRs inside the polymer beads has led to the successful surface modification of GNRs.

3.4 : Conclusions

In summary, we utilized two biocompatible polymers, PAA and PEG, to surface modify and to improve the colloidal stability of citrate-stabilized AuNPs. The resulting polymer-modified AuNPs are stable in high ionic strength conditions including human serum. In addition,

we developed a facile method for effective replacement of CTAB surfactants on GNR surface with a bifunctional thiol ligand using ionic exchange polymer beads. The resulting GNRs show a good solubility and stability against aggregation in organic solvents such as chloroform. The carboxylic acid groups on the GNRs surface provide anchor points for further modification and conjugation with other chemicals and biomolecules by covalent and non-covalent chemistry.

3.5 : List of References

1: Caruso, F. *Adv. Mater*. **2001**, 13, 11.

2: Neouze, M. A.; Schubert, U. *Monatsh. Chem*. **2008**, 139, 183.

3: Hofman-Caris, C. H. M. *New J. Chem*. **1994**, 18, 1087.

4: Davies, R.; Schurr, A.; Meenan, P.; Nelson, R. D.; Bergna, H. E.; Brevett, C. A. S.; Goldbaum, R. H. *Adv. Mater*. **1998**, 10, 1264.

5: Turkevitch, J.; Stevenson, P. C.; Hiller, J.; *Discuss. Faraday Soc*. **1951**, 11, 55.

6: Cao, C. Sim, S. J. *J. Nanosci. Nanotech*. **2007**, 7, 3754.

7: Laaksonen, T.; Ahonen, P.; Johans, C.; Kontturi, K. *ChemPhysChem* **2006**, 7, 2143.

8: Brust, M.; Walker, M.; Bethell, D.; Schiffrin, D. J.; Whyman, R. *Chem. Comm*. **1994**, 801.

9: Templeton, A. C.; Wuelfing, W. P.; Murray, R. W.; *Acc. Chem. Res*. **2000**, 33, 27.

10: Weisbecker, C. S.; Merritt, M. V.; Whitesides, G. M. *Langmuir* **1996**, 12, 3763.

11: Zhu, T.; Vasilev, K.; Kreiter, M.; Mittler, S.; Knoll, W. *Langmuir*, **2003**, 19, 9518.

12: Aslan, K.; Perez-Luna, V. H. *Langmuir*, **2002**, 18, 6059.

13: Rouhana, L. L.; Jaber, J. A.; Schlenoff, J. B. *Langmuir*, **2007**, 23, 12799.

14: Zhang, F. J.; Skoda, M. W. A.; Jacobs, R. M. J. Zorn, S.; Martin, R. A.; Martin, C. M.; Clark, G. F.; Goerigk, G.; Schreiber, F. *J. Phys. Chem. A* **2007**, 111, 12229.

15: Youk, J. H.; Park, M. K.; Locklin, J.; Advincula, R.; Yang, J.; Mays, J. *Langmuir* **2002**, 18, 2455.

16: Miyamoto, D.; Oishi, M.; Kojima, K.; Yoshimoto, K.; Nagasaki, Y. *Langmuir* **2008**,

24, 5010.

17: Chen, Y.; Cho, J.; Young, A.; Taton, T. A. *Langmuir* **2007**, 23, 7491.

18: Kimura, K.; Takashima, S.; Ohshima, H. *J. Phys. Chem. B* **2002**, 106, 7260.

19: Link, S.; El-Sayed, M. A. *J. Phys. Chem. B* **1999**, 103, 8410.

20: Nikoobakht, B.; El-Sayed, M. A. *Chem. Mater*. **2003**, 15, 1957.

21: Ying, Y.; Yang, S. S.; Lee, C. L.; Wang, C. R. C. *J. Phys. Chem. B* **1997**, 101, 6661.

22: Nikoobakht, B.; El-Sayed, M. A. *Langmuir* **2001**, 17, 6368.

23: Jana, N. R.; Gearheart, L.; Murphy, C. J. *J. Phys. Chem. B* **2001**, 105, 4065.

24: Connor, E. E.; Mwamuka, J.; Gole, A.; Murphy, C. J. Wyatt, M. D. *Small* **2005**, 1, 325.

25: Hotchkiss, J. W.; Lowe, A. B.; Boyes, S. G. *Chem. Mater*. **2007**, 19, 6.

26: Yu, C.; Varghese, L.; Irudayaraj, J. *Langmuir* **2007**, 23, 9114.

27: Pastorize-Santos, I.; Perez-Juste, J.; Liz-Marzan, L. M. *Chem. Mater*. **2006**, 18, 2465.

28: Niidome, Y.; Honda, K.; Higashimota, K.; Kawazumi, H.; Yamada, S.; Nakashima, N.; Sasaki, Y.; Ishida, Y.; Kikuchi, J. K. *Chem. Comm*. **2007**, 36, 3777.

29: Jin, R.; Wu, G. S.; Li, Z.; Mirkin, C. A. Schatz, G. C. *J. Am. Chem. Soc*. **2002**, 125, 1643.

30: Mulvaney, P.; Liz-Marzan, L. M.; Giersig, M.; Ung, T. *J. Mater. Chem*. **2000**, 10, 1259.

31: Liz-Marzan, L. M.; Giersig, M.; Mulvaney, P. *Langmuir* **1996**, 12, 4329.

32: Correa-Duarte, M. A.; Giersig, M.; Liz-Marzan, L. M. *Chem. Phys. Lett*. **1998**, 286, 497.

33: Esumi, K.; Matsui, H. *Colloid Surf., A: Physicochem. Eng*. **1993**, 80, 273.

34: Otsuka, H.; Esumii, K. *J. Colloid Interface Sci*. **1995**, 170, 113.

35: Koteiniieva, N. E.; Penarin, E. F.; Kudina, N. P. *Obshchi. Khim*. **1997**, 67, 335.

36: Pastoriza-Santos, I.; Perez-Jaste, J.; Liz-Marzan, L. M.; *Chem. Mater*. **2006**, **18**, 2465.

37: Hunter, R. J. *Foundations of Colloid Science*, Vol. 1, Clarendon Press, Oxford, **1993**.

38: Burns, C.; Spendel, W. U.; Puckett, S.; Pacey, G. E. *Talanta* **2006**, 69, 873.

39: Zheng, M.; Davidson, F.; Huang, X. *J. Am. Chem. Soc*. **2003**, 125, 7790.

40: Jebb, M.; Sudeep, P. K.; Praamod, P.; Thomas, K. G.; Kamat, P. V. *J. Phys. Chem. B* **2007**, 111, 6839.

41: Chang, J. Y.; Wu, H. M.; Chen, H.; Ling, Y. C.; Tan, W. H. *Chem. Comm*. **2005**, 416, 215.

42: Caswell, K. K.; Wilson, J. N.; Bunz, U. H.; Murphy, C. J. *J. Am. Chem. Soc*. **2003**, 125, 13914.

43: Kanal, B. P.; Zubarev, E. R. *Angew. Chem. Int. Ed*. **2007**, 46, 2195.

44: Thomas, K. G.; Barazzouk, S.; Ipe, B. I.; Joseph, S. T. S.; Kamat, P. V. *J. Phys. Chem. B* **2004**, 108, 13066.

45: Shibu, S. T.; Pramod, P.; Thomas, K. G. *J. Phys. Chem. B* **2006**, 110, 150.

46: Hostetler, M. J.; Templeton, A. C.; Murray, R. W. *Langmuir* **1999**, 15, 3782.

47: Holtz, J. H.; Holtz, J. S. W.; Munro, C. H.; Asher, S. A. *Anal. Chem*. **1998**, 70, 780.

48: Fields, G. B.; *Methods in Enzymology Volume 289: Solid Phase Peptide Synthesis.* Academic Press, New York. **1997**.

CHAPTER 4 : A HOMOGENEOUS BIOMOLECULAR ASSAY USING GOLD NANOPARTICLE PROBES COUPLED WITH DYNAMIC LIGHT SCATTERING

4.1 : Introduction

Advances in genomics and proteomics research have opened tremendous opportunities to improve disease diagnosis and therapy.[1, 2] The availability of a rapid and highly sensitive bioassay with the capability to detect a wide range of biomarkers (proteins and DNAs) would greatly benefit point-of-care and public health applications.[3] Immunoassays are one of the most extensively used tools for protein analysis.[4] The highly sensitive detection and accurate analysis of protein biomarkers are essential for early detection, treatment and management of cancer and other diseases. For a typical sandwich-type immunoassay, which is routinely used for protein analysis, a capture antibody against a specific biomarker protein is first immobilized on a microtiter plate. After the binding of antigen from a sample solution, a labeled detector antibody is allowed to bind with the immobilized antigen. The concentration of the antigen can then be determined by indirectly measuring the concentration of the probe attached to the detector antibody, which includes enzymes, fluorescence tags, and DNA-barcodes.[5, 6, 7] A typical heterogeneous immunoassay involves antibody immobilization, multiple steps of incubation and washing cycles, followed by the signal amplification and reading step. From the initial antibody immobilization to the final reading of the assay results, the entire immunoassay can usually take hours to days to complete. A traditional immunoassay is rather time-consuming and labor-intensive. To overcome these problems, the development of single-step, washing-free

homogeneous immunoassays have been of tremendous interest and value to the scientific community.[8, 9]

Other than the immunoassay, nucleic acid sequences unique to every living organism and every bacterium, virus, or pathogen provide practical targets for the identification and diagnosis of various diseases.[10] Highly sensitive detection of specific DNA sequences is extremely important and valuable for rapid detection of genetic mutations and diseases. Current detection depends heavily on fluorescent label-based sandwich DNA hybridization methods such as DNA microarrays[11] and molecular beacons.[12] In a typical DNA microarray assay, a capture DNA probe is first immobilized on a solid substrate. After multiple washing steps to remove the free probes, a target DNA is hybridized with the capture DNA probes. After another washing cycle, a second complementary DNA probe, which is often labeled with a fluorescent probe, is hybridized with the target DNA through another end. The amount of target DNA is then determined from the fluorescence intensity of the microarray. These assays have several advantages such as high throughput capability, multiplexing and high specificity. However, two major difficulties limit the sensitivity when fluorophores are used as optical probes. The first is the relatively low signal amplification. Because one DNA probe can only be labeled with one or few fluorophores, the fluorescence signal is too weak to be detected when the target DNA concentration is low. The second challenge is the poor photostability of many fluorophores. Most organic dyes suffer from serious photobleaching problem, which consequently affect the reproducibility of the assay.

Other than traditional fluorescent dyes, colloidal gold nanoparticles (AuNPs), including spherical particles, nanorods, and nanoshells with a size ranging from 10s to 100s nanometers,

have been used recently in a variety of forms for detecting protein and DNA biomarkers based on their unique optical properties.[13, 14, 15] AuNPs are known to have large light scattering cross-section. It has been reported that the cross-section of light scattering from an 80-nm AuNPs can be a millon-fold larger than the cross-section of emission from a fluorescent dye.[16] Unlike fluorescent labels, the scattering light generated by AuNPs is not prone to quenching and does not photobleach with repeated exposure to light. Therefore, the light scattering from AuNPs should serve as a very suitable signal transducer for biomolecular imaging and detection.

The most widely used assay involving AuNPs is based on the analyte-induced particle aggregation. The particle aggregation leads to the change of the SPR spectrum (i.e.: shift and broadening of the SPR peak), and the light scattering intensity. For example, AuNPs have been used in aggregation-based immunoassays in conjugation with micrometer-sized latex particles in home pregnancy test devices.[17] In this assay, both the micro sized- latex particles and the AuNPs were functionalized with antibody, which can specificly binded with human chorionic gonadotropin, β-hCC, a hormone released by pregnant women. When mixed with a urine sample containing this hormone, the micro- and nanoparticles were aggregated together to result in a visible color change from red to blue. This particle aggregation-based assay has also been used to detect specific DNA target. Mirkin and co-workers first developed a colorimetric DNA hybridization assay that detects the change in the spectral properties of oligonucleotide-functionalized AuNPs in the presence of a complementary target oligonucleotide sequence.[18, 19] The particle aggregation leads to a color change from red to blue and the formation of a new SPR peak at longer wavelengths as a result of surface plasmon coupling. However, the main limitation of this approach is its relatively low sensitivity (10 nM). The two main factors that

contribute to the low sensitivity are the inability to detect nanoparticles at low concentration and the requirement of a larger nanoparticle aggregation to achieve a detectable SPR shift in UV-vis absorption spectroscopy. To increase the sensitivity, Reynolds et al used larger- sized 50 nm or 100 nm AuNPs as the probes.[20] It was found that a small number of target DNAs could still produce a detectable signal because of the increased scattering intensity from the larger AuNPs. The 100 nm AuNP probes were observed to be more sensitive to lower target DNA concentrations than the 50 nm AuNP probes. The sensitivity was further increased by monitoring target DNA hybridization to combinatorial DNA arrays.[21] The amount of target hybridization could be quantified by imaging the grayscale of the silver-amplified 200 μm diameter array elments using a simple conventional flatbed optical scanner. Target DNA concentrations as low as 50 fM could be detected, which is a 100-fold increase in sensitivity when compared with Cy3-labeled arrays imaged by confocal fluorescent microscopy.[22] Recently, the bio-barcode amplification and surface enhanced Raman scattering was developed to improve the assay sensitivity.[23, 24] However, all these amplified approach must be conducted on the heterogeneous formats with multiple binding and washing steps which are too tedious to be carried out for routine clinic diagnoses. Also, all of these methods involve a silver coating of AuNPs on solid substrate to enhance the signal, a complicated process which also causes decreased reproducibility.

Dynamic light scattering (DLS), also known as photon correlation spectroscopy or quasi elastic light scattering, is a technique used widely for particle size and size distribution studies. This technique is based on the Brownian motion of spherical particles which causes a Doppler shift of incident laser light. The diffusion constant of particles is measured and the size of the

particles is calculated according to the Stokes-Einstein relation.[25] DLS is a very sensitive tool to monitor particle aggregation, and this capability makes DLS a potential analytical tool for a quantitative assay. DLS detection has been utilized in the latex particle immunoassay, which is based on the antigen-induced agglutination of calibrated latex particles coated with a specific antibody.[26] However, the sensitivity is quite low due to the low light scattering cross-section produced by micrometer-sized latex particles. Because of the strong light scattering property of AuNP, it is natural to hypothesize that DLS can be a very sensitive technique for quantitative detection and analysis of AuNP probes at low concentration. In this project, we developed a single-step, washing-free, and homogeneous assay for free Prostate Specific Antigen (PSA) and target DNA detection using AuNP probes and dynamic light scattering (DLS) technique. To conduct the assay, AuNPs are first functionalized with a pair of monocolonal antibody (anti-PSA) or a pair of DNA probes, which are able to form the sandwich structure upon the addition of analyte solution (free PSA or target DNA). Both antigen-antibody binding and DNA hybridization can introduce the formation of nanoparticle dimers, trimers, and high order aggregates. By measuring the degree of nanoparticle aggregation from size analysis using DLS, the concentration of free-PSA and target DNA in the sample solution can be determined.

4.2 : Experimental Section

4.2.1 : Chemicals and Materials

All the chemicals except the following few were purchased from Sigma-Aldrich. Hydrogen tetrachloroaurate (III) hydrate ($HAuCl_4$) was purchased from Strem Chemicals (Newburyport, MA). Mouse anti-human PSA monoclonal antibody (capture antibody) (cat. #

T40081A, clone # CHYH1), mouse anti-human PSA monoclonal antibody (detector antibody) (cat. # T40081B, clone #CHYH2), and ELISA kits for human free-PSA (Cat.# 10050) were obtained from Anogen-YES Biotech Laboratories Ltd. (Mississauga, Canada). The 10 ng/mL free-PSA standard solution was used for preparation of free-PSA solutions with lower concentrations obtained using sample diluent provided in the ELISA kit. All of the DNAs used in this work were purchased from Integrated DNA Technologies (Coralville, IA). The sequences are listed as follows: DNA1: 5' TAA CAA TAA TCC CTC-C_3-SS 3'; DNA2: 5' SS-C_6- ATC CTT ATC AAT ATT 3'; Target DNA: 5' GAG GGA TTA TTG TTA AAT ATT GAT AAG GAT 3'. One base pair mismatched target DNA in the middle: 5' GAG GGA TTA TTG TTA AAT ATT GAT AAG GAT 3'. One base pair mismatched target DNA in at the end: 5' GAG GGA TTA TTG TTA AAT ATT GAT AAG GAC 3'. NAP-5 columns (Sephadex G-25 Medium, DNA grade) were obtained from GE Healthcare Biosciences. Ultrapure water (18.3 MΩ cm^-) was used throughout the work.

4.2.2 : Instrumentation and Characterization

UV-vis absorption spectroscopy was recorded on a Cary 300 Bio UV-Visible spectrophotometer from Varian Inc. (Palo Alto, CA). A PD2000DLS^{PLUS} Dynamic Light Scattering Detector and a PDDLS/CoolBatch 4oT Dynamic Light Scattering detector system from Precision Detectors Inc. (Bellingham, MA) was used for dynamic light scattering (DLS) measurement. The DLS instrument was operated under the following conditions: temperature 20^{o}C, detector angle 90^o, incident laser wavelength 683 nm, laser power 100 mW. The DLS data without molecular normalization was processed using the Precision Deconvolve software.

4.2.3 : Synthesis

4.2.3.1 : Preparation of AuNP/PSA Antibody Conjugation

The polyethylene glycol (PEG)-stabilized AuNPs with an average diameter of 30 nm was synthesized using the procedure describing in chapter 3. To activate the –COOH groups on the particle surface for covalent conjugation, 30 μL of each freshly prepared ethyl dimethylaminopropyl carbodimide (EDC) and sulfo-NHS solutions at a concentration of 2×10^{-4} M were added to 1.2 mL PEG-stabilized AuNP solution, and the solution was set at room temperature for 30 min. The mixture was passed through a Sepharose cl-6B gel column (MW: 10^4-4×10^6) to remove the excessive EDC and NHS. 500 μL of the activated PEG-protected AuNPs was then added to a 1.00 mL of diluted PSA capture antibody (cAb) or PSA detector antibody (dAb) solution, which was prepared from dilution of 100 uL of rehydrolyzed antibody solution at 1.0 mg/mL with 900 μL of 0.01 M phosphate buffer saline (NaCl 0.138 M; KCl 0.0027 M, pH 7.4). After gentle shaking at room temperature for 3 hours, the mixture solution was centrifuged at 8000 rpm for 3 times to remove the excess antibody, and the conjugated AuNP product was finally redispersed into PBS buffer solution.

4.2.3.2 : Immunoassay of free-PSA using AuNP/PSA Antibody Conjugates

A volume of 50 μL of 0.20 nM AuNP/dAb conjugates were mixed with 50 μL of 0.2 nM AuNP/cAb conjugates in a 1.5 mL sterilized polypropylene tube. To each mixed nanoprobe solution, 20 μL solution of free-PSA antigen standard at different concentrations was added, mixed well and incubated for 30 min at 37°C. Five free-PSA sample solutions at the following concentrations were tested: 0, 0.1, 0.5, 1.0, 10.0 ng/mL. All standards were prepared from

diluting the thawed 10 ng/mL standards with sample dilutant solution provided in the ELISA kit. Each concentration was repeated three times. After incubation, sample solutions were analyzed by dynamic light scattering (DLS). DLS samples were prepared by diluting 10 uL of the assay solution into 1.5 mL of nanopure water in a plastic curvette (*c*=0.5 cm). After standing for 2 min, the sample solution was analyzed by DLS.

4.2.3.3 : Deprotection of alkanethiol-modified DNA

200 μL of 3' alkanethiol-modified DNA solution (DNA1, 10 OD, 70 nmol) was mixed with 40 μL of 0.1 M dithiolthretol, and 0.02 M phosphate buffer (pH 8) solution at room temperature for 2 h to cleave the 3' mixed disulfide. Aliquots of deprotected DNA1 solution were purified through a desalting NAP-5 column. 230 μL of 5' alkanethiol modified DNA solution (DNA2, 10 OD, 91 nmol) was mixed with 15 μL 0.05 M $AgNO_3$ aqueous solution and then allowed to stand for 20 mins, followed by addition of 15 uL dithiolthreitol (10 mg/mL) to remove excess $AgNO_3$ (reaction time: 5 min). The precipitate was removed by centrifuge. Aliquots of deprotected DNA2 solution were purified through a desalting NAP-5 column. The final concentration of DNA was adjusted to ~ 0.1 mM using nanopure water.

4.2.3.4 : Synthesis of the DNA-AuNP Conjugates

The conjugation of AuNPs with two DNA probes was conducted according to a previous procedure.[19] DNA-AuNP probes were prepared by derivatizing 5 mL of an aqueous 30 nm citrate-stabilized AuNPs solution (~ 0.3 nM) with 2.5 OD of fresh deprotected DNA solution (final DNA concentration is ~3 μM). After standing for 16 h at room temperature, the mixture was first buffered at pH 7 (phosphate: 10 mM), sodium dodecylsulfate (0.01%), and the NaCl

concentration was brought to 0.2 M in a stepwise manner over 1 day by adding 2 M NaCl solution. After the salting process was completed, the DNA-AuNP conjugates were purified from excess DNA by centrifugation (twice at 8000 rpm for 5 min) and washed each time with 10 mM phosphate buffer solution (pH: 7, 0.2 M NaCl, Tween 20: 0.1%). DNA-AuNP probes were finally redispersed in a 10 mM phosphate buffer solution (0.2 M NaCl, pH: 7) to a concentration of ~ 100 pM.

4.2.3.5 : Target DNA Assay using DNA-AuNP Probes

DNA1-AuNPs and DNA2-AuNPs probes (100 μL, 10^{-10} M) were mixed in a 1:1 ratio, and 10 μL of target DNA solution with different concentrations was then added. The mixture was heated to 70 degrees (over the melting point) for 5 min, and then allowed to cool at room temperature. After two hours, a drop of the assay solution (20 μL) was diluted with 2 mL deionized water and analyzed by DLS measurement.

4.3 : Results and Discussions

4.3.1 : Free Prostate Specific Antigen (PSA) Immunoassay

Several light scattering-based detection methods have been developed in immunoassay using AuNP probes.[27, 28] Jiang et al reported to the use of resonance light scattering immunoassay with AuNP labels for detection of thiamazole,[29] fibrinogen,[30] apolipoprotein A1,[31] apolipoprotein B,[31] prealbumin[32] and microalbumin.[33] This method is based on monitoring the resonance scattering intensity of the antibody labeled- 10 nm AuNP probes using the spectrofluorometer in the presence of protein analyte. The immune reaction between the

antibody labeled- AuNP probes and protein analyte causes the particle aggregation to increase the resonance scattering intensity, which can be correlated quantitatively to the protein analyte concentration. However, the resonance light scattering immunoassays have a low detection limit and narrow dynamic range. For prealbumin, the resonance scattering intensity is proportional to the analyte concentration in the range from 16.67 to 666.67 ng/mL with a detection limit of 4.1 ng/mL.[32]

To demonstrate the feasibility and sensitivity of DLS for bioassay using AuNP probes, we first examined the detection limit of DLS for a 30 nm citrate-stabilized AuNPs. The 30 nm citrate-stabilized AuNPs solutions were diluted to appropriate concentrations for DLS analysis. Figure 4-1 is the plots of the average scattered light intensity versus the particle concentration. The average scattered light intensity shows a linear relationship with the particle concentration in the picomolar range. A detection limit of 0.02 pM was obtained, which is similar to the reported result of gold nanoshell.[34]

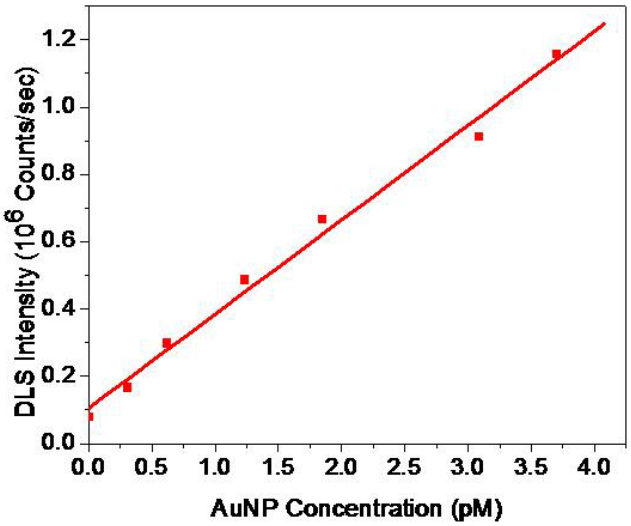

Figure 4-1: The relation between the average scattering intensity and AuNP concentration.

Prostate cancer occurs when cells of the prostate mutate and begin to multiply out of control. Prostate cancer is the second leading cause of cancer-related deaths in adult males in the United States. Since no effective cures are available for the advanced metastatic stage of prostate cancer, early detection of malignant tumor is crucial for reducing the mortality rates. Prostate specific antigen (PSA) is a glycoprotein produced and released almost exclusively by the prostate gland. Healthy males usually have low levels of PSA in their blood, while the prostate cancer patients have higher levels of PSA concentration. PSA has been used as a biomarker for prostate cancer detection and diagnosis. Free PSA is the unbound form of prostate specific antigen. The total PSA concentration of a healthy male is usually in the range of a few ng/mL and the free PSA concentration is typically less than 1 ng/mL, in the range of 10% of the total PSA. Studies have shown that the percentage of free PSA in total PSA is lower in patients with prostate cancer than those with benign prostate hyperplasia. Therefore, the free to total PSA ratio is now being introduced and studied as an additional tool for prostate cancer diagnosis.

Our group first developed a highly sensitive one-step homogeneous immunoassay for free PSA detection using AuNP probes coupled with DLS analysis.[35] As illustrated in Figure 4-2, the citrate-stabilized AuNPs were first conjugated with an anti-free PSA antibody pair through electrostatic interaction, one with a capture antibody and one with a detector antibody. When these two bioconjugated nanoparticles were mixed in a sample solution that contains free PSA antigen, the binding of free PSA will cause nanoparticles to form dimers, oligomers, or aggregates, depending on the concentration of the antigen. Through DLS analysis, the average diameter increase of the particle can then be correlated quantitatively to free PSA concentration. A higher free PSA concentration should lead to more extensive nanoparticle aggregation and

larger average nanoparticle size increase. Free PSA in the concentration range from 0.1 ng/mL to 10 ng/mL was detected by this one-step and washing-free homogeneous immunoassay.

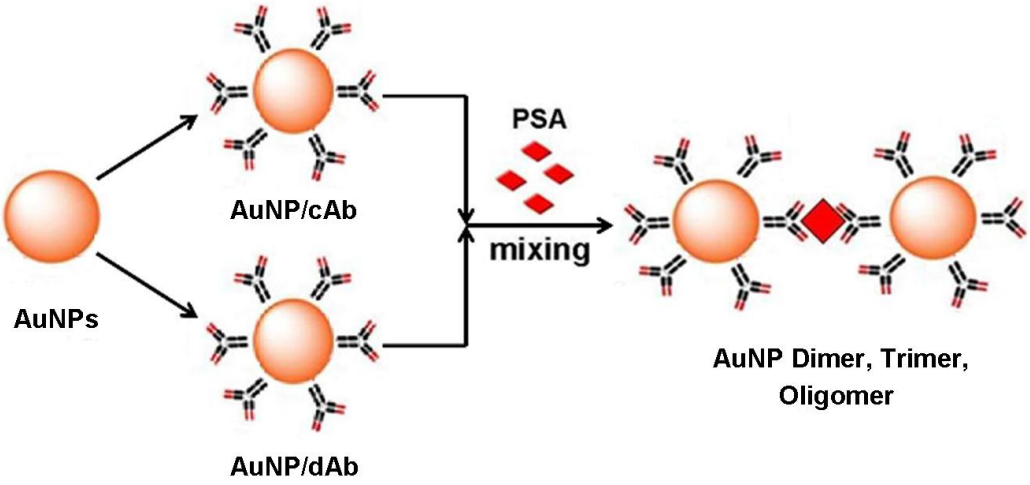

Figure 4-2: A schematic illustration of a homogeneous free PSA immunoassay using PEG-stabilized AuNP/antibody conjugates as the optical probes coupled with DLS measurement**.**

Howerver, the colloidal stability of AuNP/antibody conjugates has been a major problem that limits their further application in bioassay. Especially for the nanoparticle aggregation-based homogeneous immunoassay, it should be assured that the particle aggregation is caused by the specific antibody-antigen binding, not due to the change of salts concentration or other conditions. The nanoparticle-antibody conjugates in the reported procedure were prepared by the simple physical adsorption of antibody on the surface of citrate-stabilized AuNPs through electrostatic interaction.[35, 36] However, the electrostatic nonspecific absorption is not robust and can be easily disrupted at high ionic strength or other conditions. This problem is detrimental to the biological application development of AuNPs, which almost exclusively requires nanoparticle probes be used in high salt content buffer solutions.

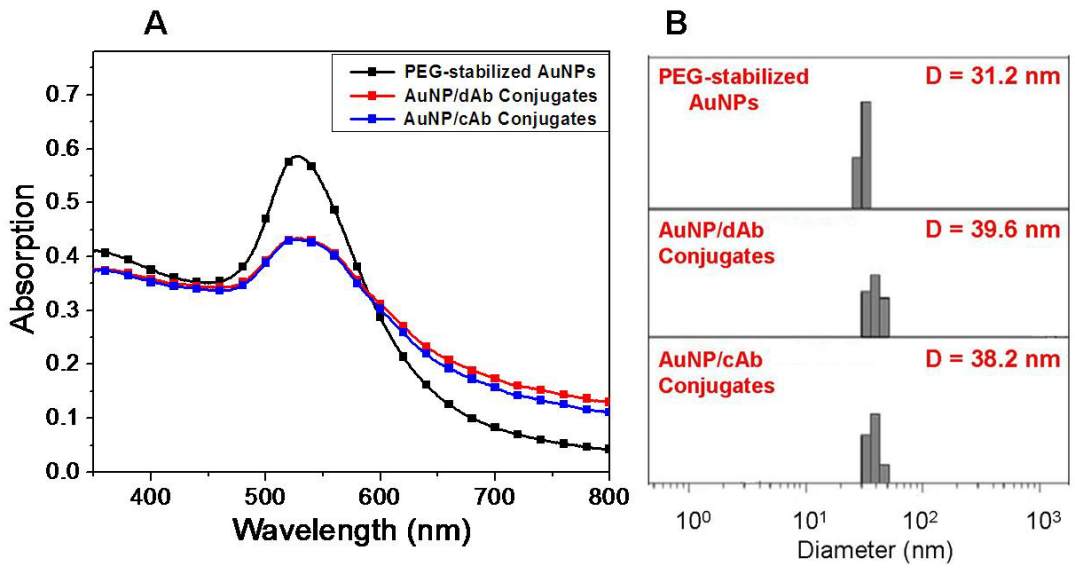

Figure 4-3: UV-vis absorption spectra (A) and DLS measurement (B) of PEG-stabilized AuNPs before and after anti- free PSA antibody conjugation.

To address this problem, in this work, robust PEG-stabilized AuNPs were used as optical probes to detect free PSA cancer biomarker. The thiol bifunctional PEG was first surface functionalized onto the citrate-stabilized AuNPs to improve its stability in electrolytic environment. The PEG coating serves as a protective layer to prevent particles aggregation and minimize nonspecific protein adsorption. The terminal carboxylic acid group on nanoparticle surface allows us to provide anchor points for further covalent conjugation with the amine groups from the antibody. Both anti- free PSA capture (cAb) and detector (dAb) antibody were convalently conjugated to the PEG-stabilized AuNPs through amide bond formation in the presence of EDC and Sulfo-NHS activation agents. After removing the excess antibody using centrifugation, the AuNP/PSA antibody conjugates were first characterized by UV-vis absorption spectroscopy. Figure 4-3A shows the UV-vis absorption spectra of PEG-stabilized AuNPs before and after coupling with PSA antibody. The PEG-stabilized AuNPs were initially a

pinkish red color with a characteristic SPR absorption peak at 520 nm. Upon conjugating with PSA antibody, the SPR band of the AuNPs did not shift to longer wavelength. However it became broadened slightly. This change is most likely caused by the surface chemistry change of the particles from a PEG layer to an antibody layer. The attachment of PSA antibody on the particle surface caused the change of the dielectric constant surrounding the AuNP core. A similar SPR spectrum change has been observed when ScFcv antibody was adsorbed on the surface of citrate-stabilized AuNPs.[37] The apparent decrease in intensity of the SPR band after conjugating with PSA antibody is due to a decrease in particle concentration during the centrifugation and washing cycles. DLS analysis results as shown in Figure 4-3B indicate that the average diameter of AuNPs increased slightly from 30.2 nm to 39.6 nm for dAb- and 38.2 nm for cAb-AuNP conjugates. A narrow particle size distribution was observed suggesting that there was no significant particle aggregation during conjugation with PSA antibody. Therefore, both UV-vis absorption and DLS analysis indicate that the anti- PSA antibody was successfully attached to AuNP surface and the conjugates remained well dispersed in the aqueous solution.

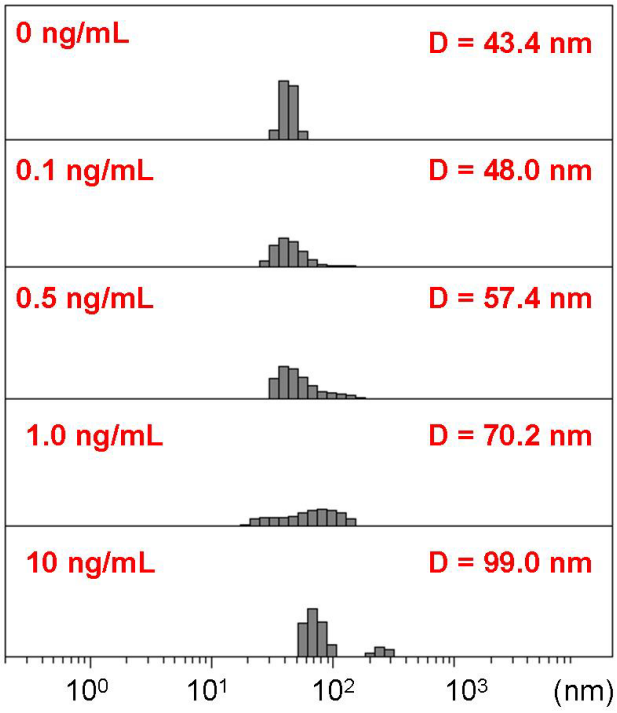

Figure 4-4: The average diameter of AuNPs determined from DLS measurement in the presence of different free PSA concentration.

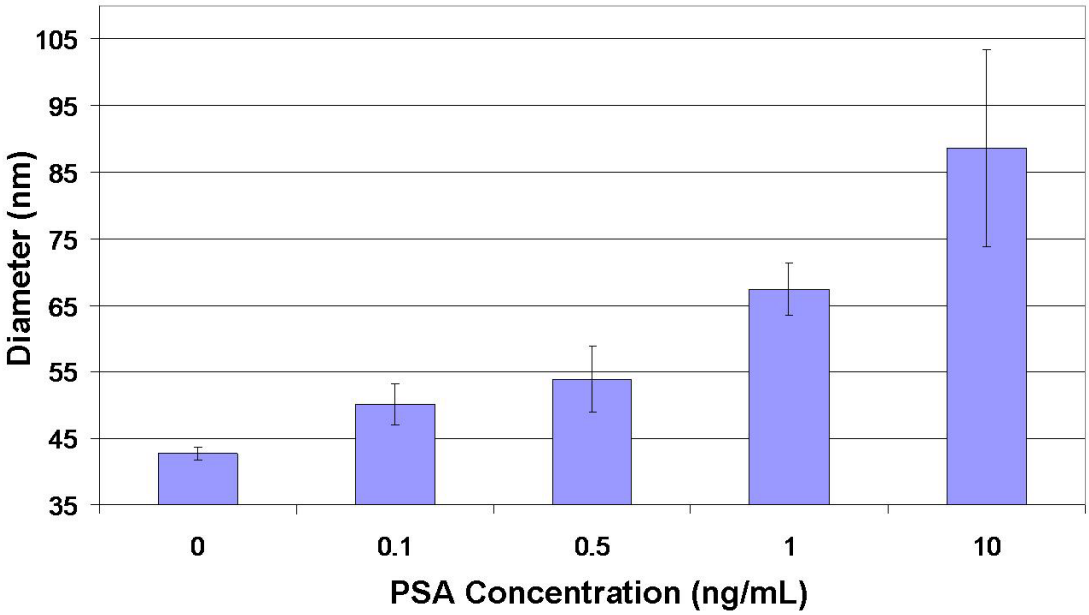

Figure 4-5: the average diameters of AuNPs as determined from DLS measurement and plotted against the PSA concentration.

The homogeneous immunoassay of free PSA was then conducted in solution using the AuNP/PSA antibody conjugate probes. The two conjugate probes (AuNP/dAb and AuNP/cAb) were mixed in a 1:1 ratio and then added to the standard free PSA solutions with different concentrations. After incubating for 1 hour, the solutions were diluted to appropriate concentrations for DLS analysis directly. It should be mentioned that the standard free PSA solutions, including the control solution, are actually prepared in a protein matrix solution to simulate the protein content of human serum samples. Figure 4-4 shows the average particle size of AuNP probes in the presence of free PSA concentration from DLS measurement. Figure 4-5 is the plot of average particle size against the PSA concentration from 0 to 10 ng/mL. With increased concentration of free PSA, the average particle sizes increased due to the formation of nanoparticle dimers, trimers and oligomers through the formation of antibody-antigen-antibody linkage in solution. In a control sample where the two AuNP/PSA antibody probes were added to the sample solution with 0 ng/mL free PSA, a certain level of nanoparticle oligomer formation with an average particle size of 43.4 nm was observed. The aggregation is most likely caused by the high content of proteins and high ionic strength of the matrix solution. At 0.1 ng/mL of PSA sample solution, the average particle size increased to 48.0 nm with a slight increase of particle size distribution. At 1 ng/mL of PSA sample solution, the average particle size increased to 70.2 nm. The particle size distribution also broadened significantly suggesting that the whole nanoparticle population now should include individual AuNP, nanoparticle dimers, trimers, and oligomers formed due to antibody-antigen binding. When the PSA concentration was further increased to 10 ng/mL, the average particle size increased to 99.0 nm. It was observed that the original peak around 30 nm from the individual AuNP was completely disappeared. A major

peak expanding from 50 to 100 nm was observed from DLS measurement indicating that the AuNP probes have been mostly converted to oligomers. Additionally, a small peak over 200 nm revealed that a small portion of AuNPs formed a larger NP aggregates due to high PSA concentration. These results indicate that the PSA concentration could be determined by monitoring antibody-antigen binding complex induced- particle aggregation as we initially suggested. The detection limit of this assay was estimated to be around 0.1 ng/mL, which is comparable with other immunological methods such as ELISA. Most recent results obtained in our group demonstrated that the lower limit of detection may be further decreased to 1 pg/mL of protein. Currently, we are working on the direct analysis of PSA biomarkers from human serum samples.

4.3.2 : Target DNA Assay

In recent years, considerable attention has been focused on the use of AuNP labels for target DNA detection.[11, 12] In this work, we used the DLS readout system to detect the DNA hybridization-induced particle aggregates, and then correlated the particle size information with the target DNA concentration. A one-step homogeneous detection of target DNA using AuNP probes is illustrated in Figure 4-6.[38]

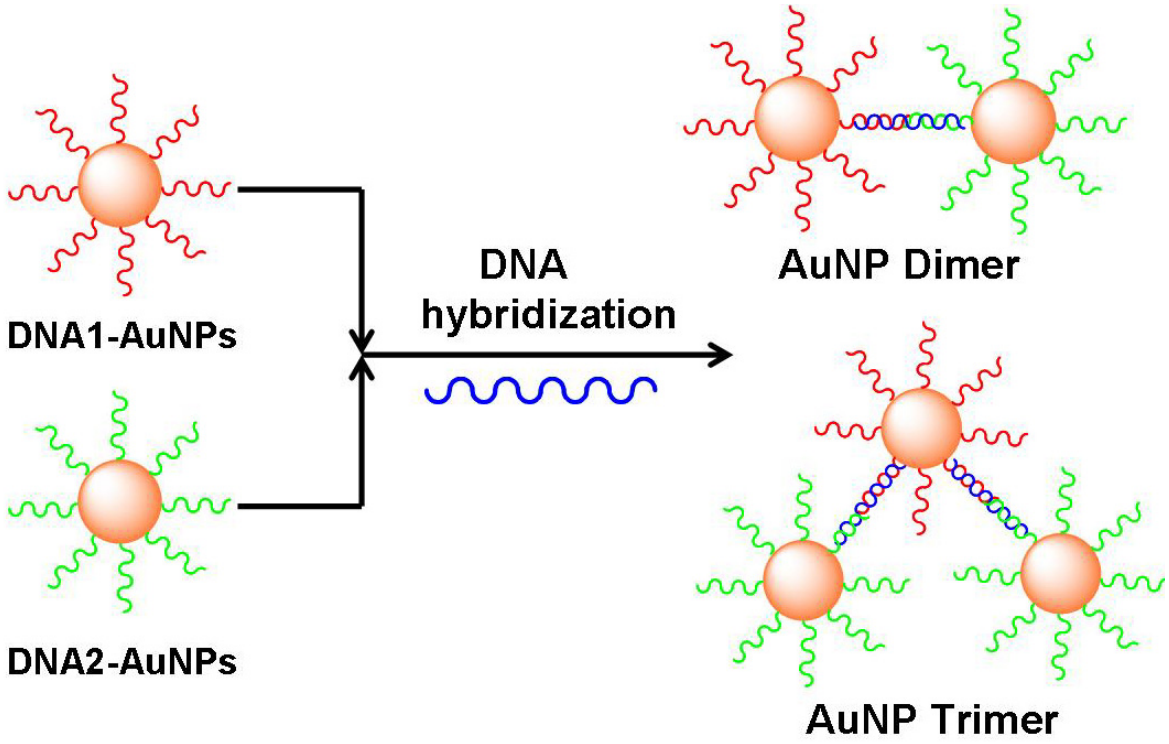

Figure 4-6: A Schematic illustration of a target DNA assay using AuNP probes.

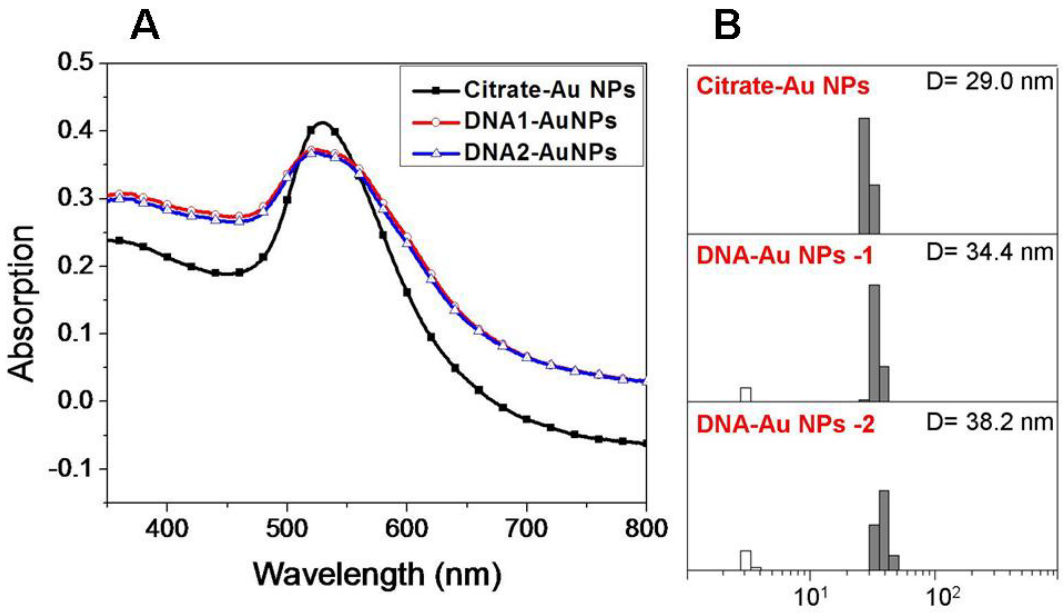

Figure 4-7: UV-Vis absorption spectra (A) and DLS measurement (B) of 30 nm citrate-stabilized AuNPs before and after conjugating with DNA probes.

Two thiol-functionalized DNA probes as previously used in the work by Mirkin et al., were conjugated to the citrate-stabilized AuNPs with a core diameter of 30 nm through thiol place exchange reaction.[39] The successful attachment of DNA probes on the particle surface was confirmed from the significant improvement of particle stability in high salt content solution although the exact number of DNA probes attached to each individual nanoparticle has not been determined yet.[40] It has been observed previously that the citrate-stabilized AuNPs were only stable in a buffer solution with a NaCl concentration less than 20 mM. In contrast, the DNA probe-modified AuNPs remained to be well-dispersed in a buffer solution containing 200 mM NaCl from UV-vis absorption spectrum measurement. As revealed from the UV-Vis absorption spectra of AuNPs before and after conjugating with DNA probes in Figure 4-7A, the SPR band of the AuNPs remained at 520 nm after conjugating with two DNA probes. DLS measurement was used to monitor the size change of AuNPs after conjugating with the two DNA probes. As shown in Figure 4-7B, the hydrodynamic diameter of the nanoparticles increased slightly from 29.0 nm to 34.4 nm for DNA1-AuNP and 38.2 nm for DNA2-AuNP, respectively. The DLS data also revealed a very narrow size distribution of AuNPs before and after DNA modification. No additional larger particles or particle aggregates are observed according to DLS analysis.

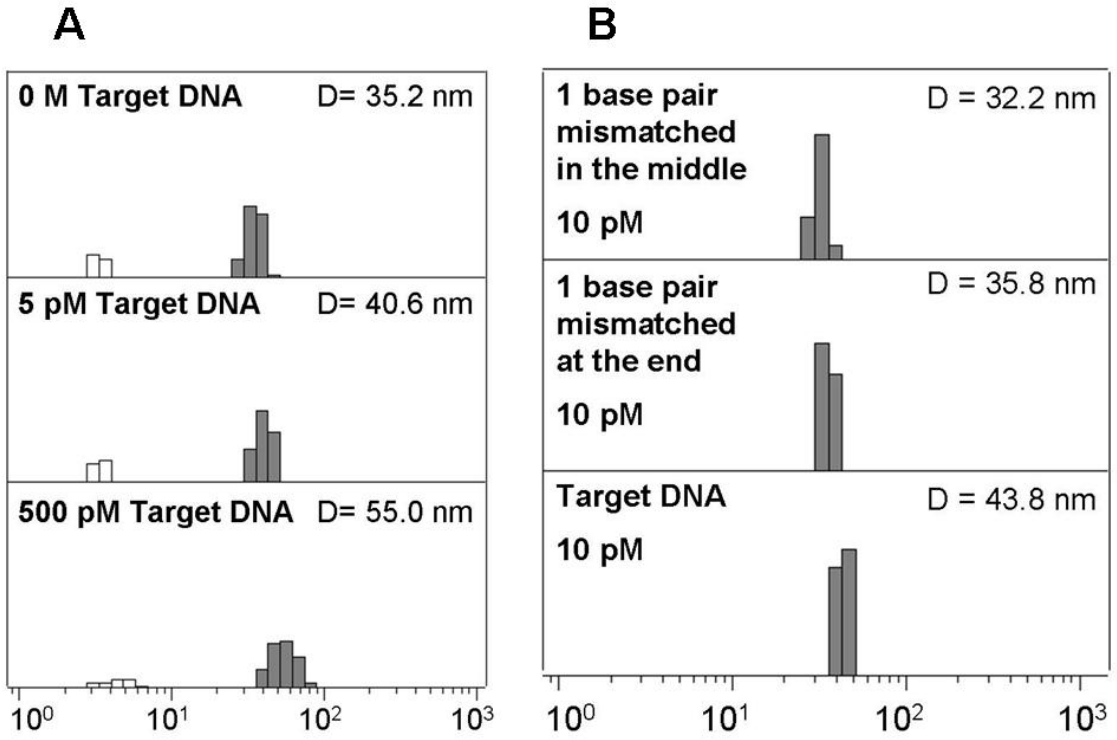

Figure 4-8: The size and size distribution (in diameter, nm) of DNA-AuNP assay solution in the presence of perfectly matched target DNAs (A), and single base pair mismatched DNAs at concentration of 10 pM (B).

For target DNA detection, a 1:1 mixture solution of the two DNA-AuNP probes at a concentration of 100 pM was added to a set of target DNA solutions with a concentration ranging from 5 pM to 5 nM. The mixed solution was incubated for 5 min at 70°C and then allowed to cool down to room temperature and set for 2 hours. The solution was then diluted 100 fold for DLS measurement. As shown in Figure 4-8A, the average size of AuNPs in the control sample with 0 M target DNA in solution is around 35.2 nm. In a sample solution containing 5 pM target DNAs, the average nanoparticle size increased to 40.6 nm. The whole nanoparticle population now should contain the individually dispersed DNA-AuNP probes, nanoparticle dimers, trimers and oligomers formed due to hybridization between target DNA and DNA

probes. The DNA hybridization not only caused the average nanoparticle size increase, but also a wider size distribution of the particle population. With increased concentration of target DNAs, the average nanoparticle hydrodynamic diameter increased accordingly. Figure 4-9 is a plot of the average particle size over the target DNA concentration from 5 pM to 5 nM. The detection limit is estimated to be 1 pM. The assay exhibits excellent intra-assay reproducibility, as judged from the small standard deviation of each sample. At the highest concentration of target DNA, 5 nM, the deviation is quite large. This is because the ratio of target DNA exceeded the probe DNA concentration substantially, approximately 50:1, leading to extensive formation of large aggregates.

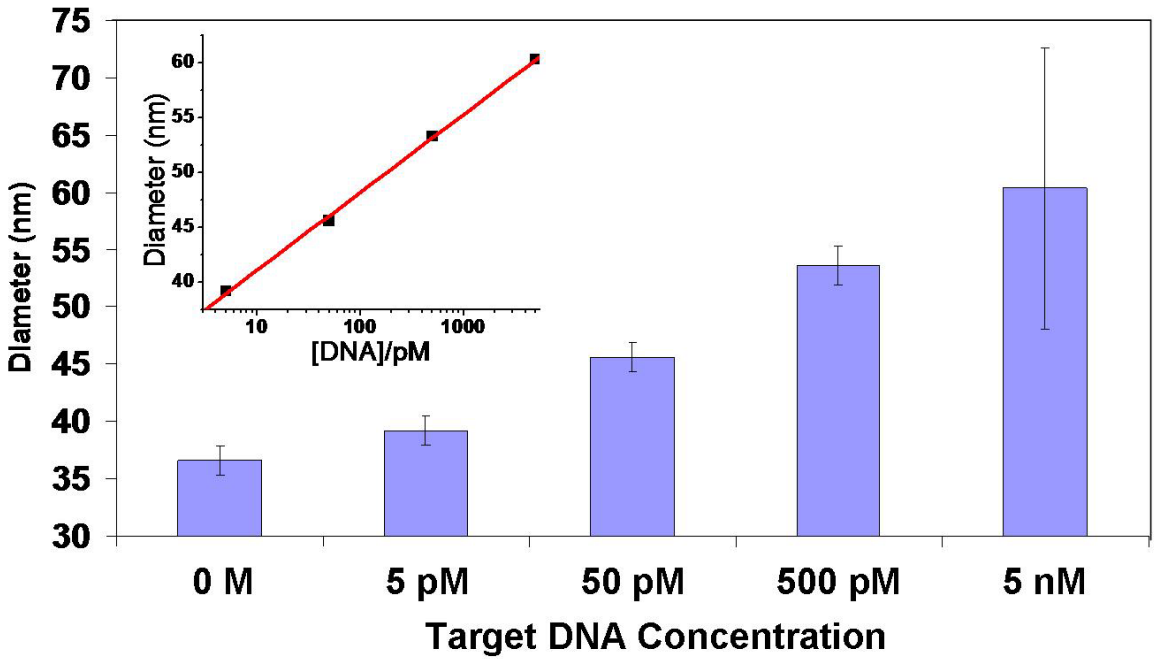

Figure 4-9: the average diameters of AuNPs as determined from DLS measurement and plotted against the target DNA concentration.

To examine the selectivity of the AuNP-based homogeneous assay, we conducted a comparison study on single base pair-mismatched DNAs from perfectly matched DNA targets. Two types of mismatched DNA targets were studied: one with a mismatched pair located the end and one with a mismatched pair in the middle of the target DNA sequence. Under the exact same assay conditions, DLS analysis revealed less degree of nanoparticle aggregation when the target DNA has a single mismatched base pair, judging from the hydrodynamic diameter of the nanoparticles as shown in Figure 4-8B. This single base pair mismatch study was conducted at a target DNA concentration of 10 pM. The result demonstrates the capability of our new assay to sensitively discriminate single base pair-mismatched DNAs from perfectly matched target DNAs, without using on the melting transition of DNA-nanoparticle aggregates as required by the reported literatures.[39]

Other than dynamic light scattering detection, several other scattering-based detection techniques have been utilized for DNA assay with improved sensitivity. A "spot-and-read" colorimetric detection method has been developed to identifying DNA sequences.[41] The hybridization solution samples were spotted onto a glass slide which is illuminated with white light in the plane of the slides. The evanescent wave- induced scattered light from AuNP is visually observed, and the individual 40- to 50- nm diameter AuNP probes scatter green light, whereas AuNP oligomers scatter yellow to orange light due to the plasmon band red-shift. This method achieved a remarkable sequence specificity that allowed discrimation of single-base mismatches. However, this method is still based on the heterogeneous assay format and involves multiple washing and incubation cycles. Also, it has been reported by Liu C.-H. et al. that the linear light scattering by AuNPs can be detected directly by a fluorescence spectrometer

equipped with a 150- W high pressure Xenon lamp and further used for quantitative DNA detection.[42] However, we did not find a clear correlation between the average scattered light intensity versus target concentration in solution from DLS measurement. The average particle diameter as determined by DLS measurement appears to provide a more accurate bioassay.

In addition to the linear light scattering techniques, recently, the nonlinear light scattering technique, such as hyper- Rayleigh scattering, has been used to detect target DNA and one base pair mismatched DNA using AuNP probes.[43] The DNA hybridization leads to particle aggregation and the hyper Rayleigh scattering intensity increases tremendously with the increase of average particle size. A detection limit of 1 nM was achieved by measuring the hyper Rayleigh scattering intensity, while the DLS-based detection gave a detection limit of 1 pM. Also, the pulsed laser used in the hyper Rayleigh scattering assay can cause the fusion of AuNPs, and decrease the sensitivity due to the photothermal effect of AuNP under laser irradiation. The complicated nonlinear experimental setup further limits their applications in high throughput screening and portable conditions.

It is important to mention here that the UV-Vis absorption spectra of the diluted assay solution were undetectable due to the extremely low concentration of AuNP probes. The sensitivity of the DLS-based DNA detection method is already three orders of magnitudes higher than that of UV-Vis absorption method. This detection limit can be improved by orders of magnitude through many possible approaches such as matching the laser wavelength of the DLS instrument with the SPR of AuNPs and their aggregates, or nanoarticles with larger scattering cross sections. According to a theoretical calculation by El-Sayed et al., by increasing the AuNP

size to 80 nm, the scattering efficiency of the nanoparticle can increase dramatically.[16] This indicates that there is plenty of room for improvement of the sensitivity of the new bioassay.

4.4 : Conclusions

In conclusion, we developed a promising one-step homogeneous sandwich assay for biomolecular detection. By taking advantage of the large scattering cross section of AuNPs and the high sensitivity of DLS measurement, protein biomarkers and target DNAs can be detected at very low concentrations (low pM range) using AuNP probes. As opposed to the traditional plate-based assay, our assay is conducted in solution which allows a much better mixing to form complex binding. The assay does not involve any washing cycle and the assay result can be read as soon as the nanoprobe-sample incubation is completed. Moreover, extremely small amount of samples are needed for the assay. With further improvement on the stability of nanoparticle bioconjugates and the light scattering intensity of nanoparticle probes, the accuracy and detection limit of the assay can be further improved. The long term goal of this project is to develop a low cost and automated DLS assay system that can be used by general publics for routine testing of their cancer-related biomarker levels from a single drop of blood sample taken from a fingertip.

4.5 : List of References

1: Etzioni, R.; Urban, N.; Ramsey, S.; McIntosh, M.; Schwartz, S.; Reid, B.; Radich, J.; Anderson, G.; Hartwell, L. *Nat. Rev. Cancer* **2003**, 3, 243.

2: Sander, C.; *Science* **2000**, 287, 1977.

3: Sidransky, D. *Nat. Rev. Cancer* **2002**, 2, 210.

4: Lequin, R. *Clin. Chem*. **2005**, 51, 2415.

5: Yu, F.; Persson, B.; Lofas, S.; Knoll, W. *Anal. Chem*. **2004**, 76, 6765.

6: Healy, D. A.; Hayes, C. J.; Leonard, P.; McKenna, L.; *Trends Biotechnol*. **2007**, 25, 125.

7: Das, J.; Aziz, M. A.; Yang, H.; *J. Am. Chem. Soc*. **2006**, 128, 16022.

8: Warnick, G. R.; Nauck, M.; Rifai, N. *Clin. Chem*. **2001**, 47, 1579.

9: Weigum, S. E.; Floriano, P. N.; Christodoulides, N.; McDevitt, J. T. *Lab Chip* **2007**, 7, 995.

10: Rosi, N. L.; Mirkin, C. A. *Chem. Rev*. **2005**, 105, 1547.

11: Duggan, D. J.; Bittner, M.; Chen, Y.; Meltzer, P.; Trent, J. M. *Nat. Genet*. **1999**, 21, 10.

12: Tyagi, S.; Kramer, F. R. *Nat. Biotechnol*. **1996**, 14, 303.

13: Penn, S. G.; He, L.; Natan, M. J. *Current Opinion in Chemical Biology* **2003**, 7, 609.

14: Jin, R.; Cao, Y.; Hao, E.; Metraux, G. S.; Schatz, G. C.; Mirkin, C. A.; *Nature* **2003**, 425, 487.

15: Schultz, D. A. *Current Opinion in Biotechnology* **2003**, 123, 5164.

16: Yguerabide, J.; Yguerabide, E. E. *Anal. Biochem*. **1998**, 262, 137.

17: Rosenzweig, Z.; Kim-Thanh, N. T.; *Anal. Chem*. **2002**, 74, 1624.

18: Jin, R.; Cao, Y.; Hao, E.; Metraux, G. S.; Schatz, G. C.; Mirkin, C. A. *Nature* **2003**, 425, 487.

19: Elghanian, R.; Storhoff, J. J.; Mucic, R. C.; Letsinger, R. L.; Mirkin, C. A. *Science* **1997**, 277, 1078.

20: Reynolds, R. A.; Mirkin, C. A.; Letsinger, R. L. *J. Am. Chem. Soc*. **2000**, 122, 3795.

21: Taton, T. A.; Mirkin, C. A.; Letsinger, R. L. *Science* **2000**, 289, 1757.

22: Taton, T. A.; Mirkin, C. A.; Letsinger, R. L. *J. Am. Chem. Soc*. **2001**, 123, 5164.

23: Cao, Y. C.; Jin, R.; Nam, J. M.; Mirkin, C. A. *J. Am. Chem. Soc.* **2003**, 125, 14676.

24: Nam, J. M.; Mirkin, C. A. *Science*, **2003**, 301, 1884.

25: Berne, B. J.; Pecora, R. *Dynamic light scattering: with applications to chemistry, biology, and physics*; Wiley: New York, **1976**.

26: Yao, B.; Collins, B.; Chen, M. *Drug Plus Int*. **2005**, 4, 21.

27: Zhang, C. X.; Wang, X.; Tang, Z. M.; Lu, Z. H. *Anal. Biochem*. **2003**, 320, 136.

28: Du, B.; Li, Z.; Cheng, Y. *Talanta* **2008**, 75, 959.

29: Liu, X.; Yuan, H.; Pang, D.; Cai, R. *Spectrochimica Acta Part A* **2004**, 60, 385.

30: Jiang, Z.; Sun, S.; Liang, A.; Liu, C. *Anal. Chim. Acta* **2006**, 571, 200.

31: Jiang, Z.; Sun, S.; Liang, A.; Huang, W.; Qin, A. *Clin. Chem*. **2006**, 52, 1389.

32: Hou, M.; Sun, S.; Jiang, Z. *Talanta* **2007**, 72, 463.

33: Jiang, Z.; Huang, Y.; Liang, A. *J. Fluoresc*. **2008**, 18, 563.

34: Xie, H.; Gill-Sharp, L. K.; O'Neal, D. P. Nanomed.: *Nanotechnol., Biol., Med*. **2007**,

3, 89.

35: Liu, X.; Dai, Q.; Austin, L.; Coutts, J.; Knowles, G.; Zou, J.; Chen, H.; Huo, Q. *J. Am. Chem. Soc*. **2008**, 130, 2780.

36: Huang, X. H.; El-Sayed, I. H.; Qian, W.; El-Sayed, M. A. *J. Am. Chem. Soc*. **2006**, 128, 2115.

37: El-Sayed, I. H. *Nano. Lett*. **2005**, 5, 829.

38: Dai, Q.; Liu, X.; Coutts, J.; Austin, L.; Huo, Q. *J. Am. Chem. Soc*. **2008**, 130, 8138.

39: Jin, R.; Wu, G.; Li, Z.; Mirkin, C. A.; and Schatz, G. C. *J. Am. Chem. Soc*. **2003**, 125, 1643.

40: Hurst, S. J.; Abigail, K. R.; Mirkin, C. A. *Anal. Chem*. **2006**, 78, 8318.

41: Storhoff, J. J.; Lucas, A. D.; Garimella, V.; Bao, Y.; Muller, U. R. *Nat. Biotech*. **2004**, 22, 883.

42: Du, B. A.; Li, Z. P.; Liu, C. H. *Angwe. Chem. Int. Ed*. **2006**, 45, 8022.

43: Ray, P. C. *Angew. Chem. Int. Ed*. **2006**, 45, 1151.

CHAPTER 5 : PHOTOTHERMAL ABLATION OF PEPTIDE AGGREGATES USING GOLD NANOPARTICLES

5.1 : Introduction

Gold nanoparticles (AuNPs) have recently attracted much attention for applications in photothermal therapy due to their efficient photon-thermal conversion properties.[1] The absorption coefficient of AuNPs with a diameter of 40 nm at the SPR band is 5 orders of magnitude higher than those of traditional organic dyes.[2] The photon-thermal conversion efficiency increases significantly when AuNPs are irradiated at a wavelength that matches the SPR absorption band of AuNPs. These unique properties of AuNPs are currently explored for therapeutic applications such as photothermal destruction of cancer cells, tumors, and bacteria.[3, 4, 5, 6, 7] When AuNPs are incorporated or incubated with cells or tissues and then irradiated with laser at a wavelength around the SPR band, the thermal energy generated by the AuNPs will cause a sharp increase on the local temperature around the AuNPs and thus destroy the surrounding cells or tissues.

Alzheimer's disease (AD) has become the sixth-leading cause of death of old populations around the world. It has been reported that 5 million Americans are living with AD.[8] AD destroys brain cells, causing problems with memory, thinking and behavior severe enough to affect normal work and social life. A key peptide, amyloid peptide (Aβ), and its aggregate formation are believed to play a central role in the pathogenesis of AD since amyloid fibrils predominantly exist in senile plaques in the brain of patients with AD.[9, 10] Aβ is produced by

proteolysis of amyloid β precursor protein and is mostly composed of either 40 or 42 amino acid. Aβ peptides are amphiphilic peptides with a hydrophilic N-terminal domain (residues 1 to 28) and a hydrophobic C-terminal (residues 29 to 40). Aβ peptides can self-assemble together into fibrils initiated by a conformational transition from random coil to β-sheet structure.[11] It has been proved that AD is usually associated with the conversion of the normal soluble Aβ peptide into neurotoxic β-sheet oligomeric structures, which are able to form insoluble amyloid depositing and accumulating in the brain. One possible strategy for AD therapy is to block the early steps of misfolding and aggregation of soluble Aβ peptides.[12, 13, 14, 15] It has been reported that short synthetic peptides, β-sheet breakers are able to specifically bind with Aβ peptides, block and reverse the abnormal conformational change, and prevent the formation of peptide aggregates.[16] However, the use of this short peptides as AD drugs has some disadvantages such as poor blood-brain barrier permeability. Recently, a synthetic 5-amino acid β-sheet breaker peptide (iAβ5p) has been utilitized to inhibit and disassemble amyloid fibrils *in vitro*, and to prevent Aβ neurotoxicity in cell culture.[17, 18] It was observed that iAβ5p was capable of inducing dissolution of preformed plaques in a rat brain model of amyloidosis. This compound showed low toxicity, low immunogenicity, and high solubility. A major disadvantage of this compound is its relative short *in vivo* half-time. Overall, currently there are no effective therapeutic methods and agents for AD.

In this work, we investigated the photothermal ablation of Aβ peptide aggregates using AuNPs as a photo-thermal energy converter.[19] A triethylene glycol (EG_3)-protected AuNPs with a core diameter of 5 nm was synthesized and then surface functionalized with carboxylic acid groups using the solid phase synthesis strategy. The chemical structure of the as-synthesized

EG_3-protected AuNPs with a single carboxyl group attached on the surface is shown in Figure 5-1. The EG_3 protecting layer makes the AuNPs biocompatible by preventing nonspecific peptide and protein adsorption onto the particle surface. After being covalently coupled with a Aβ peptide, the AuNP conjugates were mixed with pure Aβ peptide fragments in solution and then allowed to form peptide aggregates. The aggregates were irradiated with a continuous laser at a wavelength of 532 nm. Both SEM and AFM images revealed that the peptide aggregates were destroyed due to photo irradiation and a crater structure was formed and located selectively at the irradiated point. These results clearly indicated that the Aβ peptide aggregates were thermally ablated through the photothermal effect of AuNPs under laser irradiation.

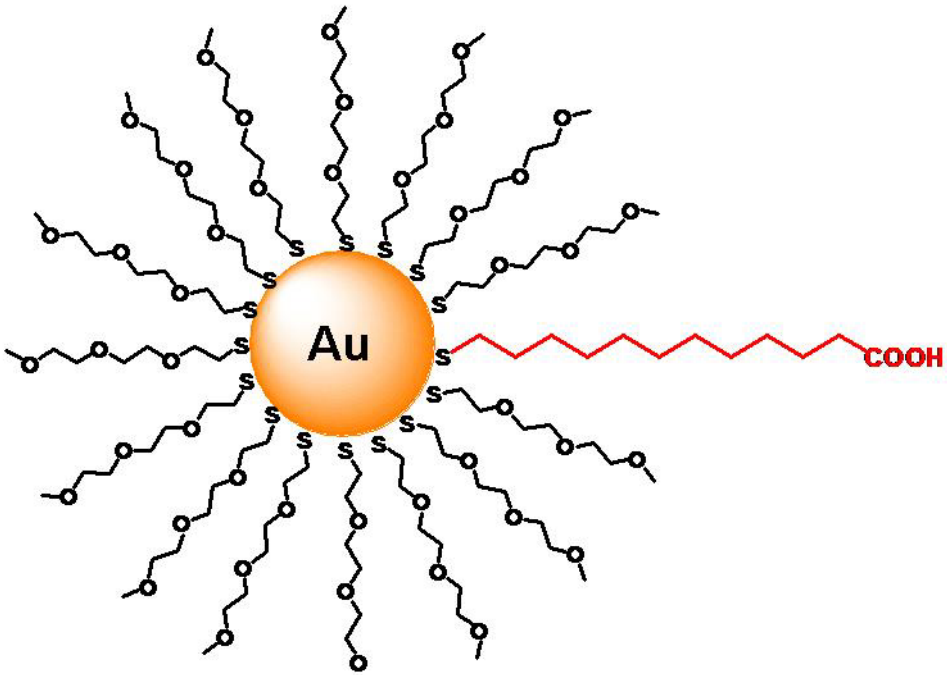

Figure 5-1: The chemical structure of monofunctional EG3-protected AuNPs

5.2 : Experimental Section

5.2.1 : Chemicals and Materials

All the chemicals except the following few were purchased from Aldrich-Sigma (Milwaukee, MI) and used without any further purification. Hydrogen tetrachloroaurate (III) hydrate ($HAuCl_4$) was purchased from Strem Chemicals (Newburyport, MA). Triethylene glycol monomethyl ether was purchased from Fluka. Ultrapure water (18.3 MΩ cm^-) was used throughout the work. The Aβ peptides were kindly provided from Professor Roger M. Leblanc's group at University of Miami.

5.2.2 : Instrumentation and Characterization

UV-vis absorption spectroscopy was recorded on a Cary 300 Bio UV-Visible spectrophotometer. TEM images were obtained from a FEI Tecnai F30 high resolution TEM at 300 Kev. Sample preparation consisted of drop coating AuNPs solution onto carbon-coated copper grids and air-dried. XPS spectrum was recorded on a VG ESCALAB 220i XPS system, which was equipped with a monochromted Al K_α source ($h\gamma$ = 1486.6 Ev) and semi-spherical energy analyzer. The characterization (AFM, SEM etc) of AuNP/Aβ peptide conjugates and their laser ablation were conducted by Dr. Robert C. Triulzi at University of Miami.

5.2.3 : Synthesis

5.2.3.1 : Synthesis of Thiol-functionalized Triethylene Glycol (EG_3-SH)

To a 200-mL round-bottom flask, 19 mL (121 mmol) tri(ethylene glycol) monomethyl ether was added in 30 mL of dry dichloromethane and 7 mL of pyridine solution. The solution

was chilled in an ice bath. 7.6 mL (81 mmol) of phosphorous tribromide (PBr_3) in 50 mL of dry dichloromethane was dropwise added while the solution was being stirred. The mixture solution was then allowed to stir at room temperature for 24 hours. The mixture was filtered through Whatman filter paper to separate the yellow colored solution from the white precipitate. The collected solution was extracted with 50 mL of saturated sodium carbonate solution, twice with deionized water, and finally once with brine. The organic phase was dried over anhydrous magnesium sulfate and filtered through cotton to obtain a yellow oil product (13.04 g).

7.19 g (31.7 mmol) of the above product was mixed with 30 mL dimethylformamide and 25 mL dichloromethane in a 100-mL, pear-shaped flask. The mixture was cooled in an ice bath. 5.4 g potassium thioacetate (47.5 mmol) was added. The solution was stirred in the ice bath for five minutes and then at room temperature for 60 minutes under nitrogen protection. The beige-colored solution was diluted with 100 mL dichloromethane and extracted 3 times with deionized water and once with brine. The organic phase was dried over anhydrous magnesium sulfate, filtered through cotton, and dried using a rotary evaporator. The sample was purified by flash chromatography using silica gel with a particle size of 40-63 μm and pore size of 60 Å. The mobile phase consisted of a solvent mixture of 5:1 petroleum ether to ethyl acetate. TLC of the purified product had an R_f value of 0.1-0.2.

The thiol-functionalized triethylene glycol (EG_3-SH) was obtained by deprotecting the thioacetate groups using a sodium methoxide in methanol solution. To a glass vial, 350 mg of sodium metal was added to 5 mL of methanol to form $NaOCH_3$ in-situ, causing the sodium metal to dissolve. To the protected ethylene glycol ligand, 60 mL of methanol was added and protected with nitrogen. The solution was stirred, and the sodium methoxide solution was added using a

syringe. After being stirred for 24 hours, the solution was neutralized with 3 mL acetic acid, followed by addition of 100 mL chloroform. The solution was washed twice with brine and dried over anhydrous magnesium sulfate, followed by filtration through cotton. The sample was dried and collected as viscous oil.

5.2.3.2 : Synthesis of EG_3-stabilized AuNPs

The EG_3-protected AuNPs were synthesized according to the reported method.[20] Briefly, to a 100-mL Erlenmeyer flask, 22.5 mL of methanol was mixed with 3.75 mL of acetic acid. To the stirred solution, 120 mg (0.3 mmol) of hydrogen tetrachloroaurate (III) hydrate and 23 mg (0.13 mmol) of EG_3-SH ligand, prepared as described above were added. The clear yellow solution was vigorously stirred while 128 mg (3.4 mmol) sodium borohydride in 3.8 mL deionized water was added dropwise. The color turned immediately dark black due to nanoparticle formation. After reacting at room temperature for two hours, the nanoparticle solution was centrifuged at 5000 rpm for 5 min to remove any large precipitates. The remaining solution was evaporated in a rotary evaporator and the nanoparticles were washed with petroleum ether twice to remove small organic molecules and then recollected in dichloromethane.

5.2.3.3 : Monofunctionalization of EG_3-protected AuNPs

The synthesis of monofunctional EG_3-protected AuNPs was prepared using a solid phase exchange method as reported previously.[21] Typically, 11-Mercaptoundecanoic acid (MUA) was immobilized on Amberlite IRA-67 ion-exchange resin in a 400:1 mole ratio (NH_2:MUA) through electrostatic interaction between the tertiary amine groups from the resin and carboxyl groups of

MUA ligands. A typical loading recipe was the following: 3 g of dried ionic resin (NH_2 group density: 3.6 mmol/g) was suspended in 8 mL dichloromethane. Following the addition of 0.03 mmol MUA, the mixture was shaken at room temperature for 12 h. After washing with dichloromethane and drying with a stream of nitrogen flow, the above-synthesized EG_3-protected AuNP solution in dichloromethane/hexane (1:1, v/v) was added to the resin. The place exchange reaction was allowed to proceed for 1 h at room temperature. During this period the resin turned black. The resin was then washed with dichloromethane and hexane until the solution became clear. The nanoparticles were then cleaved from the resin by adding 5 mL of 10% acetic acid in dichloromethane with gentle shaking at room temperature for 10 min. The solution was separated from polymer resin, collected and concentrated to obtain the crude product. The crude product was washed with petroleum ether to remove any free ligands. The nanoparticles were re-dissolved in a solvent mixture of dichloromethane/methanol (4:1, v:v) and purified by size exclusion chromatography (LH-20 gel) using the same solvent.

5.2.3.4 : Synthesis of Monofunctional EG_3-protected AuNP/Aβ Peptide Conjugation

500 μL of 0.5 mg/mL Aβ peptide methanol solution was mixed with 2 mL of 0.5 mg/mL monofunctional EG_3-protected AuNP solution (dichloromethane/methanol, 4:1, v/v). Following the addition of 40 μL DIPCDI, the reaction mixture was gently shaken at room temperature overnight. The product was purified by a size exclusion chromatography (LH-20 sephadex gel) to remove the excess peptides.

5.3 : Results and Discussion

5.3.1 : Synthesis of Thiol-functionalized Triethylene Glycol (EG_3-SH)

Huang, et al. ititially reported the synthesis of thiol-functionalized triethylene glycol ligands (EG_3-SH).[20] This method involves 6 reaction steps and required multiple purification procedures with a low yield. In this work, we developed a modified procedure to synthesize the EG_3-SH ligand as shown in Figure 5-2. This new synthesis can be completed in a shorter period of time with significantly improved yield. The initial step was to brominate the triethylene glycol monomethyl ether using phosphorous tribromide. After reacting with thiol acetate, the product was purified by successive aqueous solution extractions followed by chromatography. The product was found to have an R_f value of 0.1-0.2 while the impurities had an R_f value of 0.9. A sodium methoxide in methanol solution was then used to deprotect the acetyl group to obtain the EG_3-SH. The purified product was first characterized by ^{1}H-NMR (Figure 5-3). The spectrum is consistent with the literature report.[20] The ^{1}H-NMR peak assignment is the following: 1.55 pm (triplet, thiol proton at-SH), 2.7 ppm (quartet, methyl protons at –C2), 3.5 ppm (singlet, methyl protons at -C8), and 3.5-3.7 ppm (multiplet, methyl protons at C3-C7).

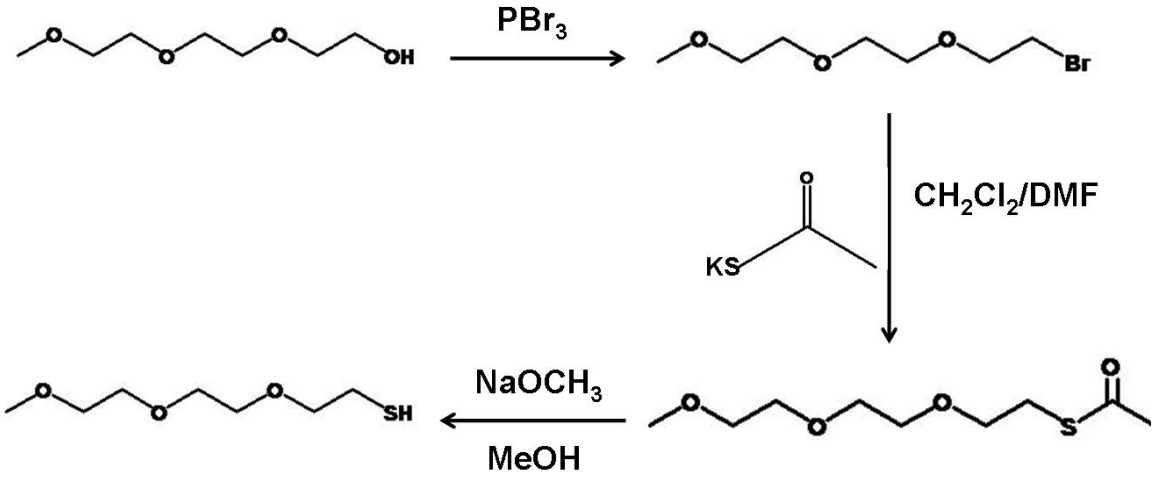

Figure 5-2: A schematic illustration to synthesize the EG3-SH ligand

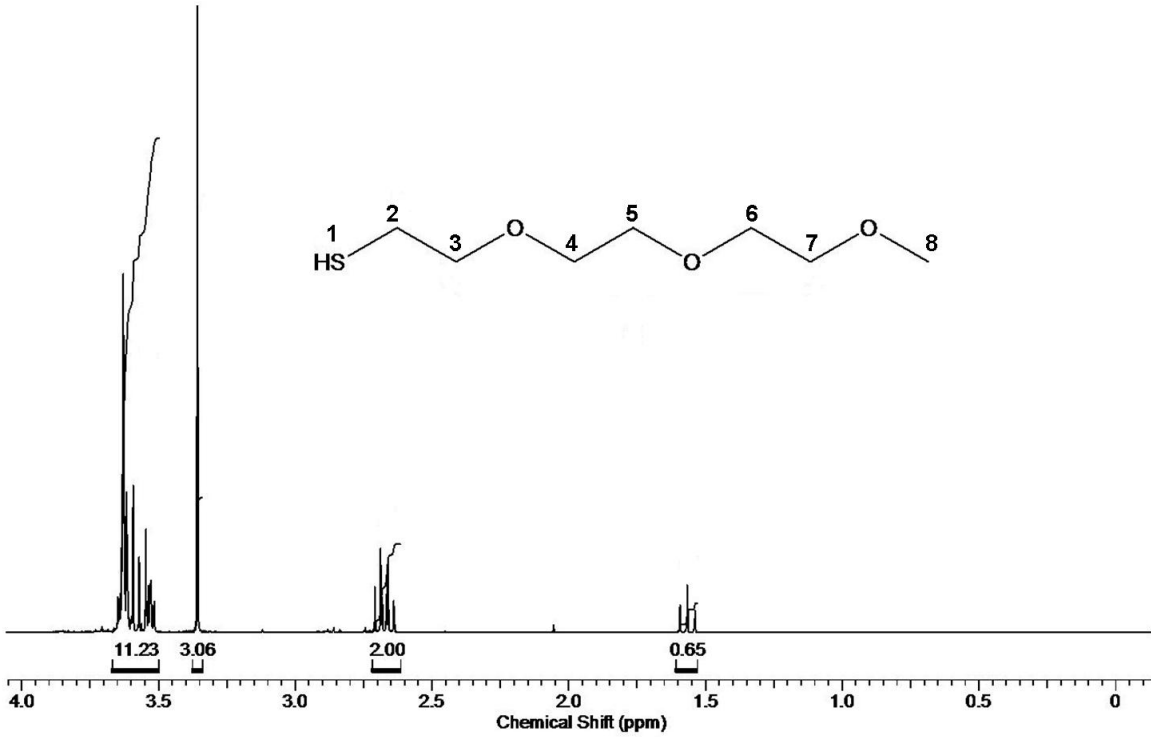

Figure 5-3: ^{1}H-NMR spectrum of the EG_3-SH ligand

5.3.2 : Synthesis and Monofunctionalization of EG_3-protected AuNPs

The EG_3-protected AuNPs was then synthesized by reducing $HAuCl_4$ using $NaBH_4$ in the presence of EG_3-SH ligands according to the literature report.[20] With an appropriately controlled ratio of [$HAuCl_4$]/[EG_3-SH], the as-synthesized particles have an average diameter of 5 nm with a relative narrow size distribution according to TEM analysis as shown in Figure 5-4A. The particles were dispersed uniformly on TEM grids and had good solubility in both aqueous and organic solvent such as chloroform and dichloromethane. This unique solubility of EG_3-protected AuNPs in both polar and nonpolar solvents makes it a good candidate for nanocomposite applications.[22] The 5 nm EG_3-protected AuNPs exhibited a characteristic SPR band around 520 nm as shown in Figure 5-4B. To analyze the nature of the monolayer on the particle surface, FTIR spectra of EG_3-SH ligands before and after attaching to the AuNPs were acquired and compared (Figure 5-5). A strong band at 1100 cm^{-1} is assigned to the symmetric vibration mode of the –C-O-C-, suggesting that the EG_3 ligands were successfully attached on the particle surface. The characteristic peak at 2870 cm^{-1} associated with the asymmetrical stretching mode of $–CH_2-$ group did not change after the ligands were attched to the particle. Additionally, compared to the free EG_3-SH ligands as seen in Figure 5-5A, it is found that the characteristic peak of the free thiol group at 2560 cm^{-1} disappeared after the EG_3-SH ligands were attached to the particle surface due to their conversion into thiolates.

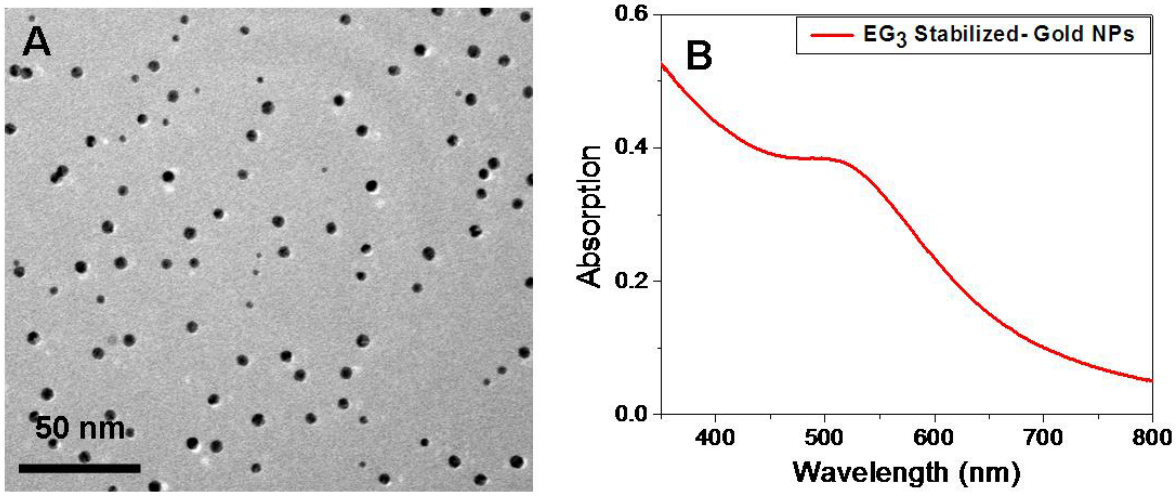

Figure 5-4: A: TEM image of EG_3-protected AuNPs; B: UV-vis absorption spectrum of EG_3-stabilized AuNPs in dichloromethane solution.

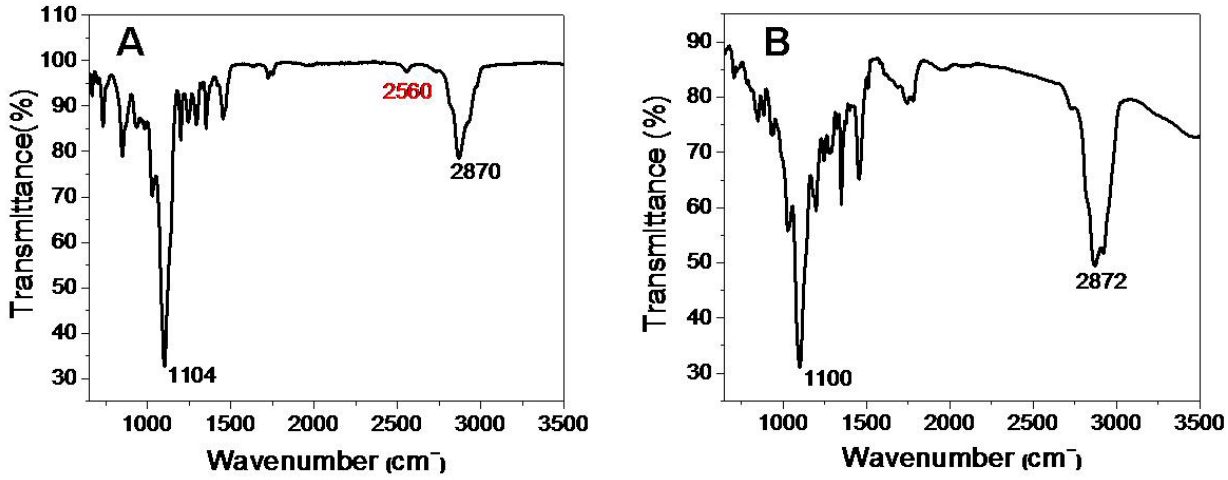

Figure 5-5: FT-IR spectra of EG_3-SH ligands (A) and the EG_3-protected AuNPs (B).

The short triethylene glycol (EG_3) molecule-protected AuNP has several advantages in comparsion to polyethylene glycol (PEG)-protected AuNPs. Small ethylene glycol molecules have well-defined lengths. In contrast, PEG polymer chains form random coil structures on the particle surface.[22] The conformational change of the PEG chain is reflected by its stretching or

retracting, which depends greatly on the polarity of the solvents. Thus, it is difficult to predict the thickness of PEG layer on the particle surface. In addition, small ethylene glycol molecules can form a densely packed monolayer on the particle surface. PEG polymer, on the other hand, forms a loose, random structure on the particle surface. Thus, the small ethylene glycol-protected AuNPs should have a better colloidal stability in complex biofluids than that of PEG-protected AuNPs. Furthermore, a mixed monolayer on the AuNP surface composed of short ethylene glycol molecules and a functional ligand can be easily conjugated with biomolecules. In contrast, for a coiled PEG polymer-covered AuNP, a functional ligand on the particle surface is usually buried or blocked in the polymer coil structures, which preclude further conjugation with biomolecules. Therefore, a short ethylene glycol monolayer-protected AuNPs is more suitable for conjugating with biomolecules.

Following the synthesis of EG_3-protected AuNPs with a relatively narrow size distribution, a solid phase place exchange method was used to surface functionalize the EG_3-AuNPs with controlled number of carboxylic acid groups.[21] This method differs slightly from the previous covalent bond-based solid phase synthesis. The solid support used in this study was the ionic exchange resins with positive charged amine groups on the surface. The bifunctional thiol ligands, 11-mercaptoundecanoic (MUA), were first loaded onto the resin beads through electrostatic interaction between the positively charged amino groups from the resin beads and the negatively charged carboxylic acid groups from the MUA ligands. The loading ratio of the amino groups to the thiol ligands was relatively high to ensure that only one thiol ligand will be exchanged with one EG_3-protected AuNPs during the following place exchange reaction. After loading the thiol ligands into the resin beads and washing away any unbound thiol molecules.

The surface-bound thiol groups underwent the place exchange reaction with EG_3-protected AuNP. The resin beads turned into black in color after 1 hour gentle shaking at room temperature. After washing off any unbound nanoparticles, those EG_3-AuNPs bound to the resin beads were cleaved using 5% acetic acid solution in dichloromethane for 10 min. The crude product was purified by washing with petroleum ether, followed by SEC purification. Since the EG_3-protected AuNPs were not covalently bonded to the resin beads, the cleavage step could be completed using relatively mild conditions in a much shorter period of time compared to previous work using covalent-bond-based solid phase synthesis.[24] A 5% acetic acid solution could cleavege the particle from the resin beads without destroying the ethylene glycol monolayer on the particle surface. To confirm that only one or a very limited number of carboxyl acid groups were present on the particle surface, a diamine coupling reaction was conducted on the obtained nanoparticle product and the coupling product was analyzed by TEM. One can observe from Figure 5-6A that the majority of the coupled product is particle dimers with a small percentage of individual particles and particle oligomers. This suggests that monofunctional AuNPs are the major product along with a small percentage of particles containing a few limited number of carboxyl groups on the surface.

Several methods have reported to conjugate the peptides to the surface of AuNPs.[25, 26, 27] Recently, it has been reported by Kogan et al that the Aβ peptide was conjugated on citrate-protected AuNPs through the formation of Au-S bonding.[28] The synthesized Aβ peptide has a cystein residue, which contains a thiol group allowing a strong interaction with AuNP surface. However, the stability of citrate-protected AuNPs decreases significantly in high salt content solutions due to the screening charge effect.[29] The addition of peptide into citrate-protected

AuNPs causes AuNP aggregation and decreases the coverage density of peptide attached on AuNP surface. In this work, Aβ peptides were conjugated to the as-synthesized monofunctional EG_3-protected AuNPs through a one-step *in situ* amide coupling reaction in the presence of DIPCDI activated agent. After eliminating the unreacted Aβ peptides using SEC (LH-20 sephadex gel), the EG_3-protected AuNP/Aβ peptide conjugates were characterized with X-ray photoelectron spectroscopy (XPS). As shown in Figure 5-6B, a weak nitrogen peak was observed on the XPS spectrum of the conjugates but was lacking from the unconjugated AuNPs. Since unreacted Aβ peptides were removed by SEC purification, therefore, it is reasonable to believe that the N signal from XPS analysis should come form the Aβ peptide covalently attached onto the particle surface.

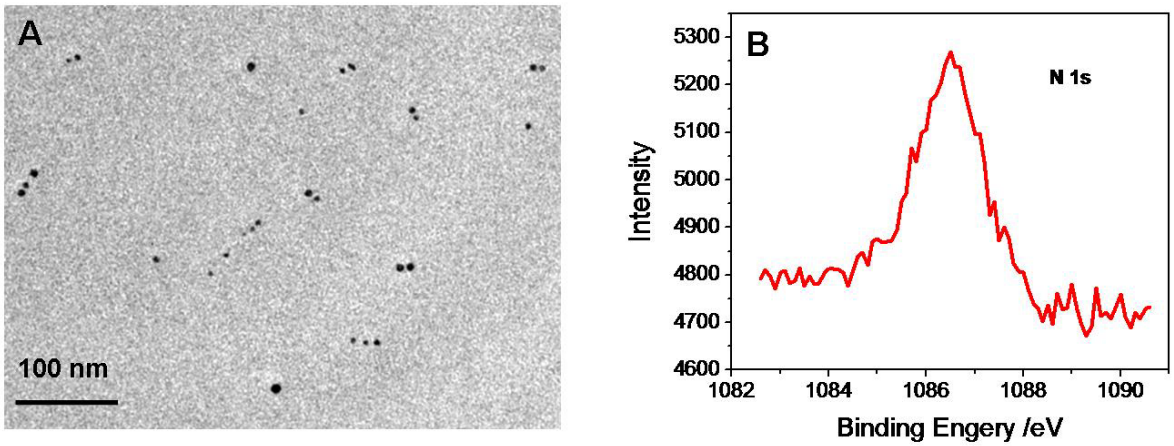

Figure 5-6: A: TEM image of diamine coupling product of the monofunctional EG_3-protected AuNPs; B: XPS spectrum of nitrogen 1S peak from the monofunctional EG_3-protected AuNP/Aβ peptide conjugates.

5.3.3 : Monofunctional EG_3-protected AuNP/Aβ Peptide Aggregation

It is known that the monomeric state of Aβ peptide can spontaneously self-assemble into oligomers, protofibrils, and amyloid fibrils.[30] This self-assembling process is in equilibrium

between soluble peptide monomer and increasingly larger insoluble fibrils. The peptpide aggregates would precipitate out of solution and force the equilibrium shift towards aggregate form. Vigorous shaking and sonication, high hydrostatic pressure, and temperature cycling have the effect of reversing the natural equilibrium and redissolving the aggregates.[31, 32, 33] The structure of the Aβ peptide aggregates has been analyzed by X-ray diffraction, and solid- state NMR spectroscopy. These data suggest that the peptide fibrils are composed of antiparallel β sheets structure.[34]

In this work, the AuNP/Aβ peptide conjugates were mixed with pure Aβ peptides and then incubated at 37ºC for 24 h. During the incubation fibrils starts growing and slowly form precipitates. The morphology of the Aβ peptide aggregates was initially characterized using an epifluorescence microscopy. The images were obtained by spreading the peptide solution on quartz substrate using Congo red staining. A random distribution of peptide aggregate structure was observed from pure Aβ peptide sample (Figure 5-7A). The epifluorescence image of the monofunctional EG_3-protected AuNP/Aβ peptide conjugates as shown in Figure 5-7B is apparently different from that of pure peptides. The randomly interwined fibrillary structures could be clearly seen under the same resolution. The microstructures of the peptide aggregates were further investigated using SEM technique. Figure 5-8A shows the SEM image of pure Aβ peptide aggregates. One can see clearly that the peptide aggregates have a non-uniform morphology with an average diameter of around 2 μm. In contrast, the monofunctional EG_3-protected AuNPs/Aβ peptide aggregates in Figure 5-8B exhibited a much more uniform aggregated fibrillary structure, which is consistent with what was observed from the epifluorescence microscopy.

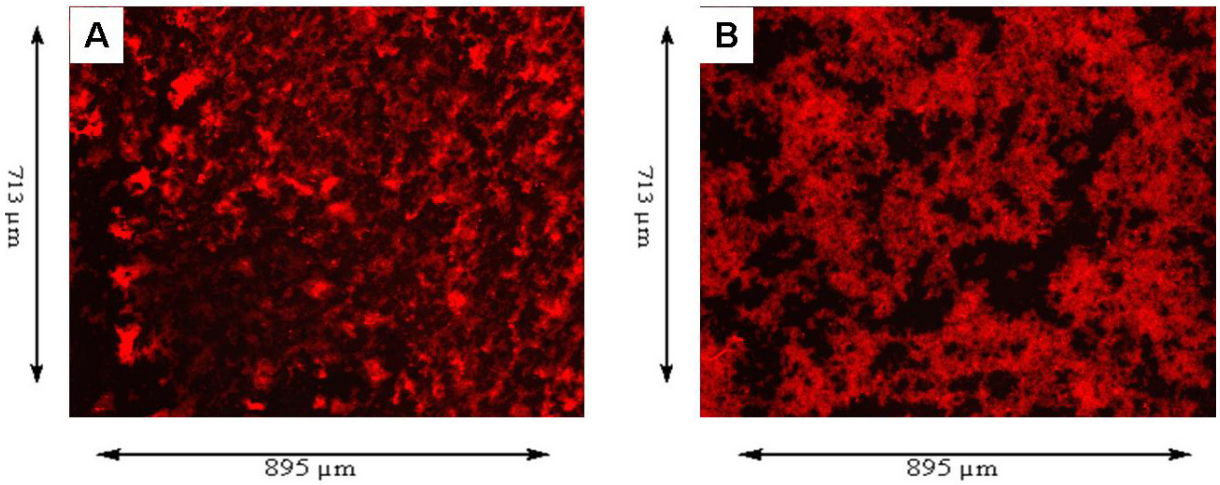

Figure 5-7: Epifluorescence micrograph of (A) pure Aβ peptides after Congo red staining, magnification 10x (B) the monocarboxylated EG_3-stabilized AuNP/Aβ peptide conjugate after Congo red staining, magnification 10x.

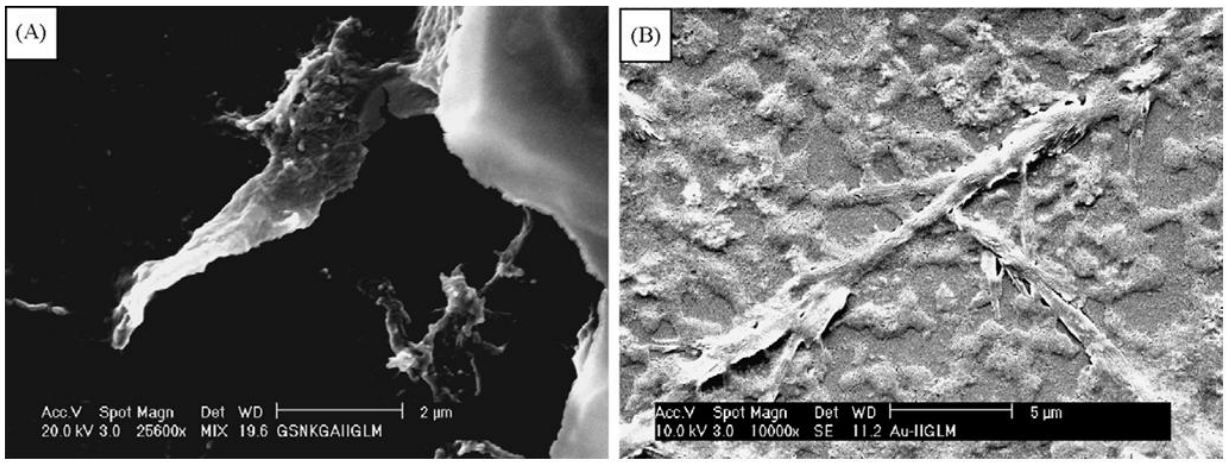

Figure 5-8: A: SEM image of the pure Aβ peptide aggregates, magnification 25,600x, scale bar: 2 µm; B: SEM image of the monofunctional EG_3-protected AuNP/Aβ peptide conjugate, magnification 10,000x, scale bar 5 µm.

It is very interesting to note that the successful attachment of Aβ peptides onto AuNP surface is very important to embed AuNPs into the peptide aggregates. When the AuNP/Aβ peptide conjugates were mixed with the pure Aβ peptide solution, after incubating at room temperature for 24 hours the peptide aggregates precipitated out of solution and finally settled

down at the bottom of a sample tube as shown in Figure 5-9B. The disappearance of the characteristic red color of AuNPs in solution indicated that AuNPs had been embedded into the peptide aggregates and then precipitated out of solution. In a control experiment, when the EG_3-protected AuNPs were mixed with pure Aβ peptides under the same conditions, the red color of the solution remained the same after 24 hours of incubation (Figure 5-9A). This suggests that the AuNP did not interact with the Aβ peptides and precipitate in the peptide aggregation process. This result also confirmed properties of ethylene glycol layer towards non-specific protein adsorption interaction. Because free Aβ peptides could self-assemble with the Aβ peptides attached on the AuNP surface together to form the peptide aggregates, as a result, AuNPs were embedded uniformly into the peptide aggregate matrices and provided a potential heating source for photothermal ablation application of the peptide aggregates.

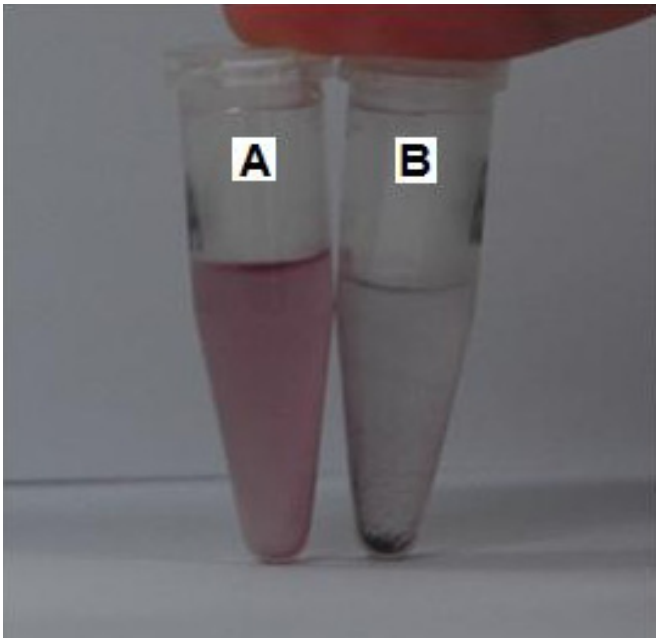

Figure 5-9: (A) The mixture of EG_3-protected AuNPs with the pure Aβ peptide in aqueous solution; (B): the mixture of the moncarboxylated EG_3-stabilized AuNP/Aβ peptide conjugates with pure Aβ peptide in aqueous solution.

It has been reported that the Aβ peptide aggregation depends greatly on the conformational changes from random coil structure to the β-sheet structures.[35] Thus, it is very important to understand the conformational change of Aβ peptide before and after being attached to the AuNP surface. Infrared analysis is a very informative tool for studying the molecular conformation of peptides. A Bio-ATR-FTIR spectrophotometer was used to analyze the conformation of the Aβ peptides after coupling to AuNP surface. Figure 5-10A shows the amide I and II band of the Aβ peptides before and after being conjugated to the particle surface. The amide I band consists of C=O stretching vibration, and appears in the region from 1620 cm^{-1} to 1690 cm^{-1}. This band is directly related to the peptide backbone conformation. The amide II is associated with the N-H deformation and C-N stretching vibrations occuring in the region from 1590 cm^{-1} to 1620 cm^{-1}, which is related to the secondary structures of the peptides. These amide modes have been known to be highly sensitive to the secondary structures of polypeptides and proteins so that it has served as an indicator of the α-helix and/or β-sheet conformations.[36] The band at 1696 cm^{-1} in Figure 5-10A is related to the secondary component of β-sheet structure. The band at 1652 cm^{-1} corresponds to the α-helical structure. In addition, the band at 1668 cm^{-1} is associated with the random coil structure and the shoulder at 1680 cm^{-1} can be assigned to a β-turn structure. Figure 5-10B shows the amide N-H stretching vibration of Aβ peptide before and after being conjugated to AuNPs. The peak at 3500 cm^{-1} is associated to the asymmetric N-H stretching vibration. A weak band at 3100 cm^{-1} is arised from the first overtone of the secondary amide II band.

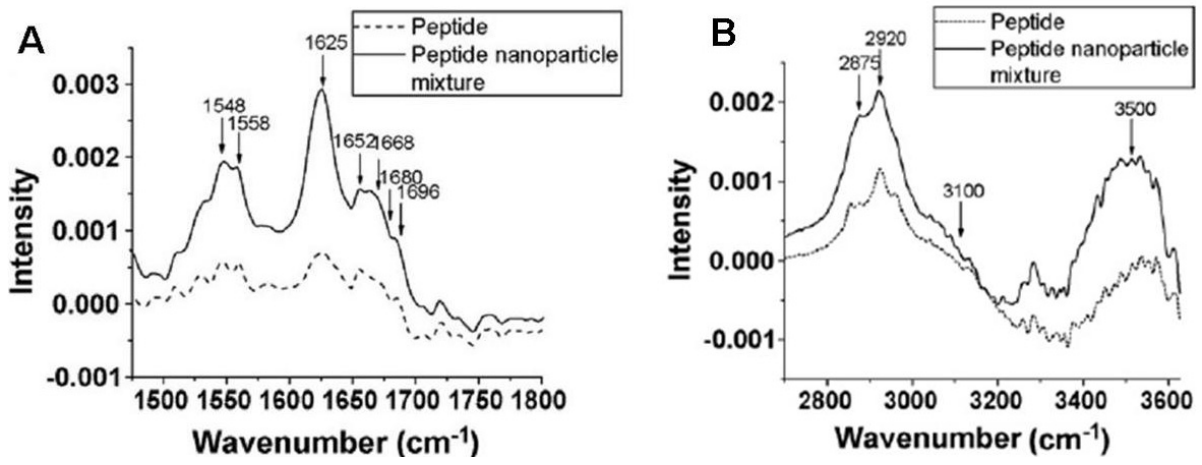

Figure 5-10: Bio-ATR-FTIR spectra of Aβ peptide before and after conjugated onto the particle surface. (A): Amide C=O stretching bands; (B): Amide N-H stretching bands.

Circular dichroism (CD) spectroscopy is another valuable tool to study the secondary structures of proteins. The CD spectrum of proteins and peptides can reveal important characteristics of their secondary structures (α-helix, β-sheet, and random coil). It has been reported that Aβ peptides exhibits conformational transition from random coil to β-sheet structure during the peptide aggregation.[35] Figure 5-11 is the CD spectra of Aβ peptides before and after being attached to the particle surface over a 72 h period. The spectrum was recorded every 24 hours. One can see clearly that pure Aβ peptide contained 28% β-sheet structure, 5% α-helix structure, and 66% of random coil structure in freshly prepared solution. After 24 hours, both β-sheet and α-helix structures increased to 36% and 9% respectively, indicating that the Aβ peptides started to self-assemble to form peptide aggregates. The β-sheet structure reached a maximum of 44% over 48 hours and finally settled at 42% after 72 hours. The peptide was further monitored for 168 h. However, little change was observed after 72 h. It is found that the increase in β-sheet structures is mainly at the expense of random coil structures of the peptides,

which is consistent to the reported literature.[35] The CD spectra of the EG_3-protected AuNP/Aβ peptide conjugates exhibited a similar result with that of pure Aβ peptide over the same period. The percentage of secondary structures compotent did not deviate from the pure Aβ peptide by more than 7% for any structural compotent with the first 72 h of aggregation. Between 72 and 168 h there was less than 3% deviation.

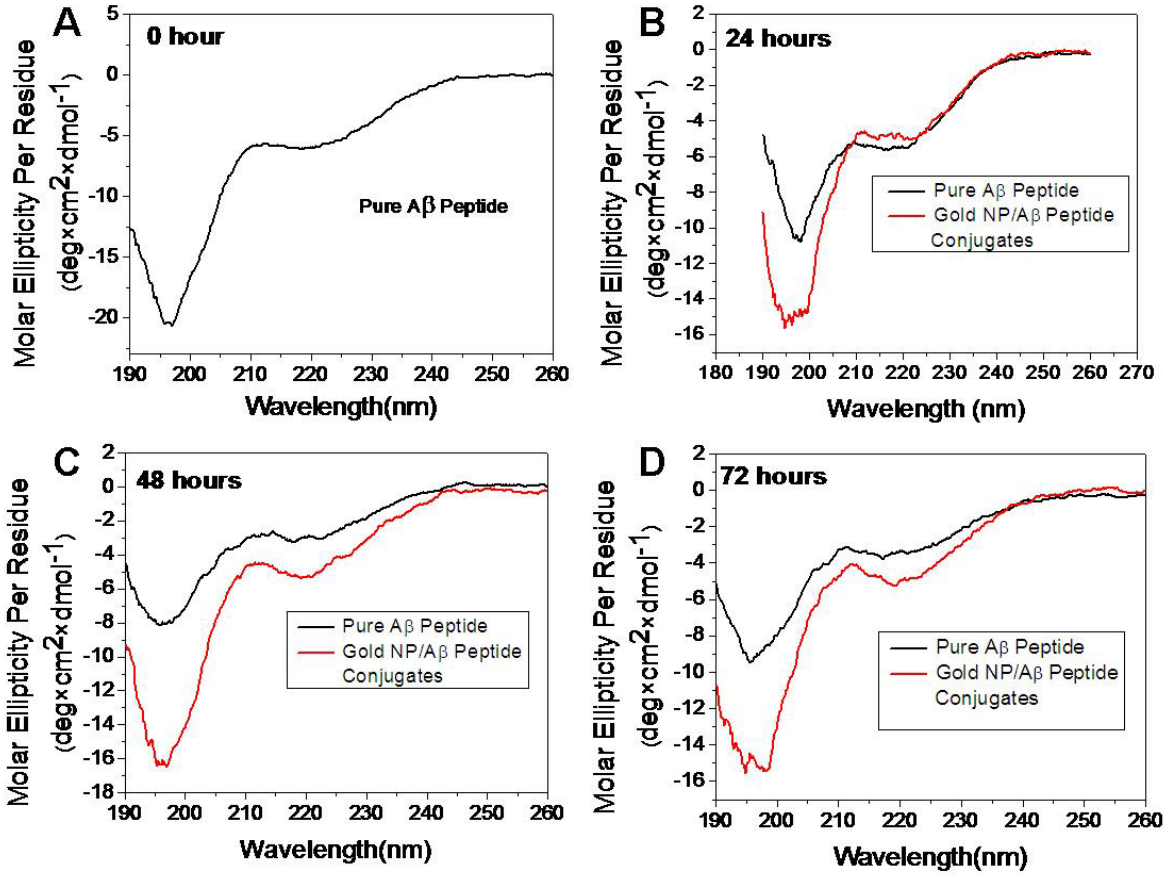

Figure 5-11: CD spectra of the pure Aβ peptide and the monofunctional EG_3-protected AuNP/Aβ peptide conjugates after (A) 0 h; (B) 24 h; (C) 48 h; and (D) 72 h.

5.3.4 : Photothermal Ablation of Aβ Peptide Aggregates using Gold Nanoparticles

To study the photothermal ablation of Aβ peptide aggregates, the Aβ peptide aggregates were transferred to a clean silicon substrate. The photothermal ablation experiments were

conducted under a continuous laser irradiation with a power of 50 mW for 5 min. The laser wavelength is 532 nm, which is close to the SPR absorption band of 5 nm EG_3-protected AuNPs. The irradiated sample was then analysed by SEM as shown in Figure 5-12. One can see clearly that a uniform peptide aggregate was covered on the substrate interrupted by a crater structure in the middle of the images (Figure 5-12A). The crater is located at the irradiated point. Figure 5-12B is a magnified (1600x) image of the ridge area around the crater. One can clearly see that the irradiated area has been cleared of Aβ peptide aggregates when compared to the area just above the ridge. This crater should be a result from AuNP induced- photothermal ablation of Aβ peptide aggregation. Another magnified view (27000x) of the center of the crater in Figure 5-12C further confirmed that the Aβ peptide aggregates have been thermally ablated and removed under the laser irradiation. In contrast, a magnified view (27000x) of the non-irradiated area above the ridge in Figure 5-12D revealed that the aggregates remained intact with only minimal damage due to thermal diffusion from the site of irradiation.

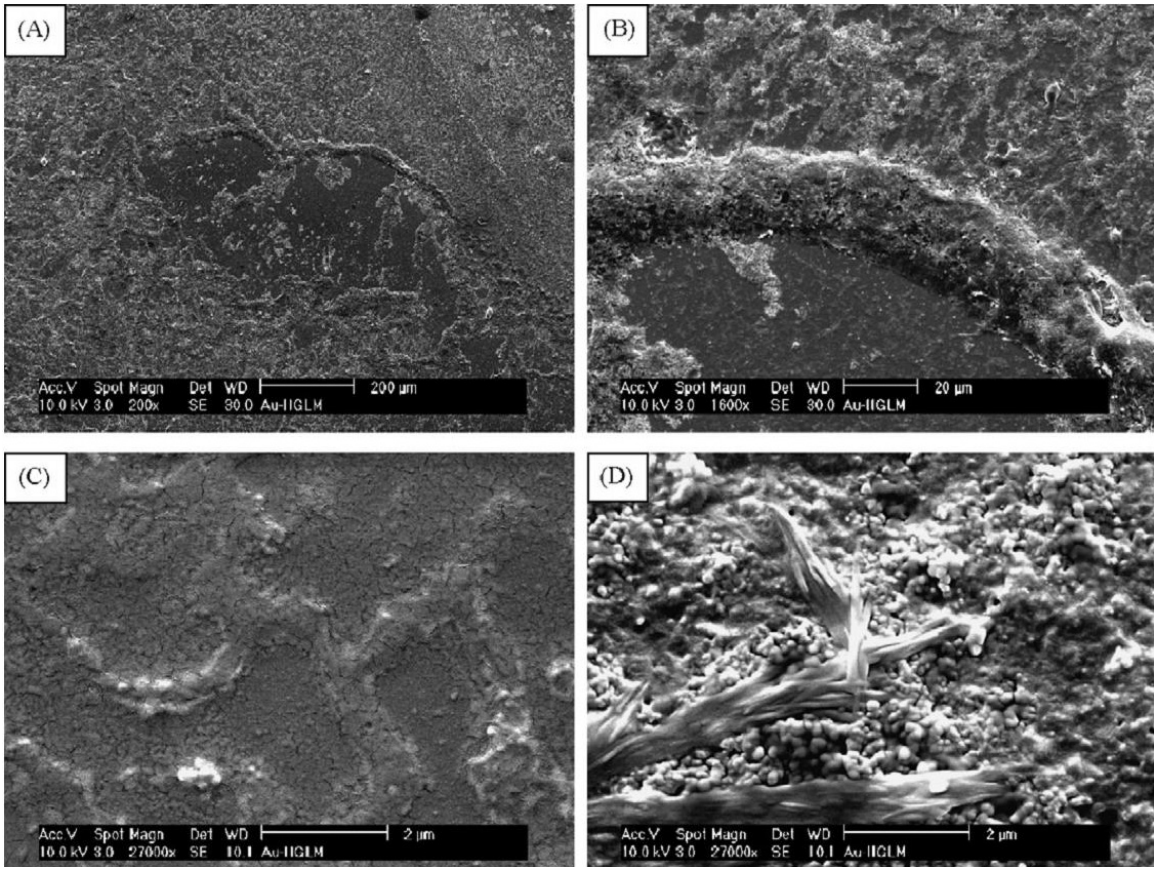

Figure 5-12: SEM images of the EG_3-protected AuNP/Aβ peptide aggregates after laser irradiation. A: the irradiated point with a magnification 200x, scale bar 200 µm; (B) magnification 1600x, scale bar 20 µm; (C) magnification 27000x, scale bar 2 µm; (D) the non-irradiated point with a magnification 27000x, scale bar 2 µm.

The photothermal ablation of Aβ peptide aggregates using AuNPs was further studied by AFM imaging. Figure 5-13A is the AFM images of the AuNP/Aβ peptide aggregates deposited on a mica substrate after laser irradiation. One can see that the peptide aggregates have a relatively smooth surface with some microhole structures. A close look at the AFM image of the AuNP/Aβ peptide aggregates in Figure 5-13B revealed that the irradiated site was free of the peptide aggregates. This smooth surface is probably due to the heat diffusion and melting of the peptide aggregates under laser irradiation. We believe that the formation of microhole structures

was due to the decomposition of the peptide aggregates at the substrate caused by photo irradiation. After the absorption of the photon energy by the EG_3-protected AuNPs, a large amount of heat was accumulated by the AuNPs, causing a dramatic temperature increase around them. The temperature was increased sufficiently to cause complete decomposition of the surrounding peptide aggregates, leading to the formation of microhole structures around the irradiated site. In a control experiment, the pure Aβ peptide aggregates were irradiated under the same condition. Since no AuNP was involved in the peptide aggregates and the Aβ peptides had a low absorption coefficient at 532 nm, it was not expected to observe any crater or hole microstructures under laser irradiation. AFM in Figure 5-14A shows that the mica surface was uniformly covered with peptide aggregates. No microhole structure was observed from the peptide aggregate (Figure 5-14B). The peptide aggregates have a globe-like structure with an average diameter of 20-100 nm. In addition, the pure peptide aggregates have a relatively rough surface compared to that of the AuNP/Aβ peptide aggregates. This experiment further confirmed that the microhole structures were the result of photothermal ablation of peptide aggregates using AuNPs under laser irradiation.

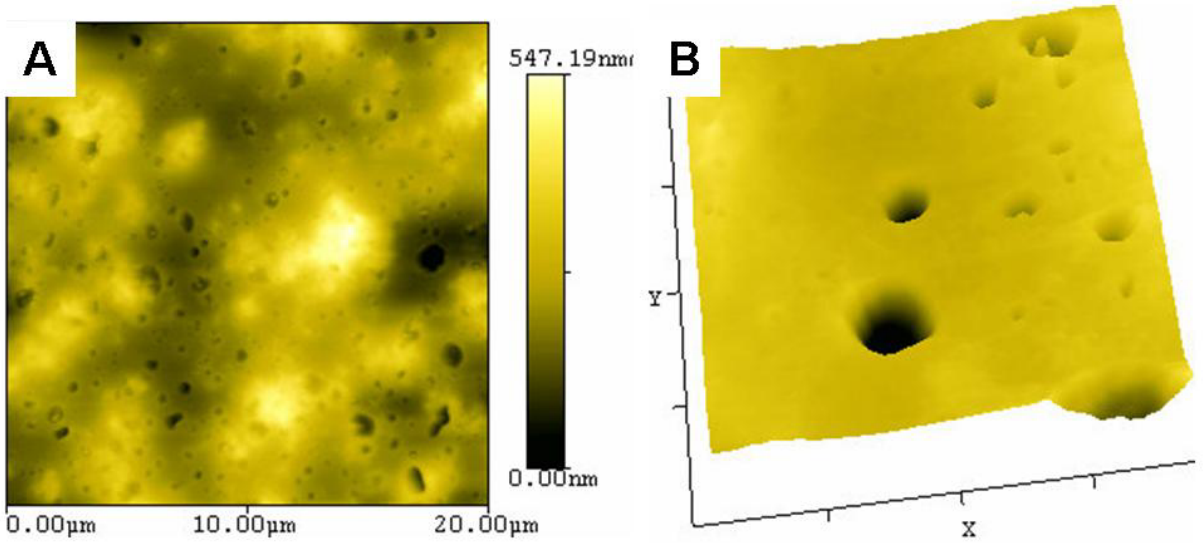

Figure 5-13: AFM images of typical topography of EG_3-protected Au NP/ Aβ peptide aggregates after laser irradiation. (A) 20 × 20 μm; (B): 3D view of the structure.

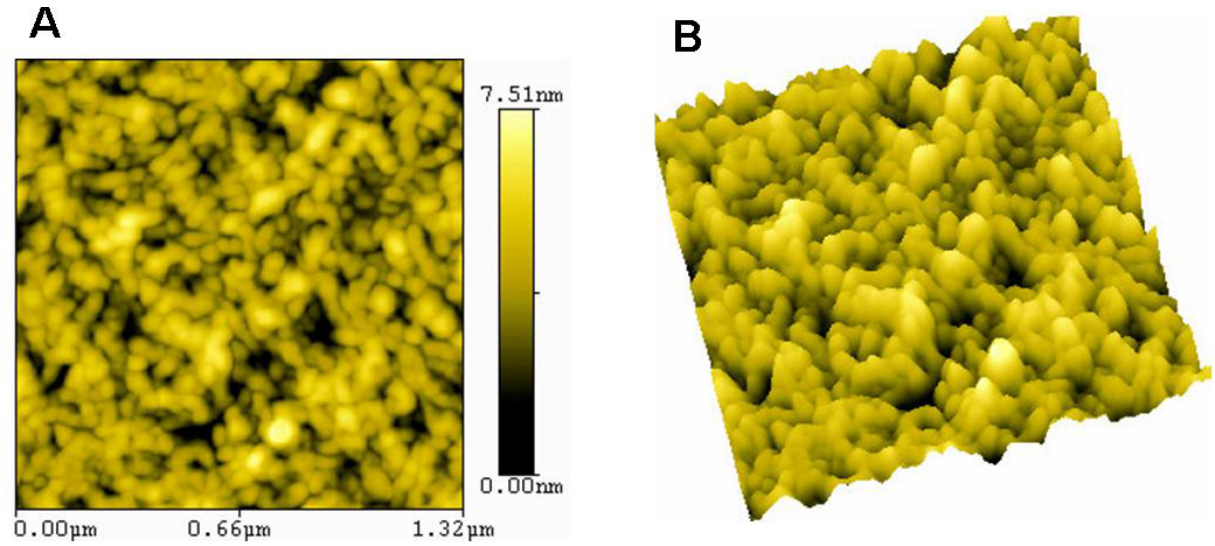

Figure 5-14: AFM images of the typical topography of the pure Aβ peptide sample after laser irradiation. A: 1.32 μm × 1.32 μm; B: 3D view of the structure.

Recently, it has been reported by Kogan et al that the clogging Aβ peptide aggregates can be redissolved remotely by using the local heat dissipated by AuNPs conjugated to the Aβ peptides.[37, 38] The AuNP-Aβ peptide conjugates was dispersed uniformly in pure Aβ peptide matrices, and then the system was irradiated with low gigahertz electromagnetic fields. These absorbed microwave energy by AuNPs was converted into heat leading to an increase of the local temperature. The heat energy released from AuNPs thermally ablates the Aβ peptide aggregates. However, the absorption of AuNPs with a diameter of 10 nm around microwave wavelength is quite low. In our work, we used the continuous laser with a wavelength of 532 nm to irradiate the peptide aggregate samples. The laser wavelength matches the maximum SPR band of AuNPs, and leads a higher absorption of photon energy by the AuNPs. Also, it is possible to tune the absorption peak to IR range using gold nanorods and nanoshells, which allows deeper penetrating of laser light into the tissues.[39, 40] We believe that there is plenty of room for improvement of this photothermal ablation of Aβ peptide aggregates using AuNPs.

5.4 : Conclusions

In summary, we have demonstrated a simple method to photothermal ablation of Aβ peptide aggregates. This process is based on the efficient photon-thermal energy conversion property of AuNPs. The Aβ peptides were covalently conjugated onto the surface of EG_3-protected AuNPs with a core diameter of 5 nm. Bio-ATR-FTIR and CD spectra show that the conformational structures of Aβ peptides did not change after attached on the particle surface, which is very important to the embedation of AuNPs into the peptide aggregate. Both SEM and AFM images of the AuNP/Aβ peptide aggregates clearly show that the Aβ peptide aggregates

was thermally decomposed by heating AuNPs under laser irradiation, and offered as a potential thermal therapy approach for AD patient.

5.5 : List of References

1: Govorov, A. O.; Richardson, H. H. *Nanotoday* **2007**, 2, 30.

2: Jain, P. K.; El-Sayed, I. H.; El-Sayed, M. A. *Nanotoday* **2007**, 2, 18.

3: Richardson, H. H.; Hickman, Z. N.; Govorov, A. O.; Thomas, A. C.; Zhang, W.; Kordesch, M. E. *Nano Lett*. **2006**, 6, 783.

4: Hirsh, L. R.; Stafford, R. J.; Bankson, J. A.; Sershen, S. R.; Rivera, B.; Price, R. E.; Hazle, J. D.; Halas, N. J.; West, J. L. *Proc. Nat. Acad. Sci*. **2003**, 100, 13549.

5: Huang, X.; El-Sayed, I. H.; Qian, W.; El-Sayed, M. A. *J. Am. Chem. Soc*. **2006**, 128, 2115.

6: El-Sayed, I. H.; Huang, X.; El-Sayed, M. A.; *Cancer Lett*. **2006**, 239, 129.

7: O'Neal, D. P.; Hirsch, L. R.; Halas, N. J.; Payne, J. D.; West, J. L. *Cancer Lett*. **2004**, 209, 171.

8: Facts About Alzheimer's Disease (www.alz.org); Alzheimer's Disease and Related Disorders Association, Inc., **2004**.

9: Iverson, L.; Mortishire-Smith, R. J.; Pollack, S. J.; Shearman, M. S.; *Biochem*. **1995**, 311, 1.

10: Bateman, R. J.; Munsell, L. Y.; Morris, J. C.; Swarm, R.; Yarasheski, K. E.; Holtzman, D. M. *Nat. Med*. **2006**, 12, 856.

11: Benzinger, T. L. S.; Gregory, D. M.; Burkoth, T. S.; Miller-Auer, H.; Lynn, .D. G.; Botto, R. E.; Meredith, S. C. *Biochemistry* **2000**, 39, 3491.

12: Selkoe, D. J. *Ann. New York Acad. Sci*. **2000**, 924, 17.

13: Howlett, D. R.; Perry, A. E.; Godfrey, F.; Swatton, J. E.; Jennings, K. H.; Spitzfaden, C.; Markwell, R. E. *Biochem. J*. **1999**, 340, 283.

14: Huang, X.; Atwood, C. S.; Moir, R. D.; Haartshorn, M. A. *J. Biol. Chem*. **1997**, 272, 26464.

15: Cherny, R. A.; Legg, J. T.; Mclean, C. A.; Bush, A. I. *J. Biol. Chem*. **1999**, 274, 23223.

16: Soto, C.; Morelli, L.; Kumar, K. A.; Castano, E. M. *Nat. Med*. **1998**, 4, 822.

17: Adessi, C.; Soto, C.; *Drug. Dev. Res*. **2002**, 56, 184.

18: Adessi, C.; Frossard, M.; Banks, W. A.; Soto, C.; *J. Bio. Chem*. **2003**, 278, 13905.

19: Triulzi, R. C.; Dai, Q.; Zou, J.; Leblanc, R. M.; Gu, Q.; Orbulescu, J.; Huo, Q. *Colloids and Surfaces B* **2008**, 63, 200.

20: Zheng, M.; Li, Z.; Huang, X. *Langmuir*, **2004**, 20, 4226.

21: Chen, H.; Liu, X.; Harish, H.; Zou, J.; Wang, J.; Dai, Q.; Huo, Q. *Adv. Mater*. **2006**, 18, 2876.

22: Miyamoto, D.; Oishi, M.; Kojimm, K.; Yoshimoto, K.; Nagasaki, Y. *Langmuir*, **2008**, 24, 5010.

23: Liu, X.; Worden, J. G.; Dai, Q.; Zou, J.; Huo, Q. *Small* **2006**, 2, 1126.

24: Worden, J. G.; Dai, Q.; Shaffer, A. W.; Huo, Q.; *Chem. Mater*. **2004**, 16, 3746.

25: Yokoyama, K.; Welchons, D. R. *Nanotechnology* **2007**, 18, 105101.

26: Levy, R. *ChemBioChem* **2006**, 7, 1141.

27: Wang, Z.; Levy, R.; Fernig, D. G.; Brust, M. *BioConjugate Chem*. **2005**, 16, 497.

28: Ivonne, O.; Araya, E.; Sanz, F.; Arbiol, J.; Toledo, P.; Giralt, E.; Kogan, M. J. *Bioconjugate Chem*. **2008**, 19, 1154.

29: Weisbecker, C. S.; Merritt, M. V.; Whitesides, G. M. *Langmuir* **1996**, 12, 3763.

30: Sato, J.; Takahashi, T.; Oshima, H.; Matsumura, S.; Mihara, H. *Chem. Eur. J*. **2007**, 13, 7745.

31: Serio, T. R.; Cashikar, A. G.; Kowal, A. S.; Sawicki, G. J.; Moslegi, J. J.; Serpell, L.; Arnsdorf, M. F.; Lindquist, S. L. *Science* **2000**, 289, 1317.

32: Foguel, D.; Suarez, M. C.; Porto, T. C. R.; Palmieri, L.; Andrad, L. R.; Lashuel, H. A.; Kelly, J.; Silva, J. L. *Proc. Natl. Acad. Sci. U.S.A*. **2003**, 100, 9831.

33: Gursky, O.; Aleshkov, S. *Biochim. Biophys. Acta* **2000**, 1476, 93.

34: Serpell, L. C.; Blake, C. C. F.; Fraser, P. E. *Biochemistry* **2000**, 39, 13269.

35: Conway, K. A.; Baxter, E. W.; Felsenstein, K. M.; Reitz, A. B. *Current Pharmaceutical Design* **2003**, 9, 427.

36: Krimm, S. *Biopolymers* **2004**, 22, 217.

37: Bastus, N. G.; Kogan, M. J.; Amigo, R.; Bosch, D. G.; Araya, E.; Turiel, A.; Puntes, V. F. *Materials Science & Engineering C* **2007**, 27, 1236.

38: Kogan, M. J.; Bastus, N. G.; Amigo, R.; Bosch, D. G.; Araya, E.; Turiel, A.; Labarta, A.; Giralt, E.; Puntes, V. F. *Nano. Lett.* **2006**, 6, 110.

39: Hirsh, L. R. *Proc. Nat. Acad. Sci*. **2003**, 100, 13549.

40: Tong, L.; Zhao, T. B.; Huff, M. N.; Hansen, A.; Wei, J. X.; Cheng, J. X. *Adv. Mater*. **2007**, 19, 3136.